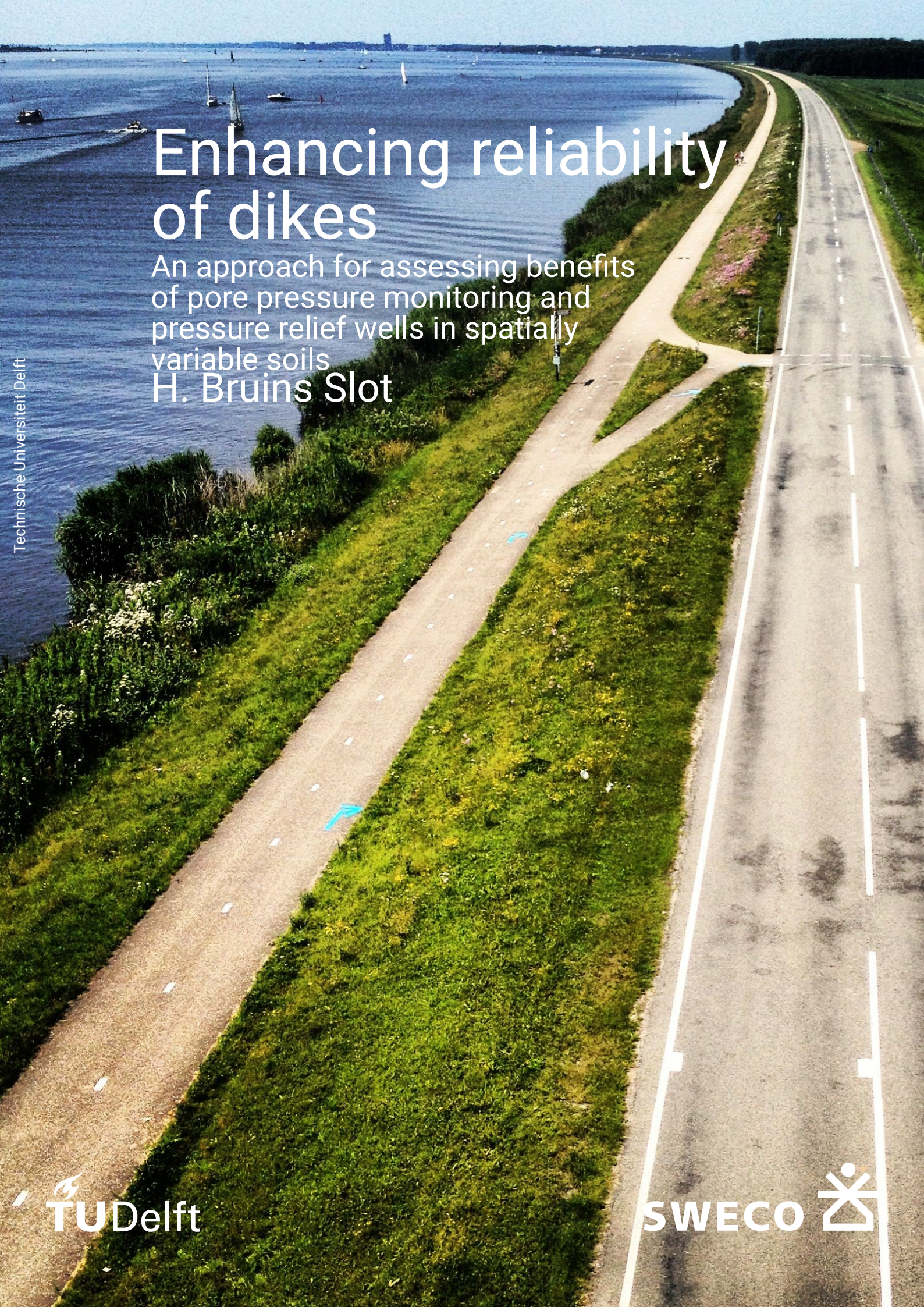

Enhancing reliability of dikes

An approach for assessing benefits of pore pressure monitoring and pressure relief wells in spatially variable soils

H. Bruins Slot

Technische Universiteit Delft

TU Delft

SWECO

Enhancing reliability of dikes

An approach for assessing benefits of pore pressure monitoring and pressure relief wells in spatially variable soils

by

Hilco Bruins Slot

to obtain the degree of Master of Science
at the Delft University of Technology,
to be defended publicly on Tuesday February 16, 2021 at 11:30 AM.

Student number:	4299744	
Project duration:	March 29, 2020 – February 16, 2021.	
Thesis committee:	Prof. dr. ir. S.N. Jonkman	TU Delft
	Dr. J.P. Aguilar-López,	TU Delft
	Dr. T.A. Bogaard,	TU Delft
	Ir. W.J. Klerk	TU Delft
	Ir. J. Steenbergen-Kajabová	Sweco

An electronic version of this thesis is available at `http://repository.tudelft.nl/`.
Cover painting by Winfred Vels

TU Delft SWECO

Preface

The Netherlands and water are inextricably linked, nearly one third of our country lies below sea level. With our fascinating system of delta works, dikes, pumping stations and polders we manage to keep dry feet. As a kid I have spent a lot of time at my grandparents who lived near a dike, I think it is for that reason I was naturally attracted to study about it. The thesis in front of you marks the completion of my MSc program Hydraulic Engineering at Delft University of Technology. I am grateful that I had the opportunity to follow this study program.

I would like to thank Sweco for giving me the opportunity to conduct my thesis at their company. Despite Covid-19 they offered me a graduation spot and made me feel very welcome. I enjoyed the weekly coffee breaks online with Team Waterkeringen a lot. I would like to thank all colleagues for their feedback and Jana in particular for all her help throughout my time at Sweco.

I would like to warmly acknowledge the help of the members of my graduation committee Bas, Juan, Thom and Wouter Jan. I have had a lot of feedback during our meetings that significantly improved the quality of my work. I would like to thank Juan in particular for giving me some valuable tips on modelling in MODFLOW and Wouter Jan for providing guidance throughout my thesis, it will take some time before you get knocked off the stage for most Microsoft Teams calls.

My greatest appreciation to all my fellow students, whom I now call friends, for all their help and support during my time in Delft. I have had a wonderful time that I will treasure for the rest of my life. Thanks to the rest of my friends for their support and friendship. I would like to thank my mom Astra, my sister Minke and the rest of my family for all their support and advice. Last but not least my deepest gratitude to my girlfriend Claire for her unconditional love and support during the final stage of my thesis.

Hilco Bruins Slot
Delft, February 2021

Abstract

The Netherlands is a country prone to flooding. Recent assessments led to the insight that protection levels of many flood defences should be increased. Integrating reinforcement measures is a difficult task as many dikes are situated in densely populated areas. Conventional reinforcement measures include berm construction or the implementation of sheet pile walls. The first can become very expensive in case houses are situated close to a dike, the latter is rather expensive and irreversibly changes dike composition.

Geotechnical failure modes piping and slope instability are most important failure modes for Dutch river dikes. In this thesis a case study is carried out on such a dike that is disqualified for those failure modes. The dike is situated in an urban area with limited space available for reinforcement works. It is studied whether pore pressure measurements behind the dike can be used to improve the reliability estimate for piping. Subsequently it is analyzed whether implementing pressure relief wells can be used to increase dike reliability for both considered failure modes.

For the case study an advanced modelling framework was used consisting of groundwater modelling software and a random field generator. The case study was divided into two parts. The first part consisted of a dike section of 100 m based on a dike section at Wijk bij Duurstede. The second part consisted of the same dike section, only now extrapolated over a length of 2 km for which variations in soil conditions become more important. First, an analysis was conducted to define the optimal amount of pore pressure sensors behind the dike. It was found that for a dike section of 100 m a total of four sensors could be used to perform reliability updates, for a dike section of 2000 m it was found that a total of six sensors could be used. For the 100 m section piping failure probability improved from 5.21E-3 per year to 1.62E-4 per year. For the 2000 m section piping failure probability improved from 5.21E-3 per year to 1.89E-4 per year.

Pressure relief well implementation behind the dike was considered as a measure to increase dike reliability for both failure modes. The system was designed based on a target reliability level for slope instability. The same modelling framework was applied. An analysis was conducted and it was shown that for the 100 m section a well spacing of 50 m would sufficiently increase dike reliability for slope instability. For the 2000 m section a well spacing of 45 m was found. For the 100 m section failure probability for slope instability increased from 8.81E-5 per year to 1.22E-6 per year, failure probability for piping increased from 1.62E-4 per year to 2.03E-7 per year. For the 2000 m section failure probability for slope instability increased from 8.81E-5 per year to 1.30E-6 per year, failure probability for piping increased from 1.89E-4 per year to 1.02E-7 per year. It was shown that for both trajectories target reliability levels for all failure modes were met.

For this case study it was shown that pressure relief wells provide a good design alternative for dike reinforcement in urban areas. A life cycle cost analysis was applied and it was shown that implementation of relief wells is economically attractive compared to traditional design alternatives berms and sheet pile walls. For the first relocation of houses forms an important cost driver, for the latter initial construction cost are high. Furthermore it was shown that implementation of pore pressure monitoring prior to the design of a relief well system yields a positive value of information.

Contents

List of Figures

List of Tables

Nomenclature

List of Abbreviations

FORM	First Order Reliability Method
FoS	Factor of Safety
LEM	Limit Equilibrium Model
LSF	Limit State Function
MCS	Monte Carlo Simulation
MEMS	Micro-electro-mechanical System
NAP	Normaal Amsterdams Peil (reference level)
PCA	Principal Component Analysis
PDF	Probability Density Function
SAR	Synthetic Aperture Radar
SHM	Structural Health Monitoring
TDR	Time Domain Reflectometry
WAM	Wijk bij Duurstede Amerongen (dike trajectory)

List of Symbols

β	Reliability index	[-]
$\Delta\phi_{c,u}$	Critical head difference	[m]
ϵ	Evidence	[-]
η	Drag factor coefficient	[-]
γ'_p	Specific weight grain	[kN/m^3]
γ_d	Model factor	[-]
γ_s	Volumetric weight aquitard	[kN/m^3]
γ_w	Volumetric weight water	[kN/m^3]
λ	Damping factor	[-]
μ	Mean	[-]
ϕ	Cumulative standard normal distribution	[-]
ϕ_{exit}	Hydraulic potential exit point	[m]
ρ	Correlation coefficient	[-]

σ	Standard deviation	[-]
τ_m	Shear stress	[kN/m]
θ	Bedding angle	[°]
a	Channel height	[m]
B	Width dike	[m]
C	Hazen-Williams roughness coefficient	[-]
D	Thickness aquifer	[m]
d	Thickness aquitard	[m]
d_{70m}	d_{70} reference value	[m]
d_{70}	70% fractile grain size distribution	[m]
e	Measurement error	[m]
$f(x)$	Probability density function	[-]
g	Gravitational constant	[m/s^2]
$g(x)$	Limit state function	[-]
H	Head loss	[m]
h	River head	[m + NAP]
H_c	Critical head difference	[m]
h_p	Hinterland phreatic level	[m + NAP]
i	Channel gradient	[-]
$i_{c,h}$	Critical heave gradient	[-]
k	Hydraulic conductivity aquifer	[m/s]
k_h	Hydraulic conductivity aquitard	[m/s]
$L(x)$	Likelihood function	[-]
L_f	Length foreshore	[m]
m_p	Model factor piping	[-]
M_r	Resisting moment	[-]
M_s	Driving moment	[-]
m_u	Model factor uplift	[-]
N	Length effect factor	[-]
p_f	Probability of failure	[year^{-1}]
Q	Flow	[m^3/s]
R	Resistance	[-]
S	Load	[-]
v	Flow velocity	[m/s]
Z	Limit State Function	[-]

1

Introduction

This Chapter provides an introduction to this thesis. Section 1.1 gives a concise background on flood defences and highlights the importance for flood protection. It is shown how research conducted in thesis fits into the current climate for dike reinforcement projects. Subsequently it will be highlighted how the length-effect, an important parameter when deriving flood defence reliability, is incorporated through random field modelling. Sections 1.2 and 1.3 elaborate on the research questions and scope for this thesis. In Section 1.4 the general methodology followed in this thesis is laid out and visually supported by means of a decision tree. Finally, Section 1.5 shows the general outline for this thesis.

1.1. Background and motivation

A substantial part of the world's population lives in areas that are prone to flooding. Flood disasters originate from a wide spectrum of reasons. Globally flood disasters affect more people than any other disaster type (CRED, 2019), which highlights the necessity for flood protection. Looking at a national level, the Netherlands is a country that has always been prone to flooding. A large proportion lies below sea level and several big rivers end in the Dutch delta. As a result roughly 60% of the country is susceptible to flooding (Vergouwe, 2014). Figure 1.1 shows flood prone areas in the Netherlands. Due to the extreme importance of flood protection, regulations have been embedded in Dutch law by the Dutch Water Act.

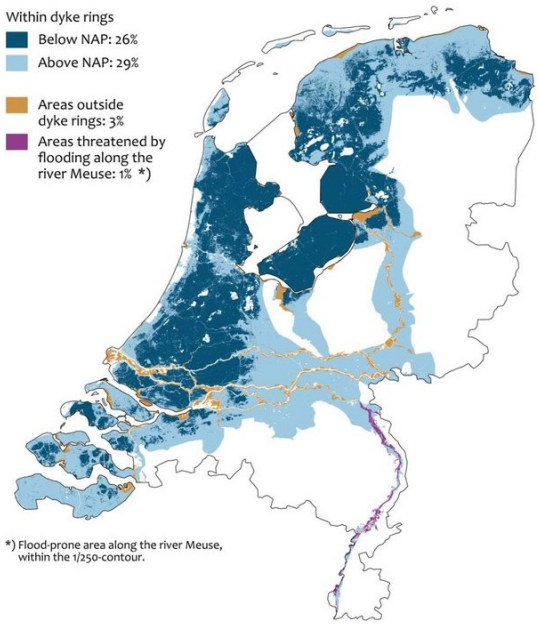

Figure 1.1: Flood prone areas Netherlands (Rijkswaterstaat, 2010).

The most common ways of flood protection consist of dunes, storm surge barriers and dikes, often also referred to as levees. A dune is a large mass of wind-blown sand. Apart from places like the dessert dunes are also found near beaches. In the Netherlands dunes play an integral role in the flood defense system along the sea. A storm surge barrier is a moveable flood barrier that is situated at a river mouth, tidal inlet or estuary and closes when water levels get extremely high. Six of such storm surge barriers have been constructed in the Netherlands and are utilized during extreme storm conditions. Dikes as referred to in this thesis are artificially constructed walls that retain water. They are usually constructed of earth and parallel to the way the river flows. This thesis focuses on man-made river dikes. A common dike composition in the Netherlands is one in which the dike consists of a clay core situated on an aquifer. An aquifer is a water conducting layer underneath a dike build up of sand and/or gravel. Since a substantial part of the Netherlands is located in flood prone areas, almost 3800 km of primary flood defences have been constructed for hinterland protection (Jonkman et al., 2018b).

In 2006 the VNK2 project was started to examine flood risk in the Netherlands. Risk is defined as likelihood times consequence. The aim of the project was to link probability of failure to consequence of flooding, in which consequence of flooding is expressed as economic damage and numbers of victims. After the project was finished in 2014 the perception of risk changed. Up until that time safety standards of flood defense systems were based on design water levels and for each sub-system, in old literature also referred to as dike-ring, acceptable probabilities of failure were derived. Present-day the system of dike division has changed and reference is only made to dike trajectories. Kind (2014) shows that based on new insights obtained through VNK2, it is possible to take targeted reinforcement measures to protect Dutch hinterland more cost-effective. Especially for dikes along the rivers Rhine and Meuse it is economically feasible to raise protection levels.

As a result many dike reinforcement projects are planned in the Netherlands. The acceptable probability of failure is determined by the most stringent criterion derived from either individual, societal or economic risk. Exceptions are made when for example nuclear power plants are included. For more information on how acceptable probabilities of failure are derived one is referred to Jonkman et al. (2018a). New safety standards range from failure probabilities of 1:100 per year to 1:30.000 per year. The VNK2 project has shown that it is not hydraulic failure such as overflow or overtopping but rather geotechnical failure modes that influence dike reliability the most. Geotechnical failure modes include slope instability, dike core sliding, piping, erosion, settlement, etc. Aguilar-López and Bogaard (2014b) showed that experts consider geotechnical failure modes piping and slope instability as the most common reasons for river dike failure in the Netherlands.

Dike reinforcement projects require long-term planning as reinforcement projects are not executed on a daily basis and the project itself takes up much time. Bernardini and Knoeff (2017) define four project phases being 1. the initiation phase, 2. the reconnaissance phase, 3. the elaboration phase and 4. the realisation phase. Figure 1.2 shows the overall process. The initiation phase refers to the phase in which the scope of the project is defined. During the reconnaissance phase a preferred alternative is selected. In the current climate there is typically a period of 5-10 years between the initiation and reconnaissance phase, here referred to as the intermediary period. The elaboration phase refers to the period in which the preferred alternative is elaborated and the project is executed in the realization phase. These project phases are not always strictly followed but provide good global understanding of the overall process.

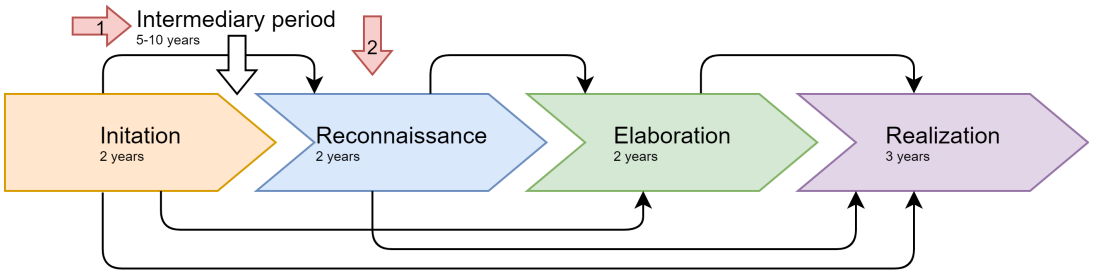

Figure 1.2: Project phases dike reinforcement (Bernardini and Knoeff, 2017). In chronological order: The initiation phase, the reconnaissance phase, the elaboration phase and the realization phase coloured respectively orange, blue, green and purple. Red arrows indicate how pore pressure monitoring fits into project planning.

At least once every twelve years safety assessments are re-evaluated for all primary flood defences in the Netherlands. If a dike is disqualified during safety assessment more detailed safety assessments can be carried out. If the dike still does not meet safety criteria reinforcement is unavoidable. Before the reconnaissance phase starts, reinforcement projects are ranked based on urgency. This intermediary period varies and can easily take up five to ten years, especially in the current situation as many dike segments are listed for reinforcement. During the reconnaissance phase design alternatives are ranked based on preferences. The desired alternative is then elaborated during the elaboration phase and implemented during the realisation phase. All phases together take up nine years of planning on average, excluding the intermediary period.

Increasing the reliability of a dike is traditionally performed through dike reinforcement. Reinforcement measures often include dike enlargement or sheet pile walls. In case of overflow a dike is heightened and for geotechnical failure modes such as piping and slope instability berms and sheet pile walls are a frequent reinforcement measure. In the Netherlands a lot of river dikes are situated in densely populated areas, which complicates traditional reinforcement. On top of that reinforcement is often relatively expensive as in densely populated areas houses are situated near the inner slope. Compensation regulations that have to be agreed on with home owners or expensive design options such as sheet pile walls are an important cost driver. As was mentioned in the previous paragraph, it typically takes five to ten years between the initiation phase of a project and the start of the reconnaissance phase. This time-frame can be used to limit uncertainties that play a role in the reliability estimate of dikes.

Civil engineers try to describe geotechnical failure modes with models. A model is a simplified version of what happens in reality. In order to describe a process a model is created in which variables are introduced that are not strictly defined, they possess a certain amount of uncertainty. van Gelder (2000) makes a general separation between two types of uncertainty: inherent and knowledge uncertainties, a terminology that will be adopted in this thesis. An important parameter in defining reliability for dikes is the length-effect: reliability decreases with increasing trajectory length. Currently reliability calculations are based on cross-sectional analysis after which results are extrapolated over the length by means of a length-effect factor. A length-effect factor represents the chance for weak spots, and therefore heterogeneity in soil. Currently, limiting knowledge uncertainties when (re-)assessing the structural integrity of a dike is not a widely supported approach, while numerous studies report positive findings (Schweckendiek, 2014; Klerk et al., 2015, 2019b).

The period between the initiation and reconnaissance phase provides time for limiting knowledge uncertainties through monitoring. This can ultimately result in an improved reliability estimate, hence a more cost-effective reinforcement project. Currently limiting knowledge uncertainties through pore pressure monitoring is not considered to be a widely supported tool for (re-)assessing a dike's reliability estimate as little is known about the effect of monitoring prior to the elaboration phase. Klerk et al. (2015) states: "Typically in the Netherlands, the assessment of flood defence reliability is based on a relatively rough analysis based on relatively limited data. Measures to increase the assessed reliability of a flood defence thus not only consist of structural measures/reinforcements, but can also be aimed at reducing knowledge uncertainties by monitoring."

It was briefly mentioned before that in the Netherlands many river dikes are situated in densely populated areas. Traditional reinforcement measures as discussed before can become very expensive and in some situations even have drastic societal impact. Pressure relief wells can provide a low-impact reinforcement measure to lower the aquifer's pore pressure and through that increase the reliability of a dike. Research on relief wells has been executed primarily in the United States of America (USA) (USACE, 1939, 1992; Sharma, 1974) and so have the practical implementations (Mansur et al., 2000). In the Netherlands documentation is scarce and because of that waterboards are reticent when it comes to implementation, still Langhorst and Bouwens (2015) recently implemented such a system on dike trajectory Schoonhoven-Langerak with success (van Meurs et al., 2018).

Currently little is known on the effect of pore pressure monitoring prior to the elaboration phase. Experience with relief wells is nil. Because of that these two measures are often overlooked in the decision process of a dike reinforcement project. The focal point of this thesis is to apply pore pressure monitoring during the intermediary period and reconnaissance phase to have a better grip on the reliability estimate and required reinforcement during the elaboration phase. An intermediary period of five years is assumed that will

be used to perform pore pressure monitoring. Subsequently it will be investigated whether pressure relief wells are a suitable reinforcement measure to increase reliability against piping and slope instability. This thesis explores the possibility applying three-dimensional analysis to derive parameters that can be used for two-dimensional stability checks. The heterogeneous character of the aquifer is modelled using random field modelling after which results will be used for two-dimensional analysis. Section 1.2 will elaborate on the research questions that are used to guide research conducted in this thesis.

1.2. Research question

This thesis focuses on the implementation of pore pressure monitoring in the aquifer in the intermediary phase to improve piping reliability estimate. Subsequently a combination pore pressure monitoring and pressure relief wells is applied in the realization phase with the aim to increase dike reliability against piping and slope instability. A case study will be performed on an actual dike trajectory in which heterogeneous soil conditions are taken into account. The main question that this thesis strives to answer is:

> *How can the effect of pore pressure monitoring and pressure relief wells on dike reliability and resulting reinforcement be assessed in spatially variable soils?*

In order to provide a well-founded answer to the research question the case study is divided into three main parts. In the first part an optimal pore pressure monitoring strategy is defined for the considered case study. Then, using the predefined pore pressure monitoring strategy, it is investigated to what extent it is possible to improve the dike's piping reliability estimate. The second part tries to define an optimal configuration strategy for pressure relief wells. Subsequently it is investigated to what extent it is possible to increase the dike's reliability against piping and slope instability. The third part will provide an overview in which the prescribed approach is compared with more traditional reinforcement methods such as berms or retaining walls. A cost overview will be provided to indicate whether the approach is economically attractive. To provide some guidance five subquestions have been created. The first two subquestions conclude part one, subquestions three and four will provide clearance on part two and the last subquestion is used to answer part three. Section 1.3 elaborates on the scope for which the research questions are answered. The subquestions are:

1. *How can spatially variable soils be incorporated in optimizing a pore pressure monitoring strategy?*
2. *What is the effect of including pore pressure monitoring on piping reliability against the considered case study?*
3. *How can spatially variable soils be accounted for in determining the configuration of pressure relief wells?*
4. *What is the effect of including relief wells on the reliability estimate for piping and slope instability for the considered case study?*
5. *To what extent can pore pressure monitoring and/or pressure relief wells contribute to more cost effective dike reinforcement designs?*

1.3. Scope

The case study considers a river dike in the Netherlands. The dike consists of clay and is situated on an aquifer. The foreshore and hinterland are overlain by a clay blanket. Because of its composition this dike is prone to geotechnical failure modes piping and slope instability. The scope of this thesis is also limited to these failure modes. Pore pressure monitoring is conducted at the hinterland toe of the dike for which optimal longitudinal spacing is derived. Results are used to improve piping reliability estimate. A relief well configuration will be derived for which the dike's berm and hinterland toe are considered as possible locations. Results will be used to increase the dike's reliability against piping and slope instability. Finally relief wells in combination with monitoring will be compared with more traditional reinforcement measures berm construction and sheet pile walls on cost-effectiveness.

The main goal in this thesis is to show whether (a combination of) pore pressure monitoring and pressure relief wells can be an effective measure for (re-)assessing a dike's reliability. Because of time constraint some simplifications are made. The aquifer is modelled as a confined aquifer. Interactions between the aquifer and

other soil layers are therefore not taken into account. Hydraulic head at the entrance point and hinterland phreatic level are assumed known and modelled as constant head boundaries. The aquifer is modelled with limited depth, the effect of aquifer storage capacity is therefore not considered. Pressure relief wells are modelled as assigned head boundaries at specific locations in the model, therefore fully penetrated relief wells are assumed.

1.4. Methodology

The aim of this thesis has been discussed extensively in Sections 1.1 and 1.2. This Section will discuss the applied methodology for the case-study. The decision-problem is most easily visualised by means of a decision tree. A decision tree is a graphical representation of a sequence of choice and chance nodes. The decision tree is depicted in Figure 1.3.

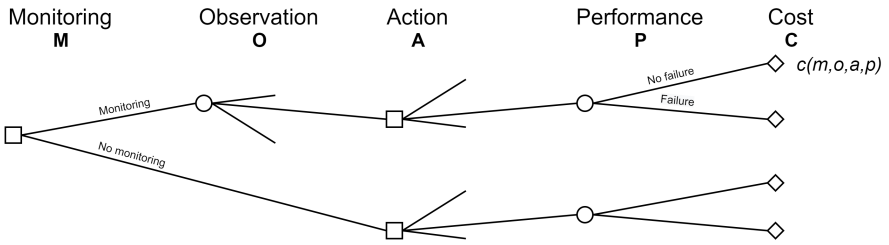

Figure 1.3: Decision tree for a sequential decision on monitoring and reinforcement used in the case study. Squares indicate choice nodes and circles indicate chance nodes.

The decision tree describes the decision process that this thesis strives to clarify. In order to assess the effect of monitoring (M) and observation (O) first an optimal pore pressure monitoring strategy is derived. To that end groundwater flow is modelled using a combination of a finite difference groundwater model and random field modelling. Spatial variation for pore pressure sensors is assessed by means of a principal component analysis (PCA) after which the results are implemented in the model. Equally spaced sensors are assumed. It is then assessed how the obtained results can be used to improve piping reliability estimate. This provides an answer to the first two subquestions.

The caption action (A) refers to possible reinforcement measures that can be taken to increase the dike's reliability. The goal is to compare traditional reinforcement measures such as berms and sheet pile walls with relief wells. To that end an optimal configuration strategy for relief wells is defined by implementing equally spaced relief wells in the aforementioned finite difference model. Relief wells are implemented by means of assigned boundary values at the location of the wells. The goal is to derive optimal spacing so that target reliability against slope instability is met. Subsequently it will be analysed whether target reliability against piping is met. This will provide answers to subquestions three and four.

As was mentioned before this thesis focuses on the implementation of monitoring and pressure relief wells. Bayesian pre-posterior analysis is applied to evaluate benefits of monitoring and pressure relief wells. Pre-posterior analysis allows to determine the best decision based on an evaluation of all outcomes with a-priori available information. Possible observations after monitoring are based on whether an observation is made or not. This depends on the given time period and whether certain water level thresholds have been exceeded in that time frame to obtain useful measurements. Using the decision tree as given in Figure 1.3 it will be investigated whether monitoring in combination with pressure relief wells is a cost-effective measure in a dike reinforcement design. This will provide an answer to research question five.

1.5. Thesis outline

Figure 1.4 provides an overview of this thesis. Chapter 2 discusses relevant theory on computing geotechnical reliability for failure modes piping and slope instability. In Chapters 6 and 7 relevant theory on pore pressure monitoring and pressure relief wells is provided. Together these Chapters provide all theoretical background for the case-study. Chapter 5 provides an introduction to the case study. The general approach is laid out and some preliminary analyses are conducted to assess the dike's reliability. In Chapter 6 a pore pressure monitoring strategy is defined and subsequently used to improve piping reliability estimate. Chapter 7 evaluates the possibility of reinforcing the dike with pressure relief wells. The Chapter ends with increased values for reliability against piping and slope instability. Finally a cost-evaluation is provided in Chapter 8 after which the case study is finished. Some general conclusions are drawn up in Chapter 9.

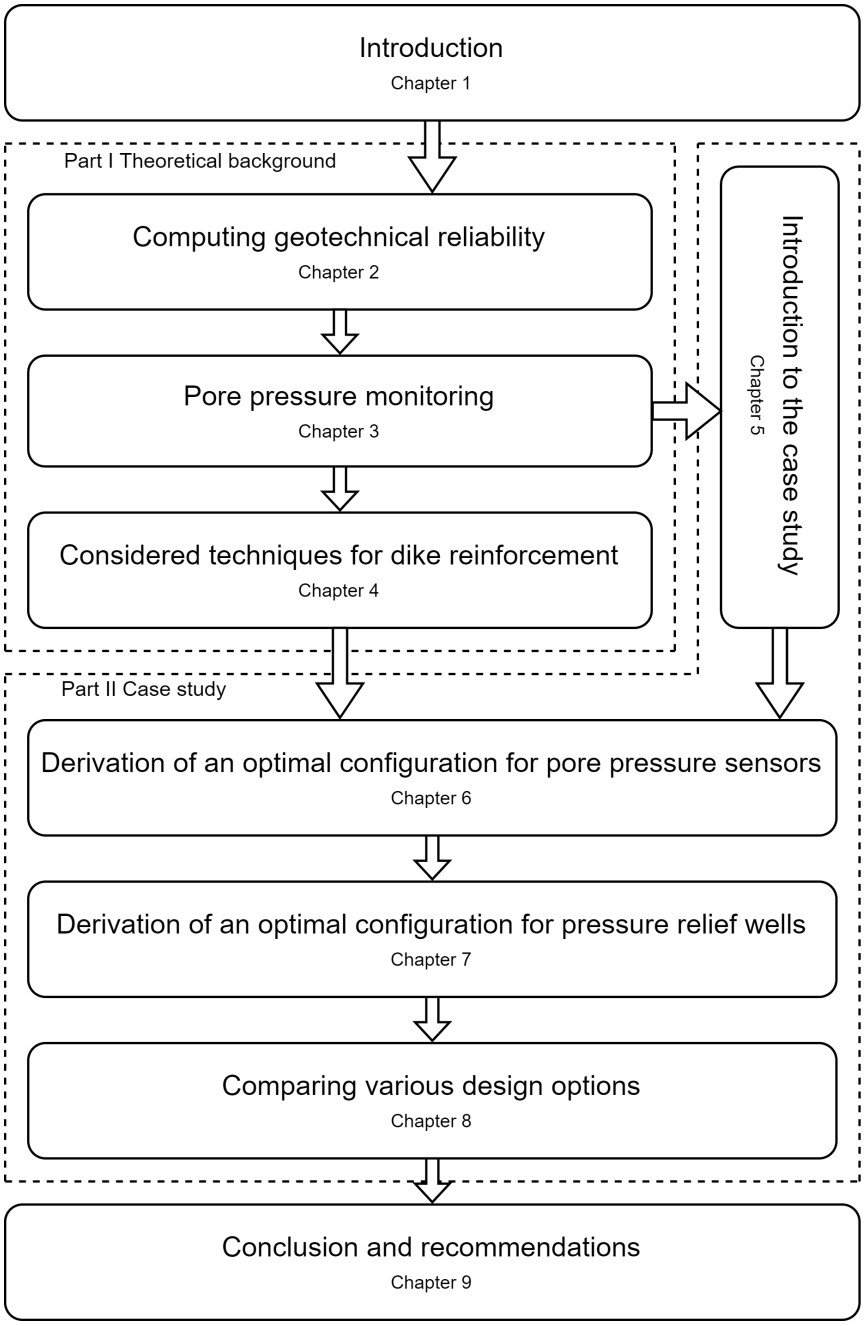

Figure 1.4: Visual overview thesis.

I

Theoretical background

2

Computing geotechnical reliability

This Chapter provides an extensive overview on the two considered geotechnical failure modes in this thesis, backward internal erosion and slope instability. Note that in this Section reference will be made to piping when only the sub-process is considered and to backward internal erosion for all sub-processes together. In the rest of this thesis reference will be made to piping referring to all three sub-processes. First, Section 2.1 will provide background on reliability analysis as it is applied in this thesis. Secondly, a small overview on theory behind the failure modes will be presented and limit state functions for each failure mode will is provided in Sections 2.2 and 2.3. Section 2.4 provides a conclusion to this Chapter.

2.1. Probabilistic framework

This Chapter will first start with a concise overview of some probabilistic theory as it is applied in this thesis. First, limit state functions (LSF) will be discussed as they will be used for reliability assessment in this thesis. Subsequently various evaluation methods for LSF's will be provided. Differences between semi-probabilistic and probabilistic calculations will be highlighted and finally insight will be given into Bayesian decision analysis as used in this thesis.

Limit state functions

Evaluation of failure probability in this thesis is executed through the analysis of limit states. Verification of safety is guaranteed by ensuring that the resistance R is larger than the load S that can act on the structure. The limit state Z is defined in a LSF as follows:

$$Z = R - S \tag{2.1}$$

Failure occurs when $Z < 0$ as the load S exceeds the resistance R. Most parameters that define strength and load conditions are not deterministic but stochastic and vary in space and time, albeit within certain boundaries. The aim of probabilistic design is to ensure that a relatively small resistance is able to withstand a relatively high load. Hydraulic structures such as dikes therefore have an acceptable probability of failure. When the probability density function (PDF) of S and R are known the probability of failure P_f is defined as:

$$P_f = P(Z < 0) \tag{2.2}$$

$$P_f = \phi(-\beta) \tag{2.3}$$

In which β is the reliability index and directly related to the P_f through the cumulative standard normal distribution ϕ. The safety assessment of dikes is calculated for cross sections. The P_f for a certain failure mode for a cross section might be composed of multiple LSF's. This will be elaborated on in Section 2.2. Multiple methods exist to evaluate a LSF. Section 2.1 highlights some of these methods and elaborates on the methods that will be used in this thesis.

Evaluation methods

Literature provides multiple techniques to evaluate a LSF (Jonkman et al., 2015; Faber, 2007). A LSF can be evaluated through deterministic calculations, in which the mean value is chosen for all parameters. Uncertainty is not accounted for. Another method is an evaluation based on semi-probabilistic calculations. For each input variable in the LSF a design value is determined. The design value is chosen as such that uncertainty in that parameter is incorporated in the design value. Distinction is made between load and strength parameters. A way to determine a design value is by taking the 5% or 95% quantile interval value of the PDF's of respectively the strength and load parameters. Another method to evaluate a LSF is through First Order Reliability Method (FORM). In a FORM calculation the LSF is linearized in the design point. The design point is defined as the most probable combination of variables at failure. For each stochastic input variable an influence coefficient α is obtained. This α describes the relative influence of the uncertainty in a certain stochastic variable to the outcome. It must be noted that linearization of the LSF does lead to a small error, which is a disadvantage of FORM. A method to overcome this disadvantage is by evaluating a LSF through Monte Carlo Simulation (MCS). In MCS random samples of the random variables are generated and used as input for the LSF. This process is repeated multiple times. Because the method uses different input values each time the answer will differ each time. The MCS is therefore assumed to be accurate when convergence is reached. Convergence means that enough samples have been drawn to represent a general population and the differences in outcome become negligible. MCS will be used throughout this thesis to evaluate LSF's.

Semi-probabilistic vs probabilistic

The focus in this study is on geotechnical failure modes piping and slope instability. In Chapter 5 a preliminary study will be conducted in which the dike section will be analysed for piping and slope instability. This analysis will be executed using the prescribed semi-probabilistic methods for piping and slope instability prescribed in respectively (Teixeira et al., 2016) and (Kanning et al., 2017). Susbsequently also a full probabilistic analysis will be executed. The essential difference between semi-probabilistic and probabilistic assessments are that in a probabilistic assessment the model is fed with all possible parameter values and their corresponding probabilities. In a semi-probabilistic assessment a failure mechanism is fed with sufficiently safe values. However sufficiently safe is a rather vague criterion and depends highly on the applied calibration procedure. The probability of failure is determined according to calibration formulas.

Bayesian decision analysis

Reliability analyses of dikes are based on statistical distributions that represent probabilities of parameters such as ground conditions that are often based on rather scarce site investigation. These uncertainties can be updated based on posterior observations, for example field measurements during high flood events. In (Schweckendiek, 2010) it is shown how piping reliability is updated based on survived loads using Bayesian techniques. Bayesian decision analysis forms the fundamental basis for optimizing reassessment of failure probability in this thesis.

Prior decision analysis comprises decisions with information that is already present (Kupper, 1971). The yet unknown state of nature is described by the PDF. Posterior decision analysis differs from prior decision analysis in the way that new information, often also called evidence ϵ, is accounted for using Bayesian updating. This will be elaborated later in this thesis. Pre-posterior analysis is about acquiring new information and updating the existing information with it. In order to decide on monitoring analysis, posterior analysis can be carried out with prior beliefs of the probabilities of the observations. This is called pre-posterior analysis and forms the cornerstone of reliability updating in this thesis. There is an important distinction to be made when performing Bayesian updating (Schweckendiek, 2014):

1. Indirect reliability updating, this concerns updating the basic distribution of random variables first after which reliability analysis is conducted with posterior distribution.

2. Direct reliability updating, this concerns updating conform the principles of conditional probability and avoids updating random variables first.

Indirect reliability updating explores the possibility of updating probability distributions of the basic random variables and subsequently recalculate the failure probability with posterior probability distributions. The

updated probability distribution of random variables is given by (van der Krogt et al., 2020):

$$f_X(x|\epsilon) = \int_{\infty}^{\infty} f_X(x|\theta) f_\theta(\theta|\epsilon) d\theta \tag{2.4}$$

In which $f_x(x|\theta)$ is the probability distribution of the random variables, $f_\theta(\theta)$ is the prior probability density function (PDF) of the parameters and ϵ represents the new evidence. The updated failure probability F is is now defined as:

$$P(F|\epsilon) = \int_{g(x)<0} f_X(x|\epsilon) dx \tag{2.5}$$

In which $g(x)$ is a limit state function as discussed in Section 2.1. What follows is an extensive elaboration on direct reliability updating as this will be applied in this thesis. The probability of failure is now given by:

$$P(F) = P(g(X) < 0) = \int_{g(x)<0} f_x(x) dx \tag{2.6}$$

In which X is the vector of the random variables and $f_x(x)$ the PDF of X. The integral can be solved numerically by previously discussed techniques such as FORM or MCS. If such an analysis is carried out with prior probability distributions of X the result is a prior probability of failure, meaning that no initially available information has been added. For reliability updating Bayes' rule is applied to obtain a posterior (updated) probability of failure:

$$P(F|\epsilon) = \frac{P(F \cap \epsilon)}{P(\epsilon)} \tag{2.7}$$

In which ϵ resembles the evidence. Distinction is made between inequality and equality type of information. Inequality type of information is defined as ϵ being described in terms of exceedance of a limit state g and equality type of information is described as when ϵ is that g is equal to a value. The relations for inequality and equality type of information are shown in respectively Equations 2.8 and 2.8.

$$\epsilon \equiv g(x) < 0 \tag{2.8}$$

$$\epsilon \equiv g(x) = 0 \tag{2.9}$$

For the case with inequality type of information reliability updating consists of using standard reliability analysis methods. Two approaches are possible, indirect and direct updating. The first method consists of first updating the basic random variables and then the reliability, the latter explores the definition of conditional probability as is shown in for example Schweckendiek (2010):

$$P(F|\epsilon) = \frac{P(F \cap \epsilon)}{P(\epsilon)} = \frac{P(g(X) < 0 \cap h(X) < 0)}{P(h(X) < 0} \tag{2.10}$$

In which g(X) is a failure limit state function. In case of equality type of information ϵ is described by Equation 2.9. Schweckendiek and Vrouwenvelder (2013) explain that for probability updating with equality type of information surface integration is involved, as h(x) = 0 describes a surface in parameters space, and standard reliability analysis methods like FORM or MCS are not suitable. A method to overcome this problem is offered by Straub (2011). The equality type of information is reformulated in inequality type of information which allows the use of standard reliability analysis methods like FORM or MCS. If a scalar measurement error e_m is involved in measuring a system characteristic, the likelihood function is given by:

$$L(x) = f_{e_m}[s_m - s(x)] \tag{2.11}$$

In which s_m resembles the measured value of the systems characteristic s(x) and f_{e_m} the PDF of e_m. In order to transform the equality problem to an inequality problem the likelihood function is rewritten into:

$$L(x) = \frac{1}{c} P(U - \phi^{-1}[cL(x)] \leq 0) \tag{2.12}$$

In which U is a standard Normal random variable and c a positive constant so that $0 \leq cL(x) \leq 1$. In case of a Normal distributed measurement error a proper choice for $c = \sigma_{e_m} \,/\, \phi(0)$, in which σ_{em} is the standard deviation for e_m. The likelihood function can now be expressed by the following equivalent observation LSF with corresponding domain:

$$h_e(x,u) = u - \phi^{-1}[cL(x)] \tag{2.13}$$

$$\epsilon_e \equiv h_e(x,u) \leq 0 \tag{2.14}$$

The conditional probability of failure can now be obtained by:

$$P(F|\epsilon) = \frac{P(F \cap \epsilon)}{P(\epsilon)} = \frac{\int_{F \cap \epsilon_e} f_x(x)\phi(u)dudx}{\int_{\epsilon_e} f_x(x)\phi(u)dudx} \tag{2.15}$$

In which ϕ is the standard normal PDF. Equation 2.15 can now be evaluated with common reliability analysis methods such as FORM or MCS. For a more extensive elaboration on reliability updating with equality information one is referred to Straub (2011).

The length effect

The concept of the length-effect is one that forms an integral role in this thesis, and is therefore important to understand. In reliability analyses for dikes the length-effect mainly refers to an increase in failure probability with increasing dike length. Figure 2.1 gives a graphical representation of the length-effect.

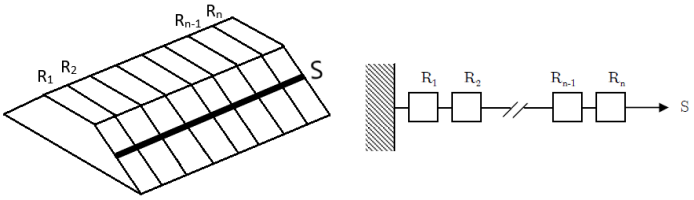

Figure 2.1: A graphical representation of the length-effect (Kanning, 2012).

Correlation lengths in loads are much higher than correlation lengths in dikes. Flood defense systems are therefore mostly modelled with loads fully correlated over the length. The length-effect can therefore be attributed to partial correlation or independence between different cross-sections in dikes. Looking at Figure 2.1, a dike can be modeled as a series system of (partly) correlated sections due to little correlation in resistance. As a result the probability of failure increases with length.

In reliability analysis for dikes probability of failure is usually calculated for a representative cross-section. In order to account for spatial variability in soil the failure probability is extrapolated over the length of the dike using a length-effect factor N. For more information on N one is referred to Appendix A. Fore a more in-depth analysis on the length effect one is referred to Kanning (2012).

2.2. Reliability analysis for backward internal erosion piping

Backward internal erosion is a process in which shallow channels develop below a structure, in this case a dike. Backward internal erosion begins at the downstream side of the dike and develops upstream, ultimately leading to collapse. Large hydraulic head in the river leads to excessive pore pressure in the aquifer underlying a dike. If pore pressure exceeds aquitard weight the clay layer bursts. This phenomenon is referred to as uplift. Excess water now seeps out of the broken aquitard. If the seepage gradient exceeds the critical heave gradient sand particles start eroding. This is also referred to as heave. More sand particles now erode and a network of pipes forms under the dike. This is referred to as piping. Once the pipe reaches the river the flow increases due to loss of hydraulic resistance. Finally the structure is undermined and collapses. Figure 2.2 shows different stages for the piping process.

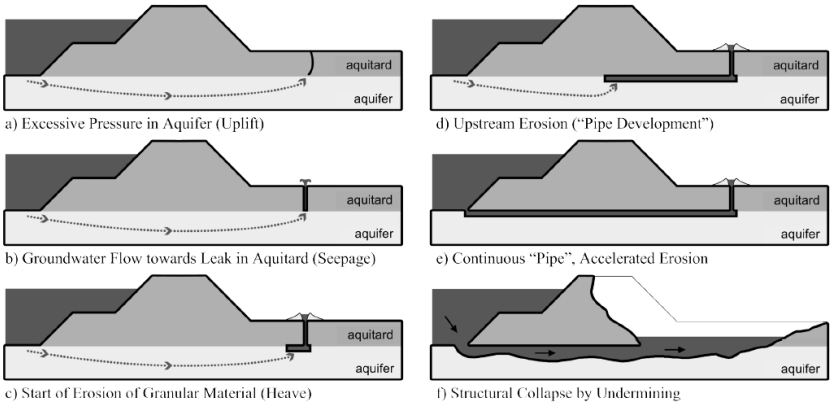

Figure 2.2: Different phases in backward internal erosion (TAW, 2004).

Uplift, heave and piping are all preconditions for piping. Backward internal erosion can therefore be described as a parallel system with limit states for respectively uplift, heave and piping:

$$F = F_u \cap F_h \cap F_p \tag{2.16}$$

Hydraulic gradient

The hydraulic gradient is an important parameter used for erosion to develop as it is used for evaluating the potential at the exit point of the pipe behind the dike ϕ_{exit}. Figure 2.3 gives an illustration of relevant parameters for analysis as applied in the Netherlands. The dike consists of a clay dike situated on a aquitard. An aquifer is present underneath the aquitard.

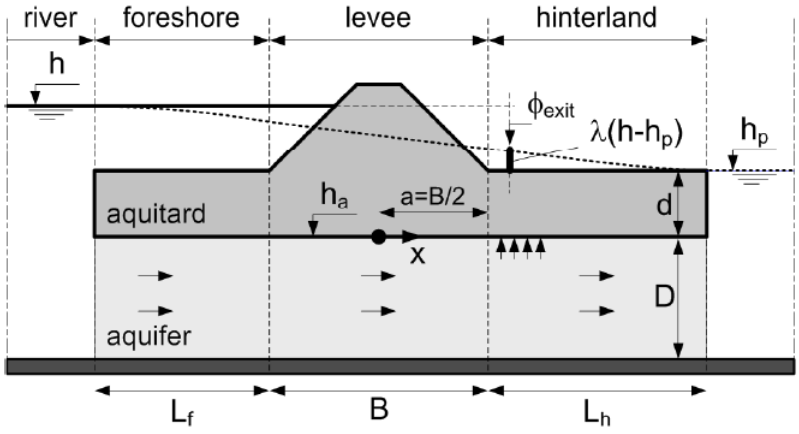

Figure 2.3: Groundwater profile for a typical Dutch river dike (TAW, 2004).

The potential at the exit point behind a dike is given by (Rijkswaterstaat, 2019):

$$\phi_{exit} = h_p + \lambda(h - h_p) \tag{2.17}$$

The damping factor λ describes the exit point potential and is defined as:

$$\lambda = \frac{\lambda_h}{L_f + B + \lambda_h} \exp^{(B/2-x)/\lambda_h} \tag{2.18}$$

In which L_f is the length of the effective foreshore, B the width of the dike, x the distance of the exit point with respect to the middle of the dike and λ_h the leakage factor for the hinterland section defined as:

$$\lambda_h = \sqrt{kDd/k_h} \tag{2.19}$$

In which k resembles the hydraulic conductivity of the aquifer, D is equal to the thickness of the aquifer, d is equal to the thickness of the aquitard and k_h is the aquitard hydraulic conductivity.

Uplift

The first of three sub-mechanisms evaluated for backward internal erosion is uplift. In simple terms it is to be evaluated if the upper impermeable blanket can be lifted. Uplift evaluation is based on a comparison between the aquitard weight and hydraulic head in the top layer of the aquifer, both measured at the exit point. If hydraulic head exceeds the aquitard's weight uplift occurs. The LSF for uplift is formulated as follows (Rijkswaterstaat, 2019):

$$Z_u = m_u \Delta\phi_{c,u} - (\phi_{exit} - h_p) \tag{2.20}$$

In which m_u is a model factor that addresses uncertainty in the critical head difference $\Delta\phi_{c,u}$, which on its turn is defined as:

$$\Delta\phi_{c,u} = d \cdot \frac{\gamma_s - \gamma_w}{\gamma_w} \tag{2.21}$$

Where γ_s represents aquitard volumetric weight and γ_w the volumetric weight of water.

Heave

Once the blanket was lifted, reduction of frictional forces among grains occurs due to fluidization of the granular mass. This allows higher fluxes between grains and initial transport of fine grains. The LSF for heave is defined as:

$$Z_h = i_{c,h} - \frac{\phi_{exit} - h_p}{d} \tag{2.22}$$

In the Netherlands a critical heave gradient of 0.7 is assumed with a standard deviation of 0.1 (Schweckendiek, 2014). Terzaghi and Peck (1967) defined that the critical heave gradient equals the balance between flow force and the weight of soil particles:

$$\gamma_w \cdot i_{c,h} \cdot V = \gamma_s^{'} \cdot V \tag{2.23}$$

In which γ_w is the volumetric weight of the water, $\gamma_s^{'}$ the specific weight of the sand, V the volume of the grain and $i_{c,h}$ the critical heave gradient. The critical heave gradient is now given by:

$$i_{c,h} = \frac{\gamma_s^{'}}{\gamma_w} \tag{2.24}$$

In which $\gamma_s^{'}$ can be defined as:

$$\gamma_s^{'} = (1-n) \cdot (\gamma_s - \gamma_w) \tag{2.25}$$

In which n resembles the sand's porosity. The critical heave gradient is now defined as:

$$i_{c,h} = \frac{(1-n)(\gamma_s - \gamma_w)}{\gamma_w} \tag{2.26}$$

Piping

Piping refers to the development of shallow channels in sand below the dike. Multiple studies have been conducted in an attempt to describe piping (Bligh, 1910; Lane, 1935; Sellmeijer, 1988; van Beek, 2015). Bligh (1910) was the first to develop an empirical rule. He realised that the stability of hydraulic structures depends on the seepage length and that a smaller grain size meant a lower resistance to piping. His study resulted in

a design formula, in which he related seepage length to the hydraulic head and soil conditions. Lane (1935) concluded that the resistance in vertical seepage paths was three times larger than the resistance in horizontal seepage paths. He therefore adapted Bligh's formula. The empirical design rules that are proposed by Bligh and Lane only allow to incorporate the soil characteristics through one percolation factor, which is in many cases too simplified. Moreover, the design rules don't offer room to incorporate additional information obtained through head monitoring.

In a later stage Sellmeijer (1988) developed a mathematical model to describe piping. He therefore looked at the limit stress state of a single particle in a pipe. His two-dimensional analysis is based on a model prescribed by White (1940) that looks at the equilibrium of grains on a bed. He later notified that larger grains stick out of the bed and modified his theory into a two force equilibrium model (Sellmeijer, 2006) with a horizontal drag force and a vertical gravity force. The forces are defined as follows:

$$F_H = \frac{1}{2\eta} \cdot \gamma_w \cdot i \cdot a \cdot d^2 \tag{2.27}$$

$$F_V = \gamma_p^{'} \cdot \frac{\pi}{6} \cdot d^3 \tag{2.28}$$

In which η represents White's constant, γ_w is the volumetric weight of the water, i is the gradient in the channel, a is the height of the channel, d is the characteristic grain diameter which is equal to the d_{70} and $\gamma_p^{'}$ is the specific weight of the grain. The movement of a grain is described by rotation and the equilibrium of forces around the contact point of two grains is given by:

$$\frac{F_V}{\cos(\theta)} = \frac{F_H}{\sin(\theta + \alpha)} \tag{2.29}$$

In which θ is the bedding angle and α is the slope of the erosion channel. Combination of Equations 2.27 and 2.28 with Equation 2.29 yields the boundary condition along the erosion channel:

$$i = \frac{\pi}{3} \cdot \frac{\eta \cdot d}{a} \cdot \frac{\gamma_p^{'}}{\gamma_w} \cdot \frac{\sin(\theta + \alpha)}{\cos(\theta)} \tag{2.30}$$

The design rule is given by:

$$\frac{H_c}{L} = F_1 \cdot F_2 \cdot F_3 \tag{2.31}$$

$$F_1 = \eta * \frac{\gamma_p'}{\gamma_w} * \tan(\theta) \tag{2.32}$$

$$F_2 = \frac{d_{70m}}{\sqrt[3]{\frac{\nu k L}{g}}} \left(\frac{d_{70}}{d_{70m}} \right)^{0.4} \tag{2.33}$$

$$F_3 = 0.91 * \left(\frac{D}{L} \right)^{\frac{0.28}{\left(\frac{D}{L}\right)^{2.8}} + 0.04} \tag{2.34}$$

In which F_1, F_2 and F_3 are respectively the resistance, scale and geometric shape factor, κ is the intrinsic permeability of the aquifer and D is the thickness of the aquifer. The LSF for the revised Sellmeijer Equation as used in this thesis is given by:

$$Z_p = m_p H_c - (h - h_p - 0.3d) \tag{2.35}$$

All previously described models describe piping as a 2D process. Obviously piping is a 3D process. van Beek (2015) however has shown that Sellmeijer Equation is well suited for modelling piping in aquifers. Kanning (2012) has shown that Sellmeijer Equation is closer to reality than Bligh or Lane. Moreover using Bligh and Lane can lead to over estimations of required piping length. The Sellmeijer Equation is therefore adopted in this thesis.

2.3. Reliability analysis for slope instability

This Section provides a conceptual description of slope instability as well as various calculation models that are being used to assess dikes for slope instability. Slope instability occurs when a soil mass loses stability and and slips along a slip plane. The equilibrium of forces is undermined. It occurs either at the inner or outer slope of the dike. This thesis will only focus on inner slope instability. Slope instability is triggered by hydrological events when water infiltrates into the dike. When water infiltrates into the dike body pore pressures increase, hence the effective stresses decrease. A schematic illustration of inner slope instability is provided in Figure 2.4.

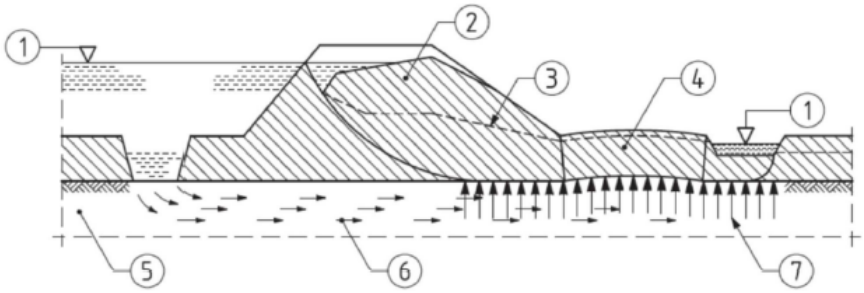

Figure 2.4: Inner slope instability ('t Hart et al., 2016).

Slope instability can occur either at the inner or outer slope. Inner slope instability occurs during conditions that were prescribed above. Outer slope instability occurs when river water level decreases rapidly. The outer slope is now no longer supported by the force of the water and might slide off due to increased pore pressures in the dike body. Outer slope instability often occurs when the river water level is on a descend and therefore poses no direct danger for flooding. Looking at Figure 2.4, the driving force behind the loss of stability is caused by the mass of soil at the left side of the center of the slip plane. The resisting force is caused by the soil at the right side of the center of the slip plane and the shear stress of the soil along the slip plane. When water infiltrates into the dike body the soil's shear decreases, hence the risk of inner slope instability increases. The risk for slope instability is assessed using limit equilibrium models (LEM). LEM compare the driving moment M_s to the resisting moment M_r to derive a factor of safety:

$$FoS = \frac{M_r}{M_s} \tag{2.36}$$

For a semi-probabilistic computation the safety format used in Dutch safety assessment is given by (Kanning et al., 2017):

$$P_f = \phi\left(-\frac{\frac{FoS}{\gamma_d} - 0.41}{0.15}\right) \tag{2.37}$$

In which γ_d is a model factor. The LEM examines any potential sliding plane and determines the most critical one. They are therefore considered to be a powerful tool for slope instability assessment. General separation is made for drained and undrained analysis. If the rate of deformation is small compared to drainage capacity of the soil the soil response is considered drained. If during deformations excess pore pressures built up and cannot be drawn away the soil is considered undrained. Drained conditions typically occur in high permeability soils such as sand and gravel. Undrained conditions are typical for low permeability soils such as clay. This thesis concerns a clay dike which will therefore be modelled using undrained conditions. In this thesis the software D-GEO Suite Stability is used for reliability assessment. D-GEO Suite Stability offers three semi-probabilistic calculation models to assess a dike for slope instability. The differences in the models can be found in the shape of the slip planes and shear stress distributions along the slip planes (Zwanenburg et al., 2013). Slope instability is considered to be one of the most important geotechnical failure modes for river dikes in the Netherlands (Aguilar-López and Bogaard, 2014b).

Slope stability assessment methods

The first considered slope stability assessment method is Bishop / Fellenius. The method is relatively simple and therefore computationally easy. In the Netherlands it is the most used method (Zwanenburg et al., 2013).

This method checks the moment equilibrium of a circular slip plane. First, the soil mass is divided into slices. For each slice the maximum shear stress τ_m is determined. The shear stress of each slice is subsequently multiplied with the arm to the center of rotation to derive the contribution to the resisting moment M_r. The forces exerted by each slice are subsequently multiplied by the arm around the center of rotation to derive the contribution of each slice to either the resisting moment M_r or driving moment M_a. Subsequently Equation 2.36 is used to derive the factor of safety. Besides moment equilibrium the model of Bishop / Fellenius also ensures vertical stability.

The second considered assessment method is called Uplift-Van. Uplift-Van method is created in order to assess the stability of the inner slope when stability is lost due to uplift conditions in the aquitard. An increase in aquifer pore pressure reduces the effective stresses under the aquitard, highlighted by 4 and 7 in Figure 2.4. A reduction in the effective stress between the aquitard and aquifer means that the aquitard can only transfer a horizontal load. Hence, Bishop is no longer applicable. The Uplift-Van method ensures moment, horizontal and vertical equilibrium. If the length of the aquitard approaches zero, and the center points of the slip circles are the same, the result of the Uplift-Van model is the same as the result of the Bishop model.

The third considered method is Spencer. Spencer method differs from the other methods as the sliding surface can be defined freely. Free to choose interconnected segments form the sliding plane. Like with Uplift-Van, Spencer ensures all three force equilibria. In field application of Spencer is limited because there is limited experience in using this method (Jonkman et al., 2018a).

Apart from LEM's, slope instability can also be assessed using a finite element model (FEM). Such computations are computationally expensive and results obtained from a finite element analysis will not provide relevant new insights for this study. They are therefore not elaborated further.

2.4. Concluding remarks

In this Chapter general theory for computing geotechnical reliability is provided. Section 2.1 showed the probabilistic framework as applied in this thesis. Subsequently Sections 2.2 and 2.3 showed how analyses for piping and slope instability fit into the probabilistic framework applied in this thesis. Stability analysis will be executed with Uplift-Van as this method allows to examine shear stress on the interface between aquifer and aquitard. Pore pressure monitoring will be applied and used to update LSF's as were discussed in this Chapter. Chapter 6 elaborates on pore pressure monitoring and shows how it is used to update failure probability for piping and slope instability.

3

Pore pressure monitoring

This Chapter elaborates on pore pressure monitoring of the dike's aquifer as it is one of the focal points in this thesis. Section 3.1 provides general background on monitoring after which Section 3.2 discusses pore pressure monitoring using standpipes in more detail. This thesis focuses on monitoring using standpipes. Section 3.3 provides an overview of other monitoring techniques relevant for failure modes piping and slope instability. Finally Section 3.4 gives some concluding remarks considering this Chapter.

3.1. Monitoring in general

Monitoring, or structural health monitoring (SHM), refers to the process of using monitoring equipment and characterization strategy to assess the structural health development of a structure. Some examples include SHM of bridges (Ko and Ni, 2005) and wind turbine support structures (Thöns, 2011). In general SHM aims at using performance observations obtained in the field to (re-)assess and predict structural health.

Dike monitoring consists of measurements and inspections on dikes with the perspective on required follow-up actions. It is widely supported that monitoring can significantly reduce uncertainties regarding the behaviour of a dike (Koelewijn and van der Meer, 2019). For every dike (reinforcement) project a monitoring plan should be constructed and updated if circumstances change (BRON). Klerk et al. (2015) concluded that head monitoring should fill an integral role in future management of dikes as an increase in loads and an increase in risk will likely result in more frequent future reinforcements. Klerk et al. (2019b) showed that especially large strength uncertainties in soil highlight the possibilities of SHM, making it very feasible for earthen flood defence structures such as dikes. Nevertheless, Klerk et al. (2019a) stress that the decision to monitor or not should depend on whether information gain will ultimately result in a different decision regarding dike reinforcement. If monitoring leads to an increase in information that ultimately influences reinforcement it is likely economically attractive.

Major contributions to the development of SHM have been provided by the FloodControl-IJkdijk research project in the Netherlands (de Vries et al., 2010). This research program was initiated in 2005 with the aim of testing new monitoring techniques and to obtain knowledge on geotechnical failure mechanisms. The focus is mainly on technological development. For example Nieuwenhuis et al. (2016) performed a study, as part of the FloodControl-IJkdijk project, in which multiple monitoring techniques were implemented and tested. It is shown that SHM can be beneficial in multiple ways as it can act as an early warning system to assess real time strength conditions during storms and it can also be used to limit knowledge uncertainties so that reinforcement works can be executed more (cost) effective.

Interest in asset management of infrastructures has increased significantly over the past decades (Frangopol and Soliman, 2016) and SHM has become increasingly important herein. The reliability of a dike is the main performance indicator to be used in defining asset management strategies, hence the link with SHM. Klerk et al. (2019b) uses a Bayesian pre-posterior analysis to show the benefits of pore pressure monitoring. In van der Krogt et al. (2020) the same approach was used with a monitoring period of five years. The Value of Information (VoI) principle is used to evaluate the results for different monitoring strategies. Within asset

management, decision analysis for SHM typically uses VoI to assess its benefits. The VoI indicates the utility of the concerned method. As was mentioned in Section 1.1 the perspective of assessing risk changed in the Netherlands. A probabilistic assessment of all primary flood defences was conducted in the VNK2 project (Jongejan and Maaskant, 2015). This assessment focused on multiple failure modes and results indicate that massive earthen berms or expensive sheet pile walls are needed for reinforcement. SHM can provide a way to improve reliability without reinforcement.

3.2. Pore pressure monitoring using standpipes

In Chapter 2 it is shown that the aquifer's hydraulic head is one of the most important factors in dike stability assessment as it directly influences soil shear stress and risk for geotechnical failure modes such as piping and slope instability. It also provides general understanding of groundwater flow and quantification of aquifer properties which are key in reliability assessment of dikes. This Section elaborates on the basic principles of hydraulic head monitoring. As this type of monitoring will be applied in this study special attention is given to involved measurement errors and ways to perform reliability updates.

Basic principle of pore pressure monitoring

Monitoring of the hydraulic head in an aquifer underlying a dike and blanket is well known practise (Melnikova et al., 2013; Parekh et al., 2016). In this thesis information on the hydraulic head is obtained through piezometer measurements. A piezometer is an observation well that is specially designed and constructed to measure the hydraulic head at a specific point. The working principle behind measuring the hydraulic head with a piezometer is that the height in the water column $h_{p,i}$ is a measure for the groundwater pressure at the location and depth z_i of the concerned piezometer and that by measuring the water level the head h_i can therefore be known. Figure 3.1 illustrates the basic principle of a piezometer. The elevation head z_i is the elevation of the measurement point with respect to reference datum. Piezometers have a certain screen length. Measured heads are therefore never point measurements, in practice the midpoint of the screen is usually used to define z_i.

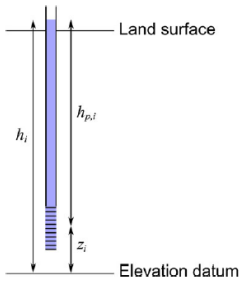

Figure 3.1: Schematic representation of a piezometer (Post and von Asmuth, 2013).

Measurement errors in pore pressure monitoring

In the reliability assessment of dikes reliable groundwater level measurements are fundamental. In this study the standpipe piezometer is used which is the most widespread type (Lancellotta, 2008). The discussion concerning measurement errors will therefore focus on standpipe piezometers. The measurement error is defined as the degree to which a measured value differs from the actual head value. Multiple factors contribute to this error and literature does not provide set in stone values. The accuracy and precision of a measuring device is often provided by manufacturers and can also be quantified. The precision of head measurements is already more difficult to quantify as operator skill and in field conditions fluctuate. Post and von Asmuth (2013) define four types of errors that will be adopted in this thesis: those due to (1) the measurement instrument, (2) conversion of pressure to water level, (3) time lag effects and (4) piezometer defects.

Errors related to the measurement instrument are listed by manufacturers and can in principle be quantified. In this thesis product specifications will be adopted from the TD-Diver (van Essen, 2016) which lists a

maximum deviation of 0.5 cm up until a piezometric height of 10 m. Water level measured in a piezometer expresses the pressure of groundwater at the measurement point ρ_i. The average density of water inside the piezometer is ρ_a. Strictly speaking the density of water varies over the depth meaning $\rho_i \neq \rho_a$, hence the measured water level shows some deviation from the actual pore water pressure. Such measurement errors become more evident for greater water depths. Another contributor to measurement errors are time lag effects. Time lag effects occur when water level inside a piezometer needs time to reach equilibrium with the prevailing groundwater pressure. Factors that influence time lag effects include transmissivity and storativity of the aquifer, volume of the observation well, screen length and local permeability of the subsoil strata. Hvorslev (1951) has shown that response times can be in the order of seconds or minutes for very permeable aquifers or hours to days for less permeable strata such as clay. Piezometer defects can occur from a variety of reasons. Potential reasons include the development of leaks, cracking or corrosion of the well screen (van der Kamp and Keller, 1993).

Literature does not provide concrete answers on how to incorporate measurement errors in modelling and its effects on reliability assessment. In this thesis working piezometers are assumed excluding (4) defect piezometers. Errors related to the measurement device (1) will be modelled as uncorrelated. Errors related to the conversion of pressure to water level (2) and time lag effects (3) will be modelled as correlated. Section 6.5 provides insight in how this is done.

Reliability updating using pore pressure monitoring

This Section will now show how hydraulic head data can be used to update probability. Bayesian techniques are used to obtain posterior probability, which is defined as prior probability plus new evidence, also referred to as likelihood. Schweckendiek (2010) showed how reassessing reliability can be done with single parameter updating and multiple parameter updating. It became clear that indirect reliability updating with numerical integration gives the same results as direct reliability updating with MCS. In this thesis direct reliability updating is used as it is easier to implement using standard reliability analysis methods such as MCS and FORM. In order to obtain posterior reliability Bayes' rule is applied:

$$P(F|\epsilon) = \frac{P(F \cap \epsilon)}{P(\epsilon)} \tag{3.1}$$

For the general principles underlying Bayesian updating one is referred to Section 2.1.

TAW (2004) presents techniques to process head monitoring data which can on its turn be used to perform reliability updates. The selected method assumes a stationary approach. An extrapolation approach is used to update the failure probability for piping. This approach seeks a relationship between top river water level and the corresponding piezometer head. This approach requires at least two high water levels of different height. However in practice more high water levels are desired as fitting a linear relationship on two high water levels is too simplified. Figure 3.2 shows the basic concept behind this theory.

Monitoring data will be generated for various high water levels. On the basis of deviations from a linear correlation an impression can be formed for deviations at other water levels. As was mentioned before a stationary approach is assumed, the element of time is therefore not accounted for. TAW (2004) argues that in such conditions a linear extrapolation approach seems justified. In many cases there appears to be a linear relationship between a hinterland monitoring well and river elevation. This linear relationship holds for both phreatic and artesian groundwater conditions. At the transition from phreatic to artesian groundwater the relationship is not linear, as depicted in Figure 3.2. Therefore, only water levels between ϕ_b and ϕ_c result in the desired linear relationship indicated by II, as shown in Figure 3.2. The relationship between river water level h and aquifer hydraulic head ϕ is mathematically shown by the following Equation:

$$\frac{\phi - \phi_0}{h - \phi_0} = \lambda \tag{3.2}$$

In which ϕ_0 is the hinterland phreatic level and λ a constant that describes the relationship. Theory discussed in Section 2.2 uses random variables and Equations 2.17, 2.18 and 2.19 to calculate aquifer hydraulic head. Linear extrapolation provides a method to use in-field piezometer measurements to find a direct relation between hydraulic river head and hinterland phreatic level. This relation can subsequently be used to perform

reliability updates.

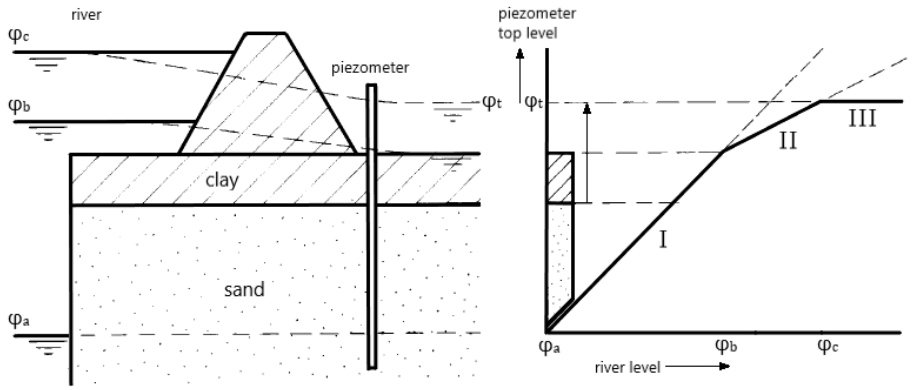

Figure 3.2: Linear extrapolation for phreatic and artesian conditions (TAW, 2004).

For uplift and heave the limit state equations are given by respectively Equations 2.20 and 2.22. The potential at the exit point behind the dike ϕ_{exit} is a direct input parameter for both limit state equations. Reliability updating is therefore straightforward. The limit state equation for piping is given by Equation 2.35. This equation does not have ϕ_{exit} as an input parameter. The difference in hydraulic head is rather expressed as the difference between river head and the summation of the hinterland phreatic level plus 0.3 times the depth of the aquitard. This limit state equation does therefore not provide a direct way to update failure probability. In order to be able to incorporate the in-field measurements the difference between the theoretical and actual hydraulic head ϕ_d is incorporated in the limit state equation:

$$Z_p = m_p H_c - (h - h_p - \phi_d - 0.3d) \tag{3.3}$$

In which the difference between in-field measurements ϕ_m and theoretical hydraulic potential ϕ_t is defined as:

$$\phi_d = \phi_t - \phi_m \tag{3.4}$$

Figure 3.3 shows ϕ_d in red. The measured difference can be regarded a reduction in load.

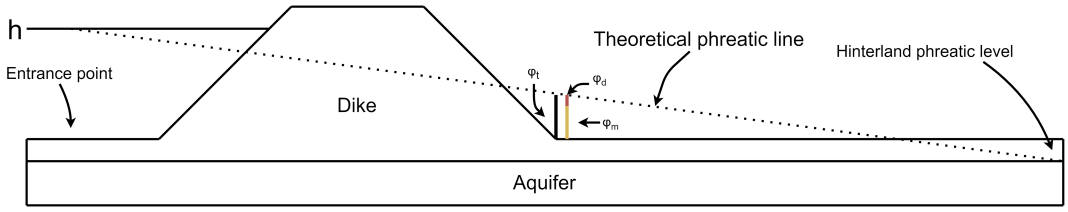

Figure 3.3: Illustration of the difference between theoretical hydraulic potential in black and measured hydraulic potential in yellow. Difference is indicated in red.

3.3. Alternative monitoring techniques

This Section will discuss alternative monitoring techniques. For the case study considered in this thesis aquifer head monitoring can be used to assess the dikes structural integrity for piping and slope instability. However that is not always the case. Therefore, this Section separates monitoring techniques relevant for piping and slope instability. A differentiation is also made for invasive and non-invasive techniques.

A vast amount of different monitoring methods exist. Aguilar-López and Bogaard (2014a) state that monitoring methods can be classified into two different types; non invasive and invasive. Non invasive monitoring consists of observing failure related variables that indicate a certain failure process. For piping observations of head difference and sand boils are common ways and for slope instability phenomena such as deformations or temperature can be measured. Invasive monitoring consists of observing the triggering variables that are directly related to the process that results in failure. For piping the aquifer hydraulic head is strongly related to the probability of failure and for slope instability the phreatic line in the dike body. The next Section provides a concise overview of invasive and non-invasive monitoring techniques, separated for piping and slope instability. A lot of techniques discussed here have been listed by Aguilar-López and Bogaard (2014a). The next Section will provide a concise overview of monitoring techniques after which they will be discussed in depth for the relevant failure modes.

Overview

This Section provides a concise overview of most relevant monitoring techniques for piping and slope instability. Figure 3.4 gives good understanding of the different scales in which monitoring can be applied.

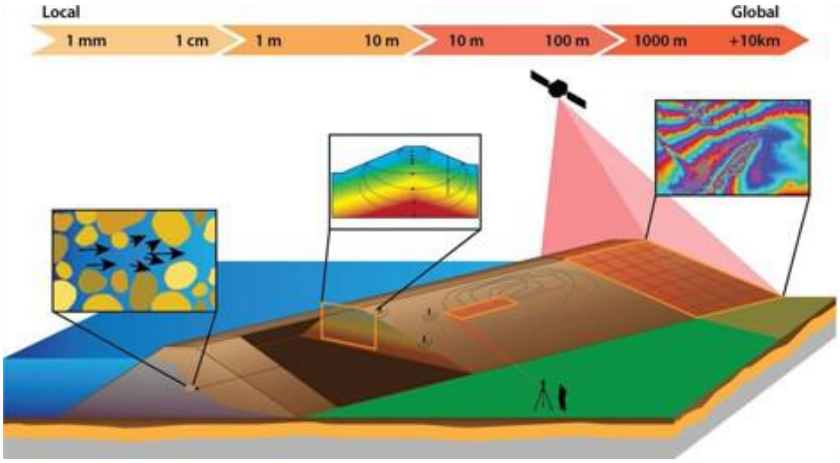

Figure 3.4: Overview of some monitoring techniques on different scales (van Vliet et al., 2011).

Table 3.1 provides an overview of available monitoring technologies. It shows for which failure mechanism they are relevant (piping or slope instability), whether the technology is invasive or not. Indications of the maximum measurement frequency and accuracy are given. It has to be said that these are indications: e.g., different types of piezometers have different accuracy's so these values might deviate. Finally a column has been added that shows the maturity of the technology, a measure to what extend a theory is proven and applied in the field.

Method of observation	Measured parameter	Failure mechanism -Piping (P) -Slope Stability (S)	Invasive (I) / Non invasive (NI)	Maximum frequency of measurements	Accuracy of measurements	Maturity
Visual inspection	Deformations, surface irregularities	P, S	NI	1 / 1 day	-	++
Infrared thermography	Temperature	P	NI	1 / 1 sec.	1 mm.	-
Piezometer	Pore pressure	P, S	I	1 / 1 sec.	10 cm.	++
Optic fibre cable	Deformation, temperature, water pressure	P, S	I	1 / 10 sec.	Strain: 1.5 % Temp: -40 - 60 C	+
Electrical resistivity	Electrical resistivity	P	I	1 / 1 min.	<1 %	-
Acoustic sensing	Sound	P, S	I / NI	1 / 1 sec.	1 - 50.000 Hertz	- -
Radar interferometry	Deformation	S	NI	1 / 2 weeks	0.10 m.	+
Airborne Laser (SAR, LiDAR)	Deformation	S	NI	1 / 2 weeks	0.15 - 0.30 m.	++
Ground penatrating radar	Deformation	S	NI	1 / 2 weeks	0.1 mm.	++
Inclinometer	Deformation	S	I	1 / 10 sec.	1.5 %	+
Tilt sensor	Deformation	S	I	1 / 1 sec.	1.5 %	+
Subsidence marker	Deformation	S	I	1 / 1 min.	1 mm.	+
Self potential	Electrical load	P	NI	1 / 1 min.	<1 %	-
Extensometer	Deformation	S	I	1 / 1 sec.	1 mm.	+
Satellite	Deformation, temperature, moisture content	P, S	NI	1 / 2 weeks	0.15 - 0.30 m.	-

Table 3.1: Dike monitoring methods

Piping

Piping was briefly elaborated in Section 2.2. Multiple methods exist to monitor parameters that indicate piping. A general separation is made between non invasive and invasive monitoring techniques. Piping is mainly driven by the hydraulic gradient in the aquifer, which is a direct result from hydraulic head difference between the river and hinterland phreatic level. The hydraulic gradient is the main trigger for piping, monitoring should therefore preferably be focused on obtaining information on the hydraulic gradient in the top layer of the aquifer.

The first and worldwide most commonly used form of monitoring is visual inspection. Many of the anomalies that can affect a dike's structural integrity are revealed by indicators at the surface (Mériaux and Royet, 2007). For piping such indicators can be sand boils, gully erosion or animal burrows. A relevant overview of the phenomena that can be monitored through visual inspection is given in (Bakkenist et al., 2012). Visual inspection is a powerful and widely used method. However, it does not allow to identify the triggering phenomena of geotechnical failure modes. The method is therefore considered to be reactive instead of pro active. Infrared thermography provides another non invasive monitoring technique. Infrared thermographic cameras detect infrared energy emitted from an object and convert it to temperature. Temperature is a parameter that can be used as an indicator for piping. In (Bersan and Koelewijn, 2015) an infrared camera was used to map the surface temperature of the downstream toe of the dike. At the exit points of flow a temperature drop of 3° compared to the surrounding region was registered.

Invasive monitoring techniques consist of measuring the triggering variables that are directly related to physical processes that result in failure. Those indicators are not visible from the outside. In situ sensors can fill that gap. Piezometers are the most used in-situ sensors used in hydraulic head monitoring (Lancellotta, 2008). As they have been discussed extensively in Section 3.2 they will not be discussed here. Other ways to measure aquifer pressure include micro electro mechanical sensors (MEMS). In the FloodControl-IJkdijk research project (de Vries et al., 2010) so called Geobeads were installed. Geobeads among other sensors contain MEMS that are able to measure pressure Weijers et al. (2009). In (Bersan and Koelewijn, 2015; Bersan et al., 2015) optic fibre cables were used to measure the pressure. Results showed that for pipe formation pressure drop was around 10% of the initial pressure. However the radius of influence was less than 1 m, making this method economically unattractive. Ikard et al. (2015) investigated seepage beneath an earthen dam using electrical resistivity. Results are promising, however application is expensive and a permanent setup is therefore unattractive to apply in a dike reinforcement design. Lu and Wilson (2012) and Planès et al.

(2016) applied acoustic sensing to measure water flow inside the aquifer. Significant changes with respect to the sound indicate piping and sound transducers and geophones were used as sensors. Nevertheless these techniques measure momentum and can therefore only be applied in sections critical to piping during critical conditions.

Slope instability

Slope instability is briefly elaborated in Section 2.3. Multiple methods exist to monitor multiple slope instability indicating parameters. Again a general separation is made between non-invasive and invasive techniques. Slope instability is mainly triggered by the position of the phreatic line in the dike body. The position of the phreatic line largely influences shear strength and volumetric weight of a dike, and by that its structural integrity. Monitoring should therefore preferably be focused on obtaining information on the phreatic line. The ideal approach would be one in which effective stresses inside the dike core are monitored.

Like for piping, visual inspection also is a widely used tool to look for surface indicators of slope instability (Mériaux and Royet, 2007). Surface indicators include soil displacement or cracks. An overview of relevant phenomena is given in (Bakkenist et al., 2012). Another non invasive monitoring technique that is commonly used is remote sensing. Remote sensing refers to monitoring based on obtaining information through electromagnetic radiation. In a way, during visual inspection, the eyes of a person inspecting the levee can be regarded as the sensor. With regards to dike monitoring there are five main remote sensing technologies. The first four are all related to monitoring deformations of the ground. Synthetic aperture radar (SAR), light detection and ranging (LIDAR) and Laser measurements are used to assess geometrical characteristics of a dike such as elevation, crown width and slopes. Multiple studies have indicated the practical applicability of Lidar (Casas et al., 2012; Choung, 2015; Bishop et al., 2003; Haarbrink and Shutko, 2008) and SAR (Jones et al., 2011, 2012; Bakkenist and Zomer, 2010). Based on the measured parameters (deformations in soil) various stability calculations can be executed to assess a dikes safety. Airborne/satellite radar interferometry is a method in which two images acquired from a slightly different position are compared to produce a three-dimensional image. A recent study conducted by Özer et al. (2019) shows the ability to detect dike deformation using satellite radar interferometry. Apart from that study much literature is available supporting this idea (Closson et al., 2003; Hanssen and Van Leijen, 2008). Ground radar is a widely used tool for SHM. Monserrat et al. (2014) highlights the effectiveness of ground based radar for measuring deformations in dikes. In Rödelsperger and Meta (2014) a ground radar sensor system is presented that is based on technologies that have already been applied in airborne SAR applications. The system is able to detect deformations of a slope or infrastructure from distances up to 4 km. Infra red monitoring enables the possibility to monitor soil moisture. Soil moisture is an indicator of slope instability. Multiple studies show promising results (Cundill et al., 2014; Hsu and Chang, 2019).

As was briefly mentioned above invasive monitoring considers measuring the triggering variables that are directly related to physical processes that result in failure. Most of the time such indicators can be measured inside the dike. In (Dahlin et al., 2008) and (Rings et al., 2008) the electrical resistivity was measured by measuring a large number of electrical potential differences for different combinations of borehole electrodes. Results showed that, given that calibration is executed, measurements can be translated to soil water content. However a setup is expensive to apply and maintain and is therefore economically unattractive for a dike reinforcement design. In (Bersan and Koelewijn, 2015) and (Schenato et al., 2017) studies were conducted in which among other things distributed strain sensors made of optic fibre cables were deployed. Nöther et al. (2008) investigated critical soil displacement in river embankments by using strain based optical fibres. The fibres were embedded in coating cables in a geotextile and measured strain when a soil displacement caused stress in the geotextile. Weijers et al. (2009) showed that MEMS such as inclinometers can be used to detect deformations in soil masses with very high accuracy. However it has to be mentioned that optical fibres have a major advantage over electrical sensors as they have a much higher spatial resolution. In (Lin and Tang, 2005) monitoring of the slope was executed with a time domain reflectometry (TDR) extensometer. The extensometer measures displacements in the soil with an accuracy of 0.5 mm. Moreover the TDR system described in (Lin and Tang, 2005) is also capable of measuring the pore pressure inside the dike body and therefore gives direct information of the phreatic line.

3.4. Concluding remarks

The desired monitoring method is one that measures the triggering variables for piping and slope instability. For piping hydraulic head in the top layer of the aquifer is the main trigger. For slope instability this is the phreatic line inside the dike body. However hydraulic head in the top layer of the aquifer can result in uplift conditions limiting shear stress between the dike body and aquifer. In that case hydraulic head in the aquifer also influences slope instability. As will be shown in Chapter 5 this is relevant for the considered case study. Head monitoring of the top aquifer layer therefore provides one method that can be used to monitor the triggering variables for piping and slope instability. In Chapter 7 it will be shown that pressure relief wells will be installed as a way of reinforcement. Piezometers can be used to (re-)assess a dikes structural integrity prior to reinforcement and act as a safeguard after.

4

Considered techniques for dike reinforcement

Dike reinforcement is used to increase reliability of dikes. Section 4.1 starts with a general introduction into dike reinforcement after which Section 4.2 discusses pressure relief wells in detail. Subsequently Section 4.3 elaborates on more traditional reinforcement techniques that are used for comparison in this thesis. Section 4.4 provides a conclusion to this Chapter.

4.1. Reinforcement in general

Dike reinforcement refers to measures that are taken to strengthen a dike. New insights or increasing loads can result in dikes being rejected during safety checks, hence reinforcement is required. Dikes fulfil more functions than flood protection alone, Jonkman et al. (2018a) lists some: living and working, traffic routes, agricultural functions, and landscape / cultural. Such values need to be included when one decides on dike reinforcement. Traditionally dike reinforcement goes hand in hand with dike heightening and widening. However in some areas such measures can have large societal impact as houses need to be demolished and people need to relocate. This thesis investigates whether, in addition to head monitoring, pressure relief wells can be used as a cheaper and more environmentally friendly reinforcement measure compared to more traditional measures such as berms and sheet pile walls. Figure 4.1 shows general classification that can be made for reinforcement types. For the type separation can be made between renovation and renewal. Renewal type changes the structural behavior, renovation maintains the general structure and increases dimensions. For the extent distinction is made between full and partial. Full refers to measures that impact all relevant failure modes and partial refers to measures that impact only one relevant failure mode. In this thesis relief wells change behavior of the system by lowering hydraulic head impacting reliability against piping and slope instability. Section 4.2 will extensively elaborate on pressure relief wells. Section 4.3 elaborates on some traditional measures relevant for piping and slope stability that will be used for comparison.

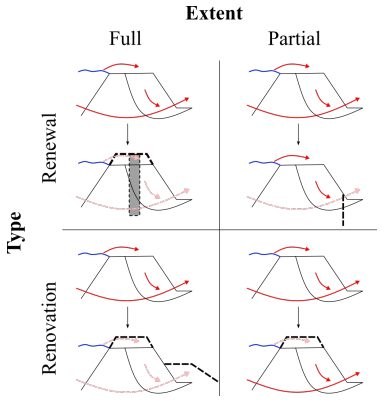

Figure 4.1: Categorization of reinforcement measures (Klerk et al., 2021).

4.2. Pressure relief wells

Pressure relief wells as discussed in this thesis refer to vertically installed wells consisting of a well screen and surrounded by filter material to prevent in wash of material. A general seperation is made between active and passive relief wells. Active wells refer to wells with hydraulic pumps, passive wells rely on artesian groundwater pressure. This thesis focuses into passive relief wells. With respect to Figure 4.1 relief wells can be regarded as a renewal type of reinforcement as it changes pore pressure and therefore the structural behavior of the system. The basic principles are discussed in Section 4.2. Some remarks on design methods for pressure relief wells are provided in Section 4.2. Finally Section 4.2 discusses other relevant background theory considering maintenance and well efficiency.

Basic principle

As was briefly mentioned in Section 4.2 this thesis focuses on passive relief wells. Passive relief wells are drilled through an impermeable clay layer into a permeable confined aquifer and their functionality is based on artesian flow. Aquifer groundwater pressure has to exceed atmospheric pressure for flow to occur. Relief wells allow confined groundwater to reach the free surface, relieving the aquifer from excess pore water pressure. As was briefly mentioned in Sections 2.2 and 2.3 this can have a positive effect on the reliability estimate for piping and slope instability. Mansur et al. (2000) have shown that relief wells can be an effective measure in controlling underseepage beneath dikes and by that limit the risk for piping. In more recent dike reinforcement projects relief wells were successfully implemented to lower the risk for slope instability (Langhorst and Bouwens, 2015). Relief wells provide a flexible control measure as the systems can be easily expanded if the initial system is not adequate. Pumping capacity can be increased by installing more wells or pumps when required. Figure 4.2 shows the basic principle for a relief well. Apart from dikes relief wells have also been used extensively in for example outlet structures or beneath stilling basins of spillways (USACE, 1992).

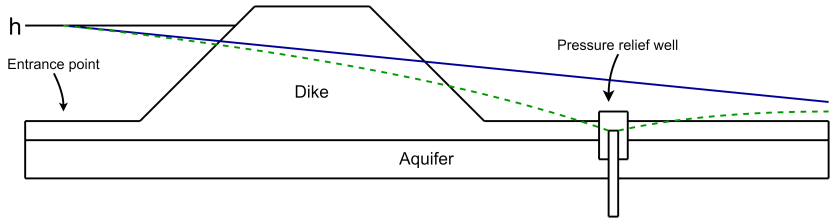

Figure 4.2: Schematic representation of the functioning of a pressure relief well. Blue line indicates aquifer pore pressure without a relief well. Dashed green line indicates aquifer pore pressure with a relief well.

Design methods

Relief wells have been used since the late 1700s for agricultural and construction dewatering (Johnstone, 1797; Terzaghi, 1927). Since the late 1930s the U.S. Army Corps of Engineers (USACE) has performed research and used relief wells for flood protection seepage control (USACE, 1939). Muskat (1937) was among the first to evaluate head distribution and flows for fully penetrated infinite well lines and started discussion on calculating flows for partially penetrating wells. Relief wells can be installed either fully or partially penetrated. Full penetration refers to the case when the well reaches the aquifer bottom layer, for partial penetration it does not. In the case of partially penetrated wells a smaller flow discharge is moving in, hence reducing the wells efficiency. Bennett and Barron (1957) were among the first to present design data for partially penetrating wells. Well discharge and drawdown expressions for partially penetrated wells were developed by Sharma (1974). Based, among other things, on these articles the USACE developed a design, construction and maintenance manual for pressure relief wells (USACE, 1992). Design rules are obtained for the maximum allowable head in between wells and assume homogeneous soil conditions. Furthermore wells are equally spaced and flow direction is assumed perpendicular to its line source. Distinction is made between a single relief well system and a multiple relief well system such as in Mansur et al. (2000). A single well system refers to the case when only one relief well is addressed. A multiple well system refers to a system of wells that are installed to ensure that groundwater level stays at an allowable level. This thesis focuses on a multiple well system. Miranda Eguez (2014) shows how the USACE method can be used to probabilistically design a relief well system. However, this thesis explores the possibility of using random field modelling in a design approach. The USACE method is found to be unsuitable for that purpose.

Well efficiency

Relief wells do require, like other engineering structures, a certain amount of maintenance to ensure their continued and proper functioning. This Section will not elaborate on maintenance measures to be taken, but more on consequences and expected head drops over time as a result of limited efficiency. It is not uncommon that the efficiency of relief wells reduces in time. Various reasons can be attributed to reduced efficiency. Design errors are often quickly noticed once relief wells are in operation and will therefore not be discussed here. Based on piezometric and flow data a well system's efficiency can be assessed once in operation. If it's functioning is considered inadequate measures can be taken. USACE (1992) identifies three major causes for reduced specific capacity with time including (a) mechanical, (b) chemical and (c) biological issues.

Mechanical issues often refer to some loss in specific flow capacity due to intrusion of foundation fines into the well's filter pack. This process is more common in case of poorly designed filter packs or improper screen placement. Other causes of clogging include backflooding of muddy surface water, which can again be attributed to poor design. Chemical filter and well screen incrustation can be a major factor in specific capacity reduction over time. Deposits can form on screen openings and significantly reduce the well's effective open area, hence reduce the well's efficiency. USACE (1992) states that the biggest forms of chemical incrustation include (a) incrustation from calcium and magnesium carbonates and (b) incrustation from iron and manganese compounds. Like with chemical incrustation it is also possible to have biological incrustation. Bacteria consist of organisms that have the ability to assimilate dissolved minerals which they can oxidize or reduce to ions. These ions can be precipitated in areas like the well opening, hence reduce the well's efficiency. This thesis will not go deeper into issues that reduce the efficiency of wells. However some conclusions need to be drawn related to head drop for design purposes later on. To that end a calculation example is provided to derive a value for head loss. USACE (1992) gives for total head loss in a well:

$$H_w = H_e + H_f + H_v \tag{4.1}$$

With H_e being entrance head loss in screen and filter, H_f friction head loss arising from flow in the pipe and H_v velocity head loss. In order to get some feeling for head loss in the filter the iterative design method proposed by USACE (1992) is used to determine flow through the well. For more info on the method or parameters one is referred to Appendix B. For this example parameters are chosen as such that they closely resemble the situation as addressed in the case study. Input parameters for the calculation are depicted in Table 4.1.

Parameter	h_a [m]	H [m]	S [m]	x_3 [m]	a [m]	k_f [m/s]	D [m]	W [m]	d [m]	C [-]	g [m/s^2]
Value	5.3	9.0	59	74	20	8E-4	37	10	0.2	100	9.81

Table 4.1: Input values iterative relief well design.

In which h_a resembles allowable head in between wells, H river head, S the distance of effective seepage entry to exit point, x_3 the distance of exit point to sink, a initial guess for well spacing, k_f aquifer conductivity, D thickness aquifer, W well penetration depth, d well diameter, C Hazen-Williams drag coefficient and g gravitational constant. Figure B.1 provides more insight into these parameters. Results show that the maximum flow through one well equals 0.044 m^3/s. Now USACE (1992) proposes empirical relations for entrance and filter head losses. The graphs are depicted in Appendix C. Results show that the expected filter and screen entrance head losses equal approximately 30 cm. Appendix D provides a more systematic approach to calculate total head loss. Appendix D shows how the Kozeny-Carman equation can be used to calculate pressure drop of flow through a filter. Miranda Eguez (2014) has shown that filter losses account for most of the head loss. Therefore two scenarios are picked for the input values. One realistic and one conservative. Input parameters are shown in Table 4.2 including kinematic viscosity of the fluid μ, gravitational constant g, porosity of the filter p, superficial flow velocity v, diameter of the filter material d_h and filter length L.

Parameter	μ [m^2/s]	g [m/s^2]	p [-]	v [m/s]	d_h [mm]	L [m]
Realistic	1.004E-6	9.81	0.40	7E-3	5	0.2
Conservative	1.004E-6	9.81	0.25	7E-3	2	0.2

Table 4.2: Input values Kozeny-Carman equation.

Results give an entrance head loss in screen and filter H_e = 0.029 m for the first scenario and H_e = 0.23 m for the second scenario. Section D gives two equations for calculating friction head loss: Darcy-Weisbach and Hazen-Williams. The advantage of Hazen-Williams is that friction coefficient C is not a function of the Reynolds number. This calculation serves for illustrative purposes, therefore Hazen-Williams is the preferred method. A calculation is performed with the following input values for flow Q, roughness coefficient C and pipe diameter d:

Parameter	Q [m^3/s]	C [-]	d [m]
Value	0.044	150	0.2

Table 4.3: Input values Hazen-Williams equation.

Results now give a friction head loss H_f of 0.008 m. The velocity head loss is calculated according to the equation expressed in Section D. Input values for the example calculation include velocity v for which a value of 1.4 m/s is taken. The result gives a head loss of 0.10 m. Equation 4.1 is now used to calculate total head loss. For the realistic scenario this equals 0.13 m and for the conservative scenario 0.33 m. Results obtained for filter and screen head loss calculation assumed no clogging. Miranda Eguez (2014) has shown that filter head losses of 0.5 m are not uncommon practise, especially in a well's later life cycle stage. The calculation has provided us with some feeling for order of magnitude. The goal of this thesis is not to thoroughly investigate the nature of the error but merely to investigate possible benefits of pressure relief wells. Therefore in this thesis a head drop of 0.5 m will be adopted to account for all head losses in the well.

4.3. Alternative reinforcement techniques

This Section elaborates on some other reinforcement techniques relevant for piping and slope stability: piping / stability berm and retaining wall. It has to be noted that more alternative reinforcement methods are available. However the aim of this thesis is to investigate whether pressure relief wells can be a viable way of reinforcement and compare it with standard reinforcement methods.

Piping / stability berm

Berms can be constructed on land and on water side. In this Section we refer to land side berms. A berm constructed at the hinterland toe of the dike decreases the overall slope angle of a dike. Relating back to Section 2.3 this increases the soil mass on the passive side of the slip plane, hence reduce the risk for slope instability. With respect to piping, a berm increases the length of the seepage path. Relating this back to Section 2.2 the seepage length is an important factor in assessing piping safety as it influences the average hydraulic gradient over the dike, which on its turn is the driving force for seepage. A hinterland berm can thus be used to increase a dike's reliability estimate with respect to piping and slope instability, making it a feasible mitigation measure. Compared to other design alternatives a hinterland berm is relatively cheap. However in urban areas space might be limited. Conventional designs with berms might then turn out to be very expensive as people need to move from there homes. Figure 4.3 shows how berm construction increases seepage length for dikes.

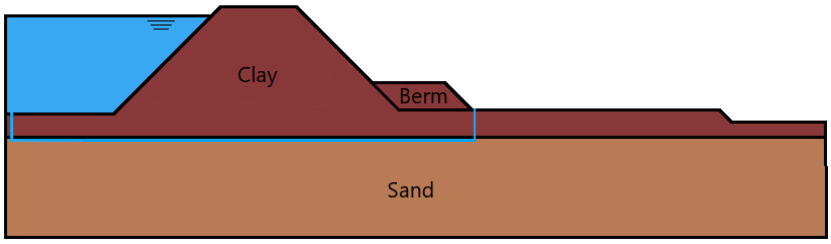

Figure 4.3: Construction of a hinterland berm to increase seepage length.

Self-retaining structures

Other design measures that have proven to be very effective against piping and slope instability are self-retaining structures. Self-retaining structures are multi functional as they block seepage paths and the same time provide a soil retaining function. Diaphragm can be installed in the crest of the dike keeping the phreatic level in the hinterland part of the dike low. However in such cases walls need to be long. Sheet pile walls can also be installed more towards the hinterland toe, maximizing the soil-retaining effect as the walls cut through the potential sliding plane as discussed in Section 2.3. Sheet pile walls are often anchored with soil anchors to maximize its soil retaining function. In urban areas where space is limited such design options might turn out to be the desired reinforcement measure. This thesis focuses on sheet pile walls. Such walls can be preferred over stability berms as relocating houses is often more expansive, not to mention societal impact. Figure 4.4 shows how a sheet pile wall increases seepage length.

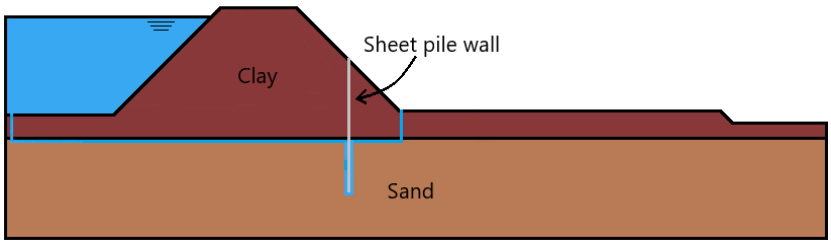

Figure 4.4: Construction of a sheet pile wall to increase seepage length.

4.4. Concluding remarks

The desired reinforcement measure is one that limits the risk for piping and at the same time slope instability. Sheet pile walls and berms have proven to be such measures. As was discussed in this Chapter relief wells can also provide that function, albeit in situations where aquifer uplift pressures significantly impact reliability against slope instability. As will be shown in Chapter 5 this is the case for the considered case study. Pressure relief wells can therefore provide one method that can be used to increase reliability against piping and slope instability. For dikes located in urban areas relief wells have as advantage that the measure is considered low-impact. Chapter 5 will provide an introduction to the case study and a preliminary analysis for the considered dike section.

II

Case study

5

Introduction to the case study

This Chapter provides an introduction into the case study that will be performed to assess the benefits of pore pressure monitoring and pressure relief wells. Section 5.1 provides an overview of the case study, including the preliminary analysis conducted in this Chapter. Section 5.2 will provide more information on the study site. In Section 5.3 the target probability of failure is determined for the dike trajectories after which preliminary analyses for piping and slope instability are conducted in respectively Sections 5.4 and 5.5. The Chapter ends with some concluding remarks and information on follow-up study in the coming Chapters.

5.1. Approach and methodology

This study focuses on pore pressure monitoring at the hinterland toe of the dike in combination with pressure relief well installation. A case study will be performed to assess whether this is a feasible approach and whether it is economically attractive compared to more traditional reinforcement measures such as berm construction and sheet pile wall installation. Figure 5.1 provides a flowchart that covers the case study. Colours indicate in which Chapter the concerned step is discussed.

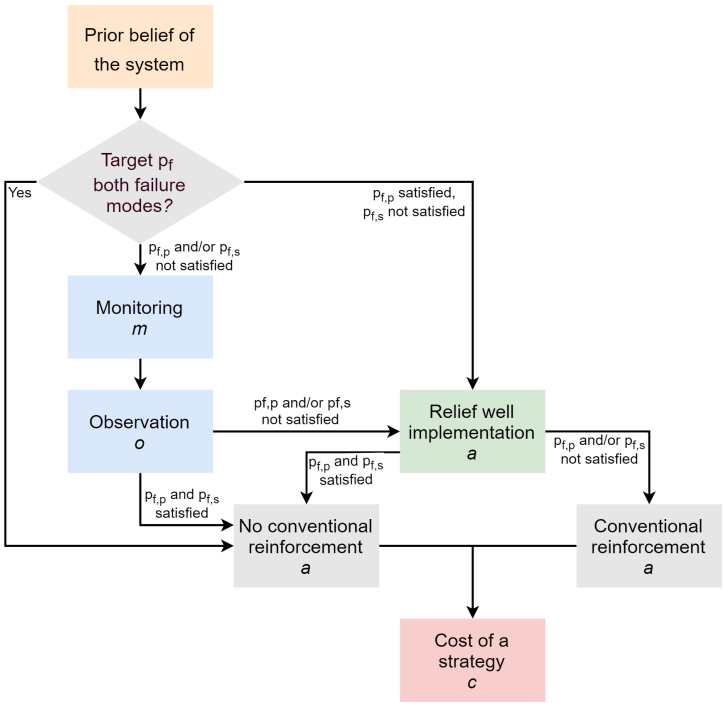

Figure 5.1: Overview of the decision model used in the case study. Colours indicate in which Chapter the considered step is discussed: orange, blue, green and red are discussed in respectively Chapters 5, 6, 7 and 8. $p_{f,p}$ and $p_{f,s}$ refer to failure probability for respectively piping and slope instability.

The case study is made up of four different phases as was highlighted in Figure 5.1. Figure 5.2 provides a clear overview that will be used throughout this thesis. Again the colours orange, blue, green and red indicate in which Chapter the relevant matter is discussed.

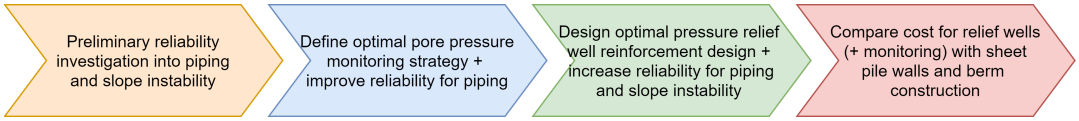

Figure 5.2: Overview of the various phases in the case study. Colours indicate in which Chapter the considered phase is discussed: orange, blue, green and red are discussed in respectively Chapters 5, 6, 7 and 8.

The first step highlighted in the case study's methodology as shown in Figure 5.1 is prior belief of the system. As was briefly mentioned in the introduction this thesis focuses on geotechnical failure modes piping and slope instability. In Section 5.3 the target probability of failure will be determined for the considered failure modes using methods prescribed in Rijkswaterstaat (2019). A preliminary analysis will be conducted for the considered failure modes piping and slope instability in respectively Sections 5.4 and 5.5. For piping a semi-probabilistic analysis is conducted with LSE's for uplift, heave and piping as was briefly elaborated in Section 2.2. The LSE for piping is based on the revised Sellmeijer model. Subsequently a probabilistic analysis will be executed to evaluate possible new insights using the same models. The analysis for slope-instability is executed through D-GEO Suite Stability with LEM Uplift-Van. For more information on the model one is referred to Section 2.3.

In Chapter 6 an approach is given for defining an optimal pore pressure monitoring strategy. This Chapter is highlighted in Figure 5.1 by the blue boxes. The approach is limited to measuring hydraulic potential at the hinterland toe of the dike and considers optimal spacing in longitudinal direction. First, a principal component analysis (PCA) is executed to evaluate the least amount of pore pressure sensors required for observing all variation in hydraulic head. The outcome will be implemented in a finite difference model that is used to compute groundwater flow through random fields that represent spatially varying soil. For every model run equally spaced pore pressure sensors are assumed. Subsequently it will be analysed how much of the variation is observed by the pore pressure sensors. The amount of pore pressure sensors are increased until the measured variation is considered sufficient for predicting hydraulic potential behind the dike. This prediction will then be implemented in the previously discussed probabilistic model for piping and used to update failure probability for the piping failure mechanism. It has to be noted that, because of the implementation of random fields, the length-effect is included in this prediction for hydraulic potential behind the dike. The derived failure probability is therefore compared with the target failure probability for a cross-section.

Chapter 7 elaborates on implementing pressure relief wells as a way to limit hydraulic potential behind the dike. This step is highlighted in green in Figure 5.1. The same groundwater flow model in combination with random fields is used, only now including the implemented relief wells. A script is written that evaluates most critical regions in the model and the corresponding phreatic lines are implemented in D-GEO Suite Stability to assess probability of failure for slope instability. This process will be repeated for various set-ups of pressure relief wells and it will subsequently be analysed if the target reliability for slope instability is met. The probability of failure after reinforcement will be determined with the same method as was done in previous Chapters using probabilistic calculations.

In Chapter 8 it will be analysed whether implementation of pore pressure monitoring in combination with pressure relief wells is a cost effective method in assuring that the dike's safety criteria are met. To that end total cost and value of information will be compared with more traditional reinforcement measures berm construction and sheet pile wall installation. Table 5.1 summarizes the main methods and theories applied in this case-study.

Chapter	Section	Topic	Applied model
Chapter 5	5.2, 5.3	Define target probability of failure	- Model runs with Riskeer and HydraRing
	5.4	Define probability of failure for piping	- Semi-probabilistic calculations using LSE's as given in Section 2.2 - Probabilistic calculations using LSE's as given in Section 2.2
	5.5	Define probability of failure for slope instability	- Semi-probabilistic calculations using Uplift-Van in D-GEO-Suite Stability
Chapter 6	6.2, 6.4 - 6.6	Define hydraulic pore pressure monitoring strategy	- PCA in combination with MODFLOW modelling in random fields
	6.7	Update probability of failure	- Probabilistic calculations using LSE's as given in Section 2.2
Chapter 7	7.2	Define configuration for pressure relief wells	- MODFLOW modelling in random fields
	7.4, 7.5	Define configuration for pressure relief wells	- Semi-probabilistic calculations using Uplift-Van in D-GEO-Suite Stability
	7.7	Increase probability of failure after implementation of pressure relief wells	- Probabilistic calculations using LSE's as given in Section 2.2

Table 5.1: All hydraulic and geotechnical models used in this thesis.

5.2. Description of the study site

The case study considers a section on the trajectory Wijk bij Duurstede - Amerongen (WAM), formally known as trajectory 44-1. The dike contemplates a typical Dutch river dike as the dike consists of (Holocene) clay, situated on (Holocene) clay and sand layers on top of a (Pleistocene) sand layer. Figure 5.4 provides a simplified representation of the dike with some dimensions. The dimensions as given are realistic, however not to scale. For the semi-probabilistic analysis hydraulic load conditions are obtained from Riskeer. For an acceptable failure probability of 1/30.000 per year this equals 9.02 m + NAP. For probabilistic piping analysis HydraRing, a separate calculation kernel from Riskeer, is used to derive hydraulic load conditions. A probability density function was fitted to the higher range of failure probabilities. Appendix E provides elaboration on this matter.

It was shown by Sweco and Arcadis (2019) that the dike is disqualified for geotechnical failure modes piping and slope instability. Acceptable failure probabilities for this trajectory are obtained from Riskeer (Deltares, 2019), a software that is used for probabilistic safety analysis of primary flood defences in the Netherlands. The upper limit of the acceptable failure probability equals 1/10.000 per year. The lower limit equals 1/30.000 per year. During design it is aimed to obtain a failure probability equal to the lower limit. The considered dike section is located near dike pole 86, which is right in front of the city Wijk bij Duurstede. Figure 5.3 shows the situation with the considered dike section outlined in red. The geographical location hampers the opportunity for hinterland expansion. The dike is enclosed by an inlet on one side and a harbour on the other side.

Figure 5.3: Aerial photo of the considered dike section for the case study. The dike section is outlined in red, there is no room for hinterland expansion of the dike. Photo by Maarten van de Biezen.

Two trajectories

The considered cross section as depicted in Figure 5.4 represents a cross section of 100 m. One of the objectives in this thesis is to explore the possibility of random field modelling as a way to incorporate the length-effect. Correlation lengths in soil are in the range of 300 m. For a trajectory of 100 m, differences in soil conductivity conditions will be small, hence there will be minor variation in hydraulic potential behind the dike. The case study will therefore be split into two case studies. The first study concerns the trajectory as is and the second study concerns the same cross section only now extrapolated over a length of 2 km. In that way the effect of varying soil conditions will become more clear. When, in this thesis, reference is made to case study 1, trajectory 1 or 100 m trajectory this all means the same. Logically this also holds for case study 2, trajectory 2 or 2 km trajectory.

5.3. Target probability of failure

Prior to the (semi-) probabilistic analyses for piping and slope instability a target probability of failure is determined that is used for analyses. As was briefly mentioned in the introduction dike reliability needs to be increased. The upper and lower limit of the acceptable failure probability equal respectively 1/10.000 and 1/30.000 per year. During design it is aimed to obtain a target failure probability equal to or smaller than the lower limit: 1/30.000 per year. The acceptable probability of failure is used to derive a target probability of failure P_f and a target reliability index β_r according to:

$$N_j = 1 + \frac{a_j * L}{b_j} \tag{5.1}$$

$$P_f = \frac{P_{r,j} \cdot w_j}{N_j} \tag{5.2}$$

$$\beta_{r,j} = -\phi^{-1}(P_f) \tag{5.3}$$

In which a_j and b_j are failure mechanism specific parameters, L the length of the trajectory, N_j resembles the length effect factor, $P_{r,j}$ the required probability of failure obtained from Riskeer, w_j a parameter that defines the maximum contribution of a failure mechanism to the system failure probability, P_f the target probability of failure and $\beta_{r,j}$ the target reliability index. Values for a_j and b_j are obtained from Rijkswaterstaat (2019) and equal resptively 0.9 and 300 for piping and 0.033 and 50 for slope instability. A more extensive elaboration on this method is given in Appendix A.

It was mentioned in Section 5.2 that this case study considers two dike trajectories. The first being the situation as is at Wijk bij Duurstede and the second being the same situation only now extrapolated over a length of 2 km. The two case studies do not have the same probability of failure as the first considers a section of 100 m and the second a section of 2 km. Equations 5.1, 5.2 and 5.3 are used to derive target probabilities of failure and reliability indices. Results are also derived for acceptable cross-sectional probability of failure as for most calculations in this thesis the length-effect will be incorporated in random field modelling rather than through a length-effect factor. Results are shown in Tables 5.2 and 5.3.

	Piping erosion	Slope instability
Cross-section	8.00E-6	1.33E-6
Dike trajectory 100 m	6.15E-6	1.25E-6
Dike trajectory 2000 m	1.14E-6	5.75E-7

Table 5.2: Acceptable probability of failure $P_{f,j}$ for piping and slope instability.

	Piping erosion	Slope instability
Cross-section	4.31	4.69
Dike trajectory 100 m	4.37	4.71
Dike trajectory 2000 m	4.73	4.86

Table 5.3: Target reliability index $\beta_{r,j}$ for piping and slope instability.

5.4. Preliminary reliability investigation on piping

As was briefly mentioned before studies have indicated that the dike is disqualified for piping and slope instability. This Section provides a conventional semi-probabilistic analysis as well as a probabilistic analysis. This Section first elaborates on the parameters that are used for the semi-probabilistic and probabilistic analyses. The results of the analyses are provided thereafter.

Parameters

For the location of the exit point two scenarios have been created. The first scenario assumes an exit point at the hinterland toe of the dike and the second scenario assumes an exit point at the location where the aquitard is thinnest. Figure 5.4 shows the exit points for both scenarios.

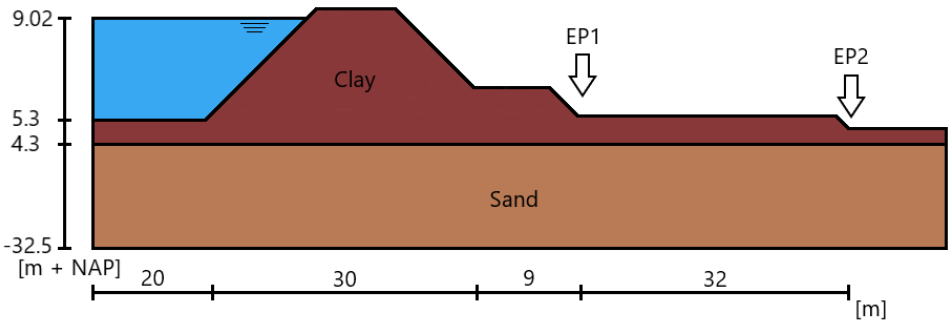

Figure 5.4: Simplified cross section of the considered dike for the case study. EP1 and EP2 indicate two exit points that are considered for piping failure.

For each of the two scenarios the probability of failure for uplift, heave and piping has been calculated. The biggest probability of failure is assumed to be normative. For scenario 1 the exit point is assumed to be equal to half the width of the dike plus the length of the berm. For scenario 2 the exit point is assumed to be located far in the hinterland where the berm width is thinnest, 1 m respectively. The width of the dike is assumed to be deterministic. Uncertainty in seepage length is accounted for in the effective length of the foreshore and the width of the berm, which are modelled as stochastic variables.

The considered cross section has a foreshore clay layer that is smaller than 1.5m, but bigger than 0.5m everywhere. It should therefore be taken into consideration for determining intrusion length (Rijkswaterstaat, 2019). The length of the effective foreshore is determined according to (TAW, 2004):

$$\lambda = \sqrt{kDc} \tag{5.4}$$

$$c = \frac{d}{k_v} \tag{5.5}$$

In which kD equals 800 m^2/day and k_v equals 1 m/day (Sweco and Arcadis, 2019). For the thickness of the clay layer d a value of 0.5m is chosen since this is the minimal thickness that is present everywhere. Now using Equations 5.4 and 5.5 this results in λ = 20 m.

The WBI default value for d_{70} for the holocene sand layer (formation from Echteld) is equal to 250 μm, with a coefficient of variation equal to 0.12. The hydraulic head in the river with an exceedance probability of 1/30.000 per year is obtained from Riskeer and equals 9.02 m. Sweco and Arcadis (2019) concluded that the conductivity of the aquifer equals k = 70 m/day. With a predetermined transmissivity value of 2577 m^2/day for kD, D equals 36.81 m. The conductivity of the aquitard k_a was determined for the foreshore and hinterland, and both equal 0.02 m/day (Sweco and Arcadis, 2019). A list of all parameters that are used for the (semi-) probabilistic calculations is provided in Table 5.6.

Semi-probabilistic analysis

As was briefly mentioned in Section 2.1 the semi-probabilistic analysis is conducted using design values for all stochastic parameters. For each parameter it is determined whether it acts as resistance or load. Respectively the 0.05 and 0.95 quantile values are determined based on the mean value, standard deviation and type of distribution. For parameters that are best described by a lognormal distribution the location ζ and scale λ parameters are determined according to formulas given in Appendix A. The design values that are used for semi-probabilistic and probabilistic calculations are to a large extent based on a default parameter list provided by Deltares (2016). The values as used for semi-probabilistic calculations are given in Table 5.6. Results that are derived through semi-probabilistic analysis are depicted in Table 5.4.

	Uplift	Heave	Piping
Exit point 1	0.262	0.218	0.395
Exit point 2	0.175	0.146	0.554

Table 5.4: Factor of safety for piping limit states derived through semi-probabilistic analysis.

The factor of safety is subsequently used to determine probability of failure P_f based on calibration formulas for uplift, heave and piping (Rijkswaterstaat, 2019):

$$P_{f,u} = \phi\left[-\frac{ln\left(\frac{F_u}{0.48}\right) + 0.27\beta_r}{0.46} \right] \tag{5.6}$$

$$P_{f,h} = \phi\left[-\frac{ln\left(\frac{F_h}{0.37}\right) + 0.3\beta_r}{0.48} \right] \tag{5.7}$$

$$P_{f,p} = \phi\left[-\frac{ln\left(\frac{F_p}{1.04}\right) + 0.43\beta_r}{0.37} \right] \tag{5.8}$$

In which β_j denotes the reliability index. For more information on these formulas one is referred to Appendix A. The probability of failure for the two different scenarios is now shown in Table 5.5.

	Uplift	Heave	Piping	Combined
Exit point 1	1.06E-1	5.20E-2	6.91E-3	6.91E-3
Exit point 2	3.53E-1	2.14E-1	3.67E-4	3.67E-4

Table 5.5: P_f semi-probabilistic analysis for different failure modes and different scenarios.

Rijkswaterstaat (2017) prescribes that probability of failure for piping is determined by the smallest probability of failure for one of the sub mechanisms $P_f = \min\left(P_{f,u}, P_{f,h}, P_{f,p}\right)$. For scenario one P_f equals 6.91E-3 and for scenario two P_f equals 3.67E-4. Scenario one has a bigger probability of failure and is therefore normative.

Description	Symbol	Unit	Q	Dist.	μ	σ	V	Design value
Thickness aquitard [1]	d	[m]	0.05	LogN.	1.65/ 1.00	0.165/ 0.100	0.10	1.39/ 0.844
Volumetric weight aquitard	$\gamma_{s,a}$	[kN/m^3]	0.05	Norm.	19.5	0.975	0.05	17.9
Volumetric weight water	γ_w	[kN/m^3]		Deter.	10.0			10.0
Conductivity aquifer	k	[m/s]	0.95	LogN.	8.10E-04	4.05E-04	0.50	1.58E-3
Thickness aquifer	D	[m]	0.95	LogN.	36.81	0.500	0.014	37.6
Conductivity aquitard	k_b	[m/s]	0.05	LogN.	2.31E-07	1.16E-07	0.50	9.52E-08
Length foreshore	L_f	[m]	0.05	LogN.	20.0	2.00	0.10	16.9
Width levee	L_d	[m]		Deter.	30.0			30.0
Exit point wrt middle of dike [1]	x	[m]		Deter.	22.6/ 54.6			22.6/ 54.6
Phreatic level hinterland	h_p	[m]		Deter.	5.30			5.30
hydraulic head river	h	[m]		Deter.	9.02			9.02
Critical heave gradient	$i_{c,h}$	[-]	0.05	LogN.	0.700	0.100	0.20	0.354
Width berm	L_b	[m]	0.05	LogN.	9.00	0.900	0.10	7.60
Drag factor coefficient	η	[-]		Deter.	0.25			0.25
Volumetric weight sand	γ_s	[kN/m^3]		Deter.	26.5			26.5
Bedding angle	θ	[°]		Deter.	37			37
d_{70} reference value	d_{70m}	[m]		Deter.	2.08E-4			2.08E-4
kinematic viscosity water	ν	[m^2/s]		Deter.	1.33E-6			1.33E-6
gravitational constant	g	[m/s^2]		Deter.	9.81			9.81
70% fractile grain size distribution	d_{70}	[m]	0.05	LogN.	2.50E-4	3.00E-5	0.12	2.04E-4
model factor uplift	m_u	[-]	0.05	Norm.	1.0	0.100	0.10	0.836
model factor piping	m_p	[-]	0.05	Norm.	1.0	0.120	0.12	0.803

Table 5.6: Geotechnical parameters for semi-probabilistic calculation. Values were provided by Sweco and Arcadis (2019). Other values are obtained from Deltares (2016).

[1] First parameter corresponds to exit point 1, second parameter to exit point 2

Probabilistic analysis

The probabilistic analysis is conducted through FORM and MCS. For that purpose the software OpenTURNS (Baudin et al., 2015) is used which is run with the programming language Python. Appendix E shows how a PDF is fitted to data acquired from HydraRing, this PDF is used for probabilistic calculations. For the rest of the data the same input was used as shown in Table 5.6. Tables 5.7 and 5.8 shows the results derived through respectively FORM and MCS.

	Uplift	Heave	Piping	Combined
Exit point 1	2.24E-1	6.36E-1	9.46E-3	9.46E-3
Exit point 2	6.10E-1	9.18E-1	1.13E-3	1.13E-3

Table 5.7: Results preliminary investigation on piping derived through FORM.

	Uplift	Heave	Piping	Combined
Exit point 1	2.39E-1	6.20E-1	1.09E-2	1.09E-2
Exit point 2	6.16E-1	9.80E-1	1.10E-3	1.10E-3

Table 5.8: Results preliminary investigation on piping derived through MCS.

The results depicted in Tables 5.7 and 5.8 indicate that there is little difference between FORM and MCS. The fragility curves derived through FORM and MCS are depicted in Appendix F. It is shown that results don't deviate much. MCS demands much more computational time than FORM and it is therefore decided to perform analyses with FORM. Figures 5.5a and 5.5b show fragility curves derived through FORM for respectively exit points one and two. Results derived through FORM show that for the first (normative) scenario probability of failure equals 9.46E-3. Importance factors are depicted in Figure 5.6.

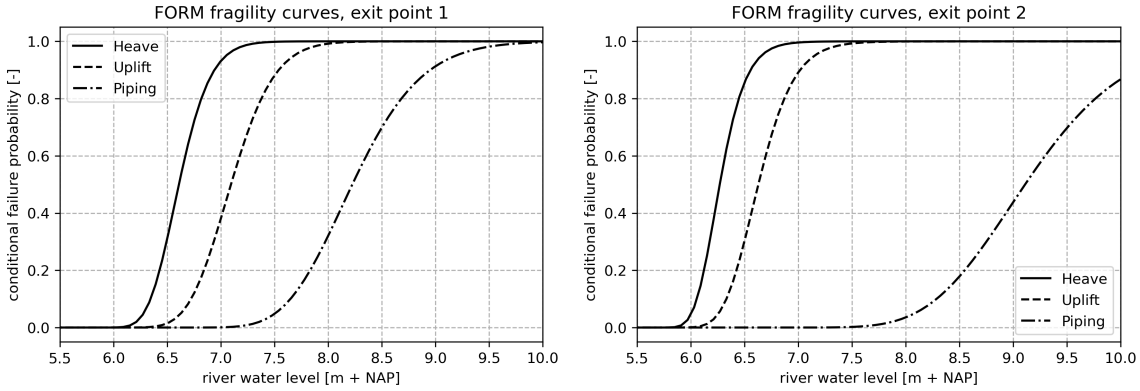

(a) Fragility curves for exit point 1

(b) Fragility curves for exit oint 2

Figure 5.5: FORM fragility curves for all three sub mechanisms of backward internal erosion.

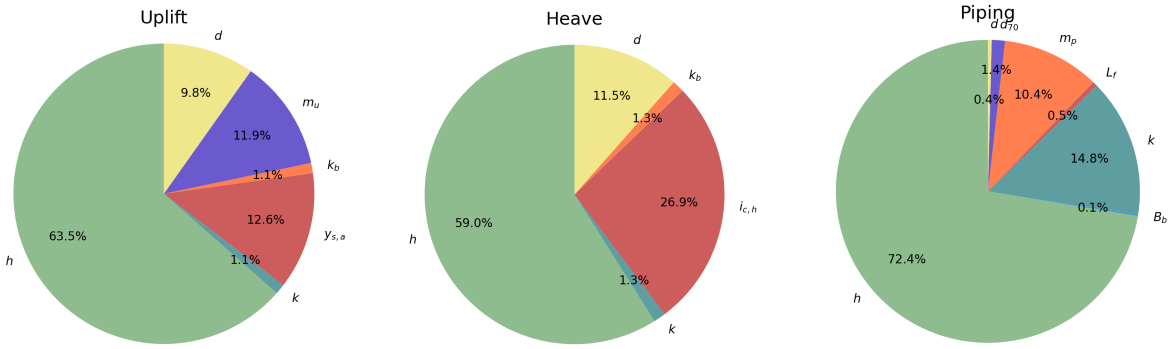

(a) Uplift

(b) Heave

(c) Piping

Figure 5.6: FORM importance factors α^2 for all three sub mechanisms of backward internal erosion. If the importance factor of a parameter was smaller than 0.1 % it was excluded from the pie charts. For all sub-mechanisms river head h has the biggest influence on failure probability for piping. Other parameters include aquifer conductivity k, volumetric weight aquitard $y_{s,a}$, aquitard conductivity k_b, model factor uplift m_u, aquitard thickness d, critical heave gradient $i_{c,h}$, berm width B_b, foreshore length L_f, model factor piping m_p and 70 % fractile grain size distribution d_{70}.

5.5. Preliminary reliability investigation on slope instability

It was shown by Sweco and Arcadis (2019) that the dike is disqualified for piping and slope instability. This Section provides a semi-probabilistic analysis for slope instability. The risk for slope instability is assessed with D-Geo Suite Stability (van der Meij, 2019). A semi-probabilistic analysis is conducted with a model that is provided by Sweco. Hydraulic load conditions are obtained through Riskeer and the phreatic line inside the dike was determined by Sweco and Arcadis (2019) and is applied in the model. The slip circle is mostly located in clay, hence undrained analysis is applied. D-Geo Suite Stability offers three methods for stability calculation: Bishop, Uplift-Van and Spencer. All three methods have been applied to the model and results are depicted in Appendix G. Results show that Bishop gives the biggest factor of safety F_d and Spencer the smallest. Table shows the results that were derived for the three methods.

Method	Bishop	Uplift-Van	Spencer
F_d	1.047	1.031	1.025

Table 5.9: Factor of safety derived through Bishop, Uplift-Van and Spencer for slope instability.

In contrast to Uplift-Van and Spencer, Bishop assumes a circular slip plane. It was shown through Uplift-Van that for the considered dike uplift pressures negatively impact the dike's stability. Moreover, one of the focal points in this thesis is to assess the effect of pressure relief well implementation as a way to increase the dike's reliability estimate. In contrast to Bishop, Uplift-Van and Spencer examine the interface between aquitard and aquifer and therefore provide a better method for determining failure probability. Uplift-Van is considered a more "stable" method compared to Spencer and as the goal merely is to investigate whether relief wells can be used as suitable reinforcement measure it is decided that Uplift-Van is the method considered in this thesis. Figure 5.7 shows the result that was obtained through Uplift-Van stability analysis.

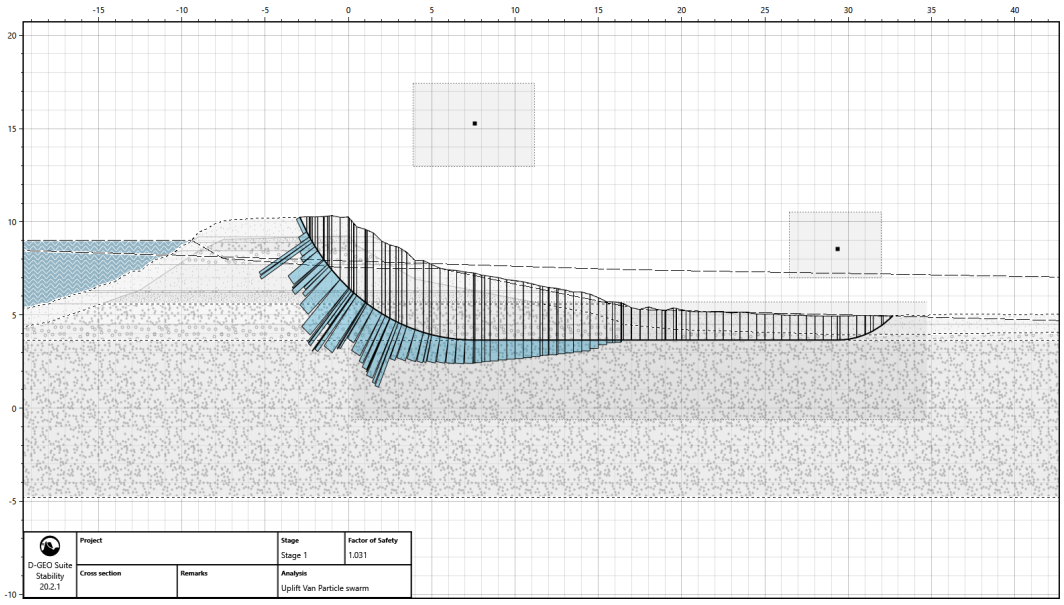

Figure 5.7: D-Stability Uplift-Van calculation, blue bars indicate shear stress.

The calibration formula derived by Kanning et al. (2017) is used to express F_d as failure probability:

$$P_{f,i} = \phi\left[-\frac{\left(\frac{F_d}{\gamma_d}\right) - 0.41}{0.15} \right] \tag{5.9}$$

In which γ_d represents the model factor, equal to 1.06 for Uplift-Van. For F_d equal to 1.031 Equation 5.9 now yields a probability of failure equal to 8.81E-5. Table 5.10 depicts the retrieved probability of failure with the acceptable probabilities of failure as were derived in Section 5.3. It is shown that currently target failure probability is not met.

Derived P_f	Target P_f 100 m	Target P_f 2000 m
8.81E-5	1.25E-6	5.75E-7

Table 5.10: Derived failure probability vs target failure probabilities. Target P_f 100 m refers to target failure probability for the first part of the case study and target P_f 2000 m refers to the second part.

5.6. Concluding remarks

In Section 5.3 it was derived that cross-sectional target failure probability for piping equals 8.00E-6. The semi-probabilistic analysis conducted in Section 5.4 showed that probability of failure equals 4.93E-3. This is much larger than the target level. Subsequently a probabilistic analysis was conducted and it was shown that probability of failure equals 5.21E-3. It is therefore concluded that the current dike section does not meet required safety criteria for failure mode piping. For slope instability cross-sectional target probability of failure equals 1.33E-6, as was shown in Section 5.3. A semi-probabilistic analysis was conducted and it showed that probability of failure for the considered dike section equals 8.81E-5. The dike section does therefore not meet required target reliability. For the remainder of this thesis when reference is made to target reliability level, it is referred to cross-sectional target reliability. The length-effect is usually incorporated in target reliability for a section of specific length through Equations such as Equation 5.1. In Chapters 6 and 7 the length-effect is incorporated through random field modelling. In Chapter 6 a pore pressure monitoring approach is presented and subsequently used to update failure probability for piping using pre-posterior analysis.

6

Derivation of an optimal configuration for pore pressure sensors

This Chapter derives an optimal head monitoring strategy taking soil heterogeneity into account. Sections 6.1 and 6.2 provide a concise overview of the framework and applied theory. Three-dimensional random fields are generated to model the aquifers heterogeneity. Subsequently, a finite-difference flow model is used to compute pore pressure in the aquifer. Section 6.3 elaborates on model specifications as used in this thesis. A principal component analysis is conducted to provide insight into the least amount of pore pressure sensors required, results are shown in Section 6.4. Subsequently model runs are executed in the groundwater model with various set-ups for equally spaced sensors. Section 6.5 elaborates on how the measurement error was included and the results of the model runs are shown in Section 6.6. Finally Section 6.7 shows how pre-posterior analysis is applied to update failure probability for piping. In Section 6.8 a sensitivity check is provided for the number of pore pressure sensors and correlation error used to define the measurement error. Section 6.9 will conclude the Chapter.

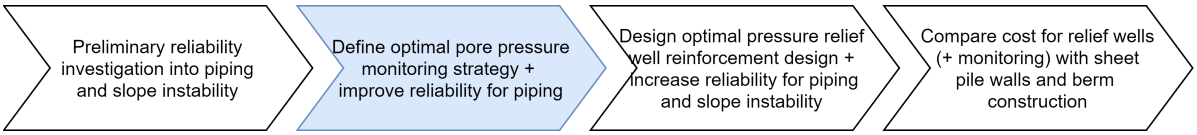

6.1. Problem description

Defining an optimal pore pressure monitoring strategy is a multi-objective problem. Ideally one would obtain a maximum amount of information and at the same time minimize cost, whilst considering constructive and legal possibilities. The optimal number of sensors is therefore a trade-off between information gain and increasing cost. This Chapter focuses on the trade-off between the amount of sensors and information gain. The desired amount of sensors depends on the desired redundancy of the pore pressure monitoring system. Redundancy refers to information that is expressed more than once, and is therefore a measure of the systems reliability. With respect to pore pressure monitoring, sensors are redundant if they provide information that correlates with information of other sensors. During measurements, deviations of 10-20 cm from the actual head are not uncommon. Placing two sensors at the same location can decrease these discrepancies. However, it can also make them susceptible to the same cause of malfunction. Spatial distribution is therefore desired. This study focuses on defining an optimal configuration of pore pressure sensors, taking measurement errors and deviations in the aquifers pore pressure into mind. Fully functioning sensors are assumed. Pore pressure sensors are placed at the land-side toe of the dike and the goal is to find the optimal longitudinal placement. In this thesis sensors are assumed to be equally spaced. The aim of implementing sensors is to update failure probability for piping. The same soil parameters are used as in the preliminary analysis elaborated in Chapter 5, Section 6.3 discusses implementation. Figure 6.1 shows the distance of interest in this study.

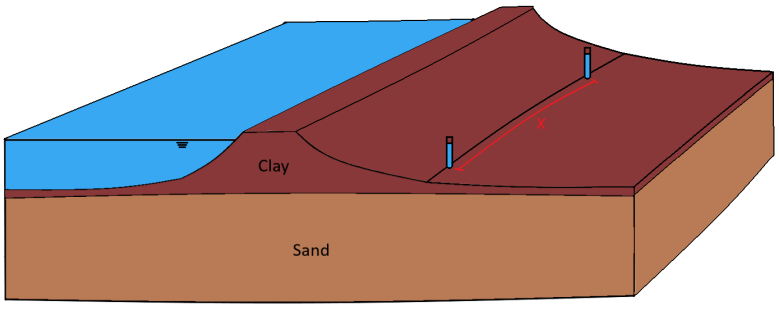

Figure 6.1: Longitudinal pore pressure sensor placement (not to scale). The x shows the distance of interest in this study. For all observations equally spaced sensors are assumed.

The general method for deriving optimal sensor configuration comprises of three steps. For the first step the minimal amount of pore pressure sensors are derived. This will be done through a principal component analysis (PCA). For the second step measurement errors are defined that should be included when deciding on the optimal sensor configuration. For the third step the set-up as was derived from PCA will be implemented in the groundwater model including the measurement error. The amount of pore pressure sensors will subsequently be increased until good estimates can be made for standard deviation in pore pressure behind the dike. For all set-ups equally spaced sensors are assumed. Section 6.2 will elaborate on details regarding the PCA and the method in general.

6.2. Method for determining optimal sensor configuration

As was discussed in Section 6.1 the ideal pore pressure monitoring strategy provides the maximum amount of information with the minimum amount of pore pressure sensors. Subsurface pressures at different locations behind the dike are correlated, information measured by one sensor shows partial correlation with that of another. Multiple strategy approaches are provided in literature to develop an optimal pore pressure monitoring strategy (Allgeier et al., 2020; Fisher and Twinning, 2011). However few strategies provide techniques to assess the actual amount of information provided by sensor combinations, which is of particular interest for this study.

Principal component analysis

Principal component analysis (PCA) is a frequently used dimensionality reduction method that is often used to reduce the dimensionality of large data sets (Tipping and Bishop, 1999). It thereby transforms a large set of variables into a smaller one without losing much of the information. Reducing the number of variables makes analyzing data much easier, however it does come at the expense of accuracy. PCA enables to capture the maximum amount of information with the minimum amount of data. Wewer (2019) shows how PCA can be used to create a starting point for developing an optimal pore pressure monitoring strategy. The next Section will provide a step by step explanation of PCA followed by a small example in which it is applied to pore pressure monitoring.

The aim of PCA is to capture as much variation in the data set as possible. The amount of variation is measured with the variance, which determines the average spread of a data point x_i from the mean value of the data μ. The variance equals the squared standard deviation σ^2:

$$Var(X) = \frac{1}{n}\sum_{i=1}^{n}\left(x_i - \mu\right)^2 \tag{6.1}$$

In PCA the continuous initial variables should contribute equally to the analysis. If there are large differences between the ranges of initial variables, variables with large ranges will dominate over variables with small ranges. Let's assume variable A that ranges between 0 and 100, and variable B that ranges between 0 and 1. Variable A will dominate over variable B because it has a much bigger range. This will lead to biased results.

In PCA it is therefore of upmost importance to transform the data to comparable scales. Standardization is performed for each variable x_i by subtracting the mean μ and dividing by the standard deviation σ:

$$z = \frac{x_i - \mu}{\sigma} \tag{6.2}$$

After standardization all variables are transformed to the same scale. One of the powerful capabilities of PCA is that it summaries the correlations between all possible pairs of variables. Correlation is determined with the covariance:

$$Cov(X,Y) = \frac{1}{n}\sum_{i=1}^{n}(x_i - \mu_x)(y_i - \mu_y) \tag{6.3}$$

The goal is to understand the relationship between the variables of the input data set. Equation 6.3 is used to investigate how the variables of the input data set vary from their respective mean with respect to each other. Results are depicted in a covariance matrix. The covariance matrix is a $p \cdot p$ matrix in which p is the number of dimensions, determined according to:

$$p = \min\{n-1, m\} \tag{6.4}$$

In which n is the amount of observations and m the amount of variables. Usually there are more observations than variables, making m normative for the matrix. For a three dimensional data set with variables x, y and z the covariance matrix has the form:

$$\begin{bmatrix} \text{Cov(x,x)} & \text{Cov(x,y)} & \text{Cov(x,z)} \\ \text{Cov(y,x)} & \text{Cov(y,y)} & \text{Cov(y,z)} \\ \text{Cov(z,x)} & \text{Cov(z,y)} & \text{Cov(z,z)} \end{bmatrix} \tag{6.5}$$

Obviously the diagonal of the matrix equals the variances of the respective variables and the upper and lower triangular portions are equal as $Cov(z,x) = Cov(x,z)$. Results depicted in the matrix are either positive or negative values. Positive values indicate correlation, so two variables increase or decrease together. Negative values indicate inverse correlation, if one variable increases the other one decreases.

The next step is to determine the principal components. Principal components are "new" variables that are constructed as linear combinations of the initial variables. Principal components are constructed in such a way that they are uncorrelated. As much information as possible is squeezed into the first principal component followed by the second, the third etcetera. So for the $3 \cdot 3$ matrix depicted above three principle components are constructed. Organizing information in principal components allows for dimensionality reduction without losing much of the information by discarding components with low information and considering the remaining components as new variables. Principal components represent the lines in the data that capture most of the variation. As was mentioned above the relationship between variation and information is that the larger the variance that is carried by one line the larger the dispersion of the data points along it, and therefore the more information it has. Principal components can therefore be regarded as new axes that provide the best angle to see and evaluate data.

In order to compute principal components belonging to the data eigenvectors and eigenvalues are to be computed from the covariance matrix. Each eigenvector has a corresponding eigenvalue and the total amount of pairs equals the number of dimensions in the data set. For the example above there would be 3 pairs. Eigenvectors define the directions of the axes with most variance and therefore the directions of the principal components. Eigenvalues define the amount of variance that belongs to that principal component. As was mentioned before, more variance means more information. Based on the computed eigenvectors and eigenvalues it can be decided to discard one in order to reduce the data set by one dimension.

As a way to clarify how PCA will be applied in this Chapter a small example will be provided in which the pore pressure at two possible sensor locations is evaluated.

Example

The behaviour of PCA is easiest to visualize by analyzing a two-dimensional data set. Consider a dike stretch of 100 m as depicted in Figure 6.1. Two possible sensor locations are located at the hinterland toe of the dike. For the sake of clarity we assume perfectly working sensors. A total of 100 different compositions of subsoil strata are created for which the pore pressure at the two sensor locations is evaluated. A total of 100 different subsoil compositions means that there will be 100 observations and two sensor locations means that there will be a total of two measurements for each observation. These measurements will be standardized, resulting in two variables. Using Equation 6.4 this results in two principal components. Figure 6.2a depicts the data that was obtained. For each observation the x-axis depicts the evaluated head at location 1 and the y-axis depicts the evaluated head at location 2. Each dot therefore represents one observation. These values are standardized according to Equation 6.2, the result is depicted in Figure 6.2b. When analyzing longitudinal sensor placement standardization does not lead to a different relation between the variables. Hence to the eye there is, except for the axes, no change in the plots depicted in Figures 6.2a and 6.2b.

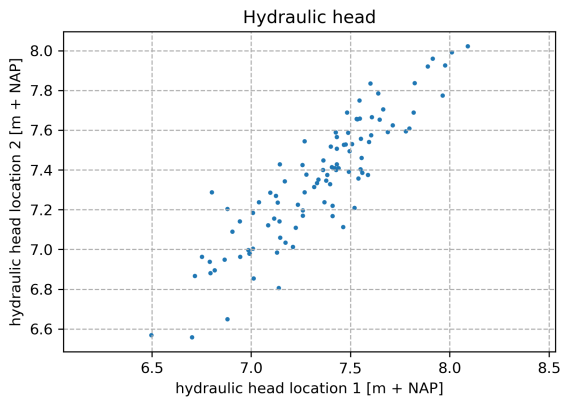

(a) Pore pressure measurements, each dot represents one observation for pore pressure measured at two different locations at the hinterland the dike.

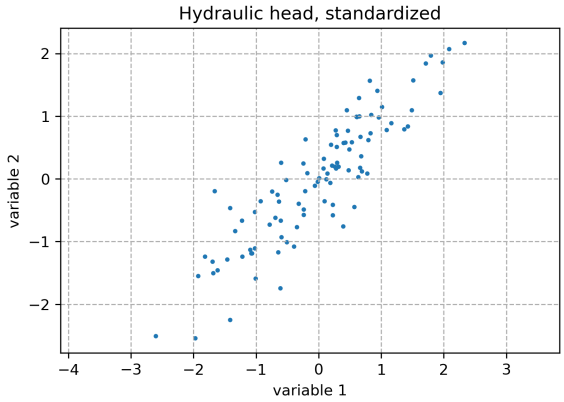

(b) Standardized pore pressure measurements. The plot looks the same as the non-standardized values because both measurements are executed at the hinterland toe of the dike.

Figure 6.2: Example for pore pressure measurements in a PCA.

A quick scan at the results depicted in Figure 6.2b shows that the two measured variables are correlated. If variable 1 is bigger than 0, variable 2 will most likely also be and vice versa. For the results depicted in Figure 6.2b the eigenvectors v and eigenvalues λ of the covariance matrix were determined according to respectively Equations 6.3 and 6.1 and are given by:

$$v = \begin{bmatrix} -0.70710678 & -0.7071067 \\ 0.7071067 & -0.70710678 \end{bmatrix}$$

With:

$$\lambda = \begin{bmatrix} 1.9128648 \\ 0.1073369 \end{bmatrix}$$

As was briefly mentioned above the eigenvectors indicate the direction of the axes where there is most variance, the direction of the principal components. The principal component of a collection of points is a vector that best fits data while being orthogonal to the first vectors. The eigenvalues describe the amount of information that is carried in each principal component. The principal components can now be constructed and are depicted in Figure 6.3a. The first principal component is highlighted with a one and the second principal component with a two.

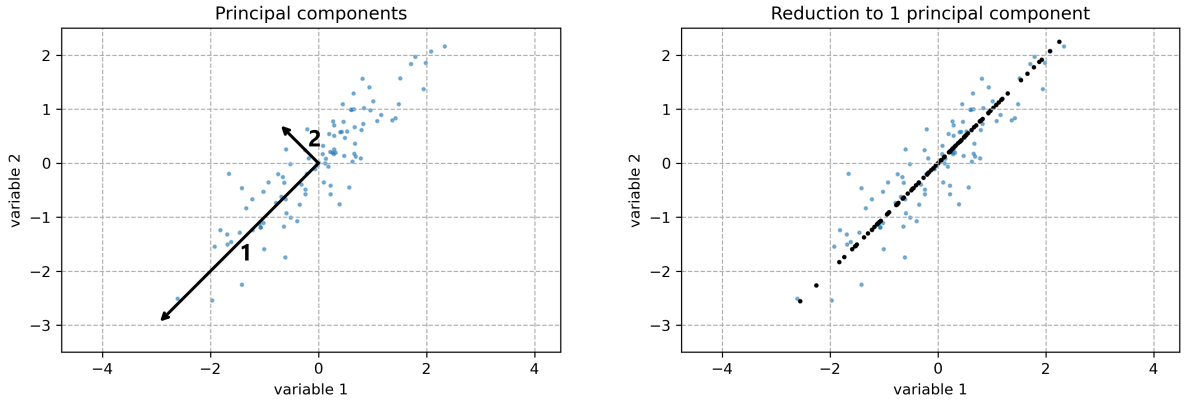

(a) Two PC's. The first PC is depicted by the first vector and the second PC by the second vector. The length of the vector indicates the amount of variation present on that vector.

(b) Reduction of two PC's to one PC. The plot shows how all data points (depicted in blue) are translated onto the first principal component. The translated points are shown in black.

Figure 6.3: Example of how PC's are derived from pore pressure measurements.

It is obvious that principal component 1 carries much more information than principal component 2 as $\lambda_1 \gg \lambda_2$. Based on the eigenvalues it can be concluded that principal component 1 carries 94.7% of the variance and principal component 2 5.3%. Based on this information it can be decided to reduce the data from a two dimensional data set to a one dimensional data set at the expanse of 5.3% of the information. Figure 6.3b shows how all data points are translated to principal component 1. The blue dots show all observations and the black dots show the newly located data points.

Relating this back to the simplified pore pressure sensor placement problem that we started with, this example shows that one principal component is capable of describing 94.7% of the variance in the spectrum. Disposing one principal component will therefore only go at the expanse of 5.3% of the information. This also indicates that one sensor will likely capture most variance in the spectrum. In this simplified example measurement errors have been ignored.

Subsequent analysis

The PCA will deduce the high dimensional sensor placement problem and indicate the minimum amount of sensors required to observe all variation in the spectrum. However the PCA does assume fully functioning sensors, neglecting measurement errors. In Section 6.1 it was mentioned that for sensor measurements errors of 10-20 cm are not uncommon, hence it cannot be neglected in the analysis. Therefore, the indicated amount of sensors in the PCA will be implemented in the aquifer model. Equally spaced sensors are assumed. Subsequently it will be checked how much of the actual variation in pore pressure is captured within the sensor measurements. Based on that it will be decided how much sensors are implemented.

6.3. Specifications of the groundwater model

This Section will elaborate on the model that will be used for observing the aquifer's pore pressure. First, the random field generator used in this study is discussed. Secondly an elaboration will follow on the flow model that is used to compute pore pressure using random fields. Lastly, some verification runs are executed to verify a model simplification. Other assumptions and simplifications that were made are also highlighted.

Modelling subsoil heterogeneity

Subsoil heterogeneity is modelled using random fields. A random field defined as a random function over an arbitrary domain. The random fields used in this thesis are generated using GSTools (Schueler and Mueller, 2020). GSTools runs through the programming language Python and provides geostatistical tools for, among other things, random field generation. These random fields are generated using the randomisation method,

described in Heße et al. (2014). First, a random field is generated using the Gaussian covariance model, given by the following correlation function:

$$\rho(r) = \exp\left(-\frac{\pi}{4} \cdot \left(\frac{r}{l}\right)^2\right) \tag{6.6}$$

In which l resembles the correlation distance, often also referred to as length scale. For the random fields generated in this study a correlation length of 300 m is adopted from Rijkswaterstaat (2019). Subsequently, this model is transformed into a log-normal distribution as this best describes hydraulic conductivity in soil (Mesquita et al., 2002; Kosugi, 1996). In this study, values for hydraulic conductivity will be adopted from Sweco and Arcadis (2019) with a mean value of 70 m/d. A default value of 0.50 is taken for the coefficient of variation (Rijkswaterstaat, 2019). An example of a random field is given in Figure 6.4a.

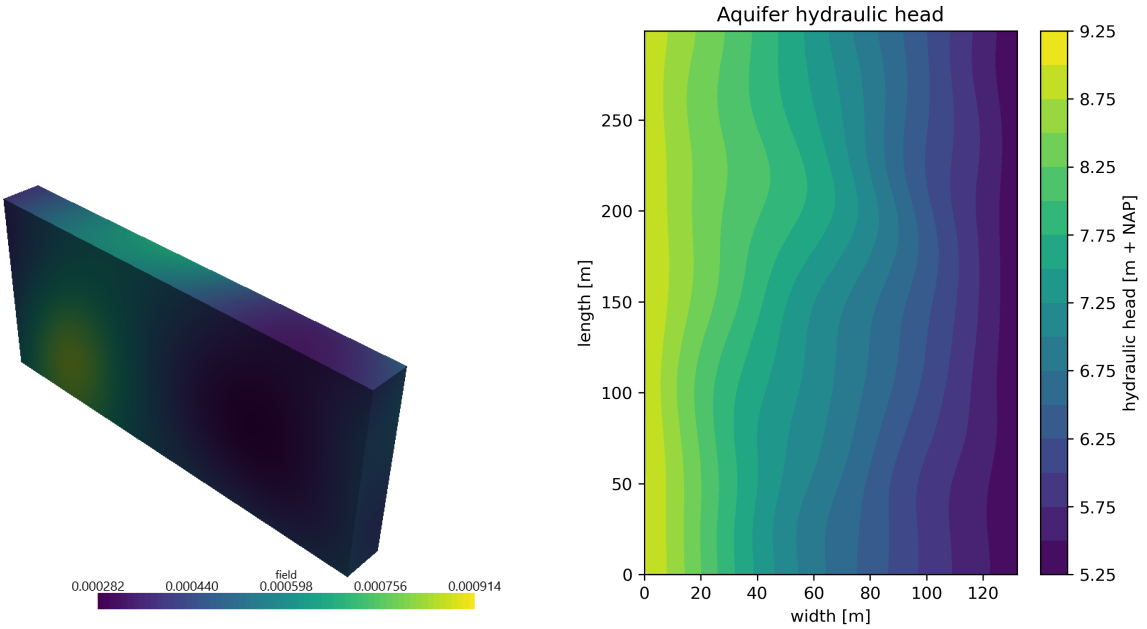

(a) Example of a random field, the scale indicates permeability with units in m/s.

(b) Result of a model run. The plot shows pore pressure at the aquifer's top layer.

Figure 6.4: Examples of random field modelling

Flow model

Groundwater flow is modelled using MODFLOW (Harbaugh, 2005), which is a finite-difference flow model computer code that solves the groundwater equation. Groundwater flow is simulated using a block-centered finite-difference approach. FloPy (Bakker et al., 2016) is used to script the model development with the programming language Python. The partial differential equation for a confined aquifer solved in MODFLOW is given by:

$$\frac{\delta}{\delta x}\left(k_{xx}\frac{\delta h}{\delta x}\right) + \frac{\delta}{\delta y}\left(k_{yy}\frac{\delta h}{\delta y}\right) + \frac{\delta}{\delta z}\left(k_{zz}\frac{\delta h}{\delta z}\right) + W = S_S\frac{\delta h}{\delta t} \tag{6.7}$$

In which k represents hydraulic conductivity along the x, y and z coordinates, h the potentiometric head, W the volumetric flux, S_S the specific storage and t time. Figure 6.4b provides an illustrative example of the result of a MODFLOW run with a random field. The plot represents the top layer of an aquifer. The left and right side represent assigned boundaries of respectively 9.02 and 5.3 m. Each contour line represents a head drop of approximately 0.25 m.

Model validation

As was stated in Section 6.3 a correlation length of 300 m is used. With an aquifer depth of 37 m one might think that depth does not really have an influence on the pore pressure measured in the top layer, since soil conditions hardly change over 37 m. To that end a verification run was performed in which five different aquifer depths were tested. Runs were executed for aquifers with a depth of 37, 20, 10, 5 and 1 m. Results are depicted in Figure 6.5. The x-axis depicts the number of runs, each run consisting of a different random field, and the y-axis depicts the mean pore pressure measured after n runs. After 2000 runs convergence was reached for all depths. For aquifer depths of 37, 20, 10, 5 and 1 m the pore pressure measured in the top layer equals respectively 7.354, 7.352, 7.358, 7.356 and 7.358 m. Results therefore show that for a correlation length of 300 m, aquifer depth does not influence the pore pressure measured in the top layer of the aquifer. Therefore in the following runs will be conducted with a limited aquifer depth of 1 m to save on computational time.

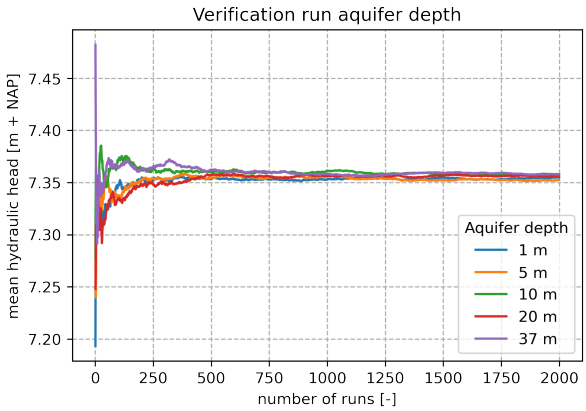

Figure 6.5: Mean pore pressure for different aquifer depths. After 2000 random field generations convergence is reached and it is shown that the effect of aquifer depth on pore pressure in the top layer is limited.

As was briefly mentioned in Section 5.2 the case study will be conducted for two trajectories. The first trajectory is a stretch of 100 m. It was shown in Figure 6.5 that results are not affected by limiting the aquifer depth from 37 to 1 m. In Section 5.4 it was determined that the hinterland phreatic level can be assumed at 133 m from the entrance point. The aquifer is therefore modelled as a conductivity grid of $100 \cdot 133 \cdot 1$ cells, with each cell representing 1 m^3 of soil. The second trajectory consists of a stretch of 2000 m. Again aquifer depth is not important and therefore modelled with 1 cell.

Other simplifications

Groundwater flow is modelled as confined aquifer flow. Interactions between the aquitard and aquifer are not accounted for. Boundaries are modelled with assigned pore pressure values. Following results that were obtained in Sweco and Arcadis (2019) a head drop of 0.028 m/m is assumed. The top layer of the aquifer is found at 3.65 m + NAP. Most runs are executed with a river hydraulic head of 9.02 m + NAP. Therefore the hinterland phreatic level is modelled at 3.65 m + NAP at a distance of 192 m from the entrance point. Figure 6.6 shows the relevant distance. The location of the hinterland phreatic level indicates the cell where constant phreatic level is assumed. The location of the entrance point is also given in Figure 6.6.

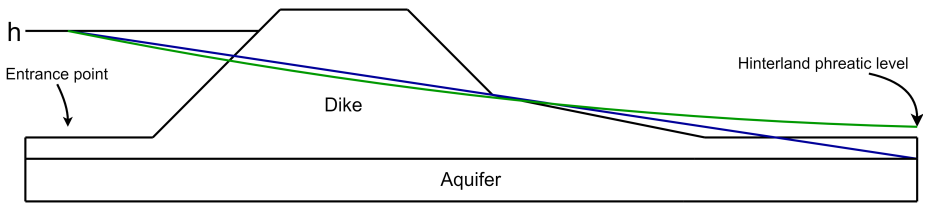

Figure 6.6: Simplified cross-section to show how hinterland phreatic level is modelled. The blue line shows how the line how it is modelled in MODFLOW. The green line shows a more realistic phreatic line.

In this Chapter runs are executed for different river water levels. The theoretical distance where the hinterland phreatic level stays constant was determined for a river water level of 9.02 m + NAP. The flow model now models the phreatic level as a straight line (excluding heterogeneous characteristics of the soil). Figure 6.6 shows the theoretical phreatic line as calculated by the model in blue. The green line gives a more realistic representation of the phreatic line with a slight parabolic gradient. The hinterland phreatic level is therefore not fixed but depends on the hydraulic head in the river. In order to incorporate this effect in the model, the hinterland phreatic level should be adjustable. However this is not possible as the grid in the model is fixed. It is therefore decided to incorporate this effect through a varying head boundary at the last row of cells. Equation 6.8 describes hydraulic head at the last row of cells.

$$\phi_h = -0.076 + \frac{3.726}{\left(\frac{9.02-5.3}{h-5.3}\right)} \tag{6.8}$$

In which ϕ_h represents pore pressure at the hinterland boundary for a given hydraulic river head h. The relation was fitted for two boundary conditions. In this Chapter runs are executed for river water levels varying between 5.3 and 9.02 m + NAP. Boundary conditions are therefore defined for those two water levels. The first boundary condition follows from the assumption that for a river water level of 9.02 m + NAP the hinterland phreatic level is found at 192 m from the entrance point. The second boundary condition follows from the assumption that for a river water level of 5.3 m + NAP and a head drop of 0.028 m/m the result should be a hydraulic head of 3.65 m + NAP at the hinterland toe of the dike. Section 6.7 provides more information on this.

6.4. Determining the minimum amount of pore pressure sensors

In Section 6.1 it was mentioned that this thesis focuses on two different trajectories. The first trajectory consists of a stretch of 100 m in front of Wijk bij Duurstede and the second trajectory is a fictitious dike section in which the cross section of the first trajectory is extrapolated over a length of 2 km. For the PCA, runs are executed for both trajectories. The PCA does not assume measurement errors. The following Sections will provide graphs to show the results for the PCA's conducted for the 100 m and 2 km trajectories. A small Table will be provided showing discretization ($l \cdot w \cdot d$), the amount of random field generations and amount of sensor locations. The latter equals the amount of principal components and therefore the dimensionality of the initial problem.

Dike trajectory 100 m

Figure 6.7a shows the result for the PCA for the first trajectory, assuming fully functioning sensors. The x-axis displays the amount of principal components and the y-axis the cumulative variance measured by the sensors. Apparently, one fully functioning sensor placed at the hinterland toe of the dike captures 100% of the variation in the spectrum. This does make sense as no measurement errors are included and for a trajectory length of 100 m in combination with a correlation length of 300 m for the soil's conductivity deviations in aquifer pore pressure are assumed to be small. For in-field pore pressure measurements at least two sensors are required to capture variation. Based on this analysis it is therefore concluded that at least two sensors are required to capture all measurements. Table 6.1 depicts some specifications on the model runs. Figure 6.7a shows the results.

Specification	Discretization	Random field generations	Possible locations
Dike trajectory 100 m	$100 \cdot 192 \cdot 1$	2000	100
Dike trajectory 2000 m	$2000 \cdot 192 \cdot 1$	2000	2000

Table 6.1: Model run specifications. Discretization refers to the amount of grid cells used for the model. Random field generations indicates the amount of model runs that have been executed and possible locations shows the amount of possible pore pressure sensor locations. It is assumed that every cell behind the dike offers space for one sensor.

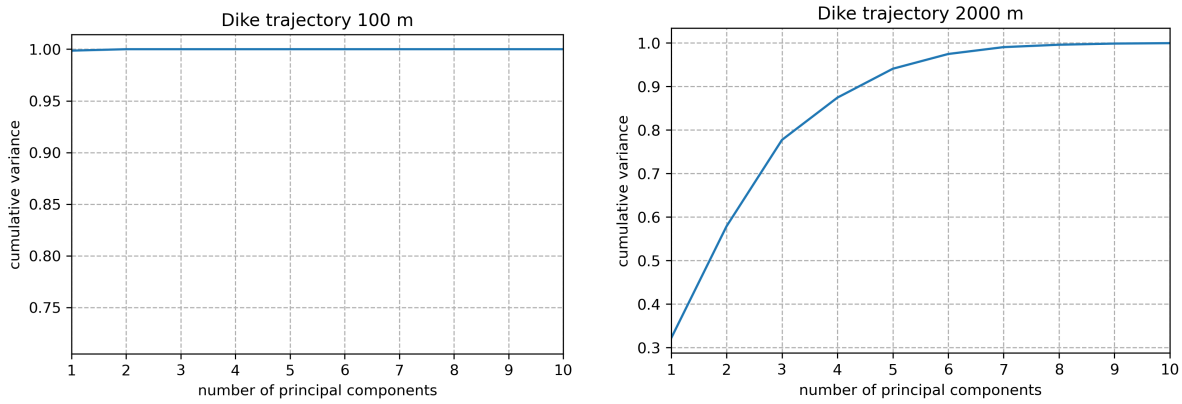

(a) Cumulative variance derived through PCA for the 100 m trajectory.

(b) Cumulative variance derived through PCA for the 2000 m trajectory.

Figure 6.7: Cumulative variance as function of number of pore pressure sensors.

Dike trajectory 2000 m

Figure 6.7b shows the result that was obtained for the PCA for the second trajectory, again assuming fully functioning sensors. The x-axis displays the amount of principal components and the y-axis the captured cumulative variance. Apparently, eight fully functioning sensors capture 100% of the spectrum's variation. It has to be mentioned however that measurement errors have not been included in this analysis. Based on this analysis it is concluded that at least 5 sensors are required to capture enough measurements. Table 6.1 depicts some specifications for the model runs.

6.5. Inclusion of a measurement error in pore pressure monitoring

In Section 6.1 it was mentioned that pore pressure sensor measurements are susceptible to errors, deviations of 10-20 cm are not uncommon. It can therefore not be neglected in the analysis. The nature of the error has been covered extensively in Section 3.2. Four types of errors were identified: those due to (1) the measurement instrument, (2) conversion of pressure to water level, (3) time lag effects and (4) piezometer defect. For this study we assume working sensors. Errors caused by the measurement instrument e_m are most easy to define as they are listed by manufacturers. For the current study we assume standard standpipes which have a maximum error of 0.5 cm up until 10 m of piezometric head (van Essen, 2016). Therefore, 95% of the measurements is in the range of $\pm$ 0.5 cm. They are therefore modelled as standard normally distributed: $N \sim (0, 0.0025^2)$. Literature does not provide stone set values for other types of errors. In a previous study Schweckendiek (2014) modelled those errors as $N \sim (0, 0.1^2)$, which seems like a reasonable estimate and will therefore be adopted in this study. Measurement errors due to (1) time lag effects and (2) conversion of pressure to water level show large correlation, especially for this study in which measurement errors are added each subsequent meter. To ensure that measurement errors are correlated each consecutive error e_n is written as a function of e_{n-1} with correlation coefficient ρ:

$$e_n = \rho e_{n-1} + e_n^* \sqrt{1-\rho^2} \tag{6.9}$$

In which e_n^* is also standard normally distributed according to $N \sim (0, 0.1^2)$ and independent of e_{n-1}. The first term in Equation 6.9 represents the correlated part of e_n and the second term the uncorrelated part.

Most analyses are conducted with a constant river head of 9.02 m. Only in Section 6.7 analyses are conducted with varying river water levels. A higher hydraulic river head automatically means a higher piezometric level at the hinterland toe of the dike. The main contributor to the correlated error is the effect of time lag. It's straightforward that time lag increases as pore pressure difference increases as the piezometer needs more time to adjust to higher head differences. In order to incorporate this process the dependent part of the measurement error e_d is written as follows:

$$e_d = e_n \cdot \frac{h - \phi_0}{\phi - \phi_0} \tag{6.10}$$

In which e_d represents the dependent part of the error neglecting head difference, h the varying river head between 5.3 and 9.02 m. The total measurement error e_t now follows from a summation of the independent and dependent part of the error:

$$e_t = e_m + e_d \tag{6.11}$$

As was briefly mentioned before literature does not provide fixed values for dependent measurement errors, hence there is no fixed value for correlation coefficient ρ. In this analysis the correlated errors will be assigned each consecutive meter, making them highly dependent. To visualize the effect of correlation coefficient ρ a small example is provided. It considers a dike section of 100 m with 100 sensors at the hinterland toe of the dike. The correlation length for soil conductivity is set at 300 m. Six cases are considered for different correlation coefficients. Results are obtained through 1000 random field generations for each case. For the sake of clarity errors caused by the measurement instrument e_m are not included and the graphs are solely based on the correlated error e_n. The results are depicted in Figure 6.8. The graph shows that for sensors with more correlation in measurement error, less sensors are required to measure more variation. It is shown that for ρ = 0.0 (no correlation) one principal component captures 59 % of the spectrum's variation, whereas for full correlation (ρ = 1.0) one principal component would capture 100 %. The results for ρ ranging between 0.8 and 0.98 are also shown in the plot.

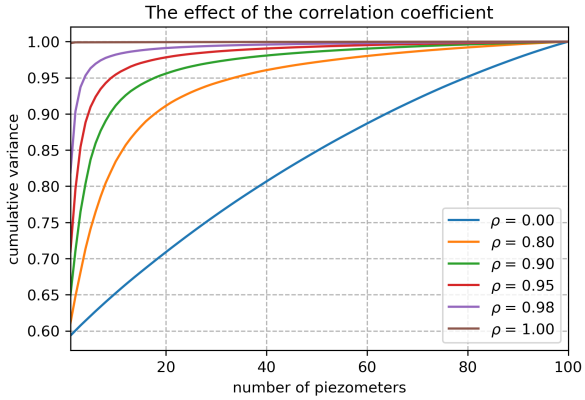

Figure 6.8: Cumulative variance as function of number of piezometers for different ρ. It is shown that for higher ρ less sensors are required to measure more variation.

In the rest of this thesis a correlation coefficient ρ of 0.9 is assumed for adjacent grid cells. The result of the PCA that shown in Figure 6.7 shows that for trajectory one at least two sensors are required to observe all variation and for trajectory two at least five sensors to observe 94%. The next step is to perform sensor measurements in the aquifer model and add the measurement error. Subsequently it is analysed how much variation of the actual pore pressure present in the field is captured by the sensor measurements. For this analysis Equation 6.11 is used.

Dike trajectory 100 m

The result of the PCA conducted in Section 6.4 has shown that for trajectory one at least two sensors are required. A script is written in which two sensors are implemented in the most ideal set-up, meaning equally spaced. For all runs the sensors are located at the same point. A measurement error is assigned to each sensor conform the method explained in Section 6.5. The results shows that two sensors only capture 50.3 % of the variation in pore pressure present in the field. Therefore runs have also been executed for set-ups with three, four, five and six sensors. Again the most ideal equally spaced sensor set-ups are implemented. The results are depicted in Table 6.2. Figure 6.9 provides a visual representation of the results.

Dike trajectory 2000 m

The result of the PCA has shown that for trajectory two, five principal components capture 94% of the variation. Like for the first trajectory again a script is written for the second trajectory in which five sensors are implemented. Measurement errors are included and again an ideal sensor set-up is assumed. The first run shows that five sensors capture 72.2 % of the present pore pressure in the field. Therefore runs are executed for set-ups with six, seven, eight and nine sensors. Again the most ideal sensor set-ups are implemented as was explained in the previous paragraph. The results are depicted in Table 6.2. Figure 6.9 provides a visual representation of the results.

Number of sensors	2	3	4	5	6	7	8	9
Dike trajectory 100 m	0.503	0.732	0.854	0.906	0.961	-	-	-
Dike trajectory 2000 m	-	-	-	0.722	0.886	0.915	0.923	0.942

Table 6.2: Percentage observed variation in pore pressure

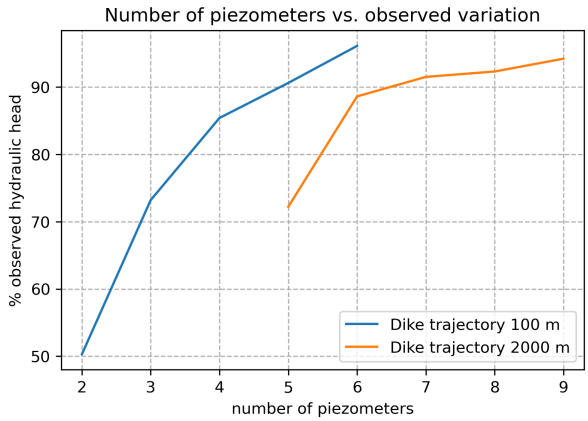

Figure 6.9: Number of piezometer vs observed variation for both dike sections.

Defining standard deviation for pore pressure measurements

The obtained results are a measure of how much percent of the occurring pore pressure in the field is observed by the sensors, and therefore provides a confidence interval. More sensors automatically means more measured variation. The more variation is measured the smaller the measurement error gets. Based on the obtained results it is decided that for the first trajectory four sensors will be implemented and for the second trajectory six sensors. The obtained measurements are assumed to be Gaussian distributed. The mean value μ is simply given by the average of the sensor measurements. As for any probability density distribution, the integral over the definition area provides the probability density. For the 100 m dike section four sensors capture 85.4% of the pore pressure, hence probability density, such that:

$$\int_{\phi_{min}}^{\phi_{max}} \frac{1}{\sigma\sqrt{2\pi}} e^{\frac{1}{2}\left(\frac{x\mu}{\sigma}\right)^2} dx = 0.854 \tag{6.12}$$

In which ϕ_{min} and ϕ_{max} represent the minimum and maximum measured pore pressure by the pore pressure sensors. Both values deviate equally from the mean value, which requires small adjustment in some cases. If for example the mean value is measured at 7.00, the minimum at 6.90 and the maximum at 7.11, ϕ_{min} would equal 6.90 and ϕ_{max} 7.10. This method therefore does come at the expanse of some minor inaccuracy. The standard deviation is now calculated with a standard probabilistic z-test according to:

$$\sigma = \frac{x-\mu}{z} \tag{6.13}$$

In which the z-score is determined by the percentage of pore pressure captured, x represents the upper boundary (ϕ_{max}) and μ the measured mean.

6.6. Results for pore pressure monitoring

The results that are derived through linear extrapolation for the 100 m trajectory and the 2000 m trajectory are depicted in respectively Figures 6.10a and 6.10b. Results for the 100 m trajectory were obtained with four pressure sensors and results for the 2000 m trajectory were obtained with six pressure sensors. The red line indicates the mean value of the correlation between river head and pore pressure behind the dike for artesian conditions. The blue shaded area shows the 95% confidence interval based on measurement uncertainty and length-effect. As was briefly mentioned in Section 6.5 larger differences in pore pressure result in larger measurement errors, hence the confidence interval widens as river water level increases. This effect is clearly visible for the 100 m trajectory depicted in Figure 6.10a. For the 2000 m trajectory the effect of the increasing measurement error is less visible as uncertainty is dominated by the length-effect.

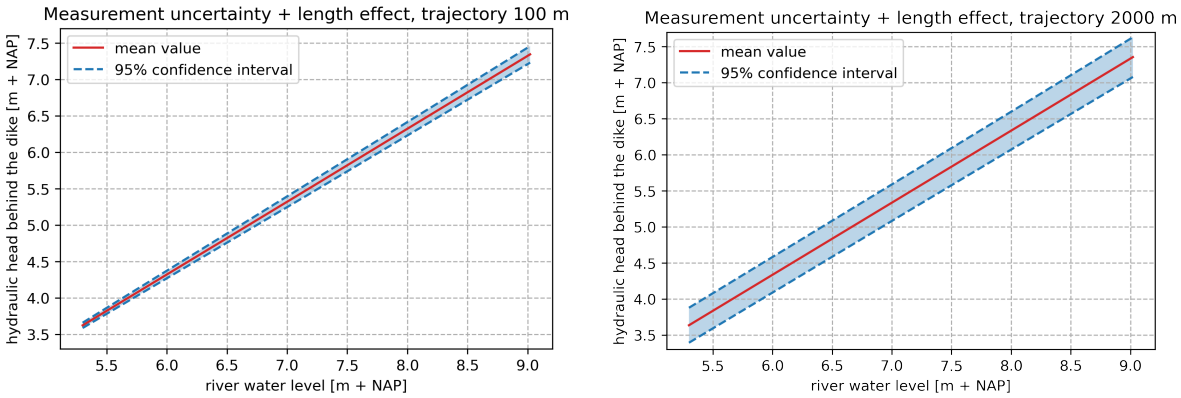

(a) Dike trajectory 100 m, results obtained with 4 sensors.

(b) Dike trajectory 2000 m, results obtained with 6 sensors.

Figure 6.10: Linear extrapolation of river head to pore pressure behind the dike.

Based on Figure 6.10 a parameter λ was derived that can be used to translate river head to pore pressure. Results that were derived for the measurement error and length-effect are depicted in Table 6.3.

	μ	σ
Dike trajectory 100 m	0.553	0.0153
Dike trajectory 2000 m	0.553	0.0371

Table 6.3: Values for uncertainty in λ derived through pore pressure measurements.

6.7. Reliability update for piping

An extrapolation approach is used to update the failure probability for piping. The approach seeks a relationship between high river water levels and their corresponding piezometer levels. On the basis of deviations from a linear correlation an impression can be formed for deviations at other water levels. For this study the element of time is not taken into account. A stationary approach is assumed. TAW (2004) states that for such conditions the extrapolation approach seems justified. Section 3.2 gives more background theory on this approach. Artesian groundwater conditions are required for the extrapolation approach to be justified. Looking at the simplified cross section of our dike, displayed in Figure 5.4, the seepage length of water equals approximately 59 m. Sweco and Arcadis (2019) showed that for this trajectory a head drop of 0.028 m/m can be assumed. The top layer of the aquifer is found to be at 3.65 m + NAP. The required river water level is now easily calculated as seepage length times the head drop plus the top layer of the aquifer, which equals approximately 5.30 m. For the extrapolation approach to be justified therefore multiple measurements need to be executed during river water levels of > 5.30 m + NAP.

Method

As was briefly mentioned linear extrapolation is applied to update the phreatic head behind the dike and ultimately the failure probability for piping. The relationship between the river water level h and the aquifer

hydraulic head ϕ was explained in Section 3.2 and is stated here again:

$$\frac{\phi - \phi_0}{h - \phi_0} = \lambda \tag{6.14}$$

In which ϕ_0 is the hinterland phreatic level and λ the constant that describes the relationship. Measurements of ϕ with their respective river water level conditions yield constant λ. Measurements of ϕ are susceptible to measurement errors as was explained in Section 6.5. Using the theory described in Section 6.5 and Equation 6.14 this uncertainty is translated to λ, making λ a stochastic variable dependent on the hydraulic head. This newly defined stochastic parameter λ is subsequently used to determine the river's hinterland phreatic level, and update the reliability estimate for piping.

Update

In the previous Section a value was derived for λ for both trajectories. These values are used to calculate the aquifer potential at the exit point. For heave and uplift, given by respectively Equations 6.15 and 6.16, the potential at the exit point is a direct input parameter in the limit state equations. The limit state equation for piping, given by Equation 6.17, does not offer the same possibility. The gain in knowledge is here integrated into the formula as the difference between the theoretical potential and the updated potential. For clarity the limit state equations as used for updating uplift, heave and piping are given below:

$$Z_u = m_u \Delta\phi_{c,u} - (\phi_{exit} - h_p) \tag{6.15}$$

$$Z_h = i_{c,h} - \frac{\phi_{exit} - h_p}{d} \tag{6.16}$$

$$Z_p = m_p H_c - (h - h_p - \phi_d - 0.3d) \tag{6.17}$$

In which ϕ_d represents the update in knowledge, defined as the old potential $\phi_{exit,old}$ minus the new potential $\phi_{exit,new}$. For more background info on the limit state equations one is referred to Section 2.2. The updated fragility curves are displayed in Figure 6.11. Figure 6.11a shows the updated fragility curves for the 100 m trajectory and Figure 6.11b for the 2000 m trajectory.

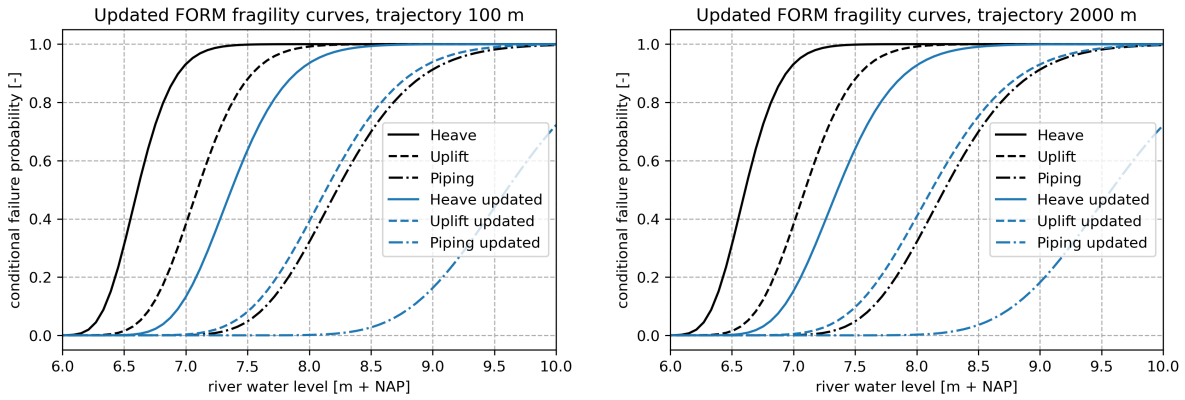

(a) Dike trajectory 100 m, update for 4 pore pressure sensors.

(b) Dike trajectory 2000 m, update for 6 pore pressure sensors.

Figure 6.11: Updated FORM fragility curves. The continuous lines indicate heave, dashed lines indicate uplift and the dashed line with dots indicates piping.

The updated reliability estimates for trajectories one and two are depicted in Table 6.4.

	Uplift	Heave	Piping	Combined
Dike trajectory 100 m	1.40E-2	1.11E-1	1.62E-4	1.62E-4
Dike trajectory 2000 m	1.52E-2	1.16E-1	1.89E-4	1.89E-4

Table 6.4: Failure probability for piping with pore pressure monitoring derived through FORM.

Table 6.5 shows the overall reliability update for backward internal erosion. The updated failure probability does not meet the target failure probability.

	Old [year^{-1}]	Update [year^{-1}]	Target [year^{-1}]
Dike trajectory 100 m	5.21E-3	1.62E-4	8.00E-6
Dike trajectory 2000 m	5.21E-3	1.89E-4	8.00E-6

Table 6.5: Improved failure probability for piping derived through FORM.

Figure 6.12 shows the effect of updating λ based on the expected values for hydraulic head monitoring. The black plot depicts the prior belief of λ and the blue plots show the posterior distribution for λ, in which the dashed line represents the 2000 m trajectory and the continuous line the 100 m trajectory. The result clearly shows that the prior belief results in an overestimation. Furthermore the PDF for the 2000 m trajectory is wider than for the 100 m trajectory. The variation covered for the 100 m trajectory equals 85.4% and for the 2000 m trajectory 88.6 %. The fact that posterior distribution for the 2000 m is wider can therefore be attributed to the length-effect.

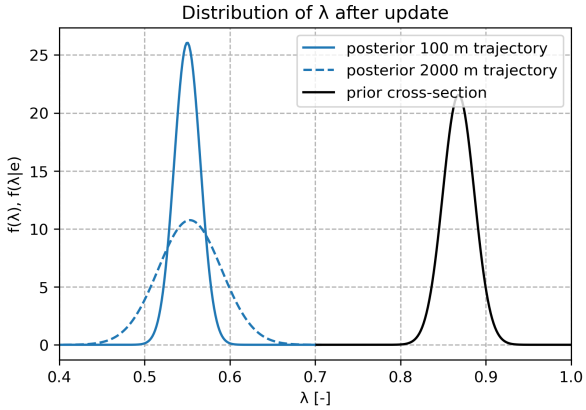

Figure 6.12: PDF for prior and posterior distribution of λ which is used for translating river head to pore pressure behind the dike.

6.8. Sensitivity check for number of sensors and correlation coefficient

In Section 6.5 an assumption was made for the number of pore pressure sensors and correlation coefficient ρ. Therefore, a sensitivity analysis is carried out to check how other values for ρ and the number of sensors influence the outcome.

Number of sensors

The same methodology that was applied in Sections 6.6 and 6.7 is used to determine piping failure probability for set-ups with a different number of pore pressure sensors. This failure probability was then used to calculate the reliability index. Table 6.6 shows derived failure probability. Resulting reliability index is depicted in Figure 6.13. Results indicate that when more pore pressure sensors are used better reliability updates for piping can be performed. However for all set-ups it was not possible to achieve target failure probability.

Number of sensors	2	3	4	5	6	7	8	9
Dike trajectory 100 m	3.82E-4	2.32E-4	1.62E-4	1.53E-4	1.48E-4	-	-	-
Dike trajectory 2000 m	-	-	-	2.52E-4	1.89E-4	1.83E-4	1.81E-4	1.79E-4

Table 6.6: Probability of failure for various pore pressure measurement set-ups.

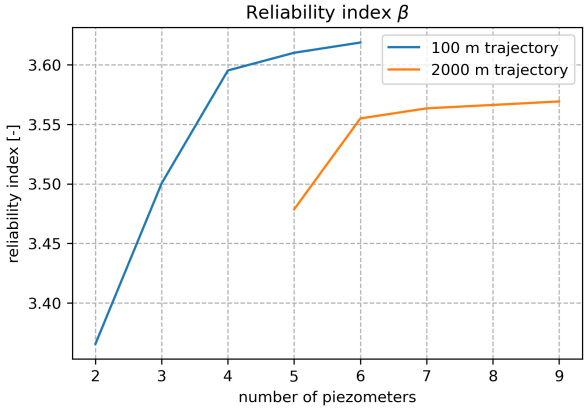

Figure 6.13: Reliability index for piping as function of number of sensors for both dike trajectories.

Correlation coefficient

The effect of correlation coefficient ρ for the measurement error will be shown according to an example for the 100 m trajectory. In Section 6.5 it was stated that for analyses in this thesis a ρ of 0.9 was assumed. This Section serves to illustrate what results would look like if a ρ of 0.5 would be assumed. Figure 6.14a shows the result for a correlation coefficient of 0.9. Figure 6.14b shows the result for a ρ of 0.5. The plots don't deviate much. Table 6.7 shows results that were obtained for λ and the respective piping failure probability. It is shown that a correlation coefficient of 0.5 hardly changes failure probability.

	μ	σ	P_f
$\rho = 0.5$	0.553	0.0153	1.62E-4
$\rho = 0.9$	0.553	0.0207	1.66E-4

Table 6.7: Comparing values for uncertainty in λ for different correlation coefficients ρ for the measurement error.

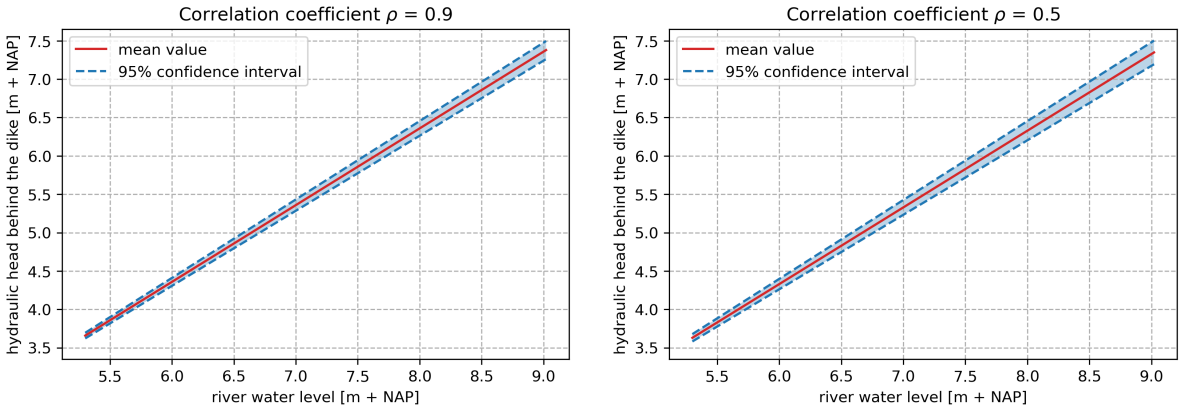

(a) Uncertainty plot for $\rho = 0.9$.

(b) Uncertainty plot for $\rho = 0.5$.

Figure 6.14: Comparing uncertainty bounds for different correlation coefficients ρ for the measurement error.

6.9. Concluding remarks

This Chapter provides answers to subquestions one and two. It was shown how PCA was used to define the least amount of pore pressure sensors necessary for measuring variance in pore pressure behind the dike. The result was implemented in a finite difference model that was used to compute groundwater flow through random fields. Measurement errors were assigned to the sensors. Results showed that for the 100 m trajectory four sensors measure 85.4 % of the variation and for the 2000 m trajectory six sensors measure 88.6 %. It was shown how measurements obtained by the pore pressure sensors can be used to derive an updated λ which was used to improve piping reliability estimate. For the 100 m trajectory reliability improved from 5.21E-3 per year to 1.62E-4 per year. For the 2000 m trajectory reliability improved from 5.21E-3 per year to 1.89E-4 per year. For both trajectories target reliability was not reached, however significantly improved. In Chapter 7 an optimal configuration for pressure relief wells will be derived and subsequently used for improving reliability for slope instability and piping.

7

Derivation of an optimal configuration for pressure relief wells

This Chapter explores the possibility of implementing a pressure relief well system as a way to lower the risk of piping and slope instability. Section 7.1 provides an introduction to the problem and Section 7.2 elaborates on the applied method in this Chapter. In Section 7.3 specifications on the groundwater model are given. Sections 7.4 and 7.5 provide results on stability analysis for various relief well set-ups. Reliability after installation of relief wells is presented in Sections 7.6 and 7.7. Finally Section 7.8 gives some concluding remarks for this Chapter.

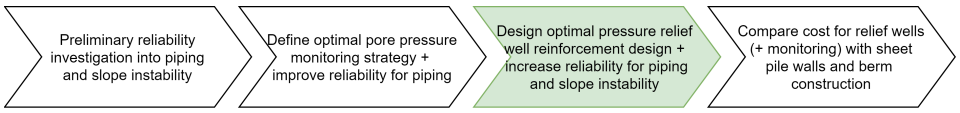

7.1. Problem description

An optimal placement strategy for a pressure relief well system is a multi-objective problem. Ideally one would install as much wells as possible to lower the aquifers hydraulic head and at the same time minimize cost, whilst considering constructive and legal possibilities. For example in the Netherlands it is predetermined by law that a permit is required for surface water discharge. In this study we assume that legal issues do not play a role. The optimal pressure relief well setup is therefore a trade-off between lowering the aquifers hydraulic head and increasing cost. The strategy therefore mainly depends on the aquifers desired head, and the possibility to expand the relief well system in the future. Relief wells can be installed at the land-side toe of the dike. However, it is also not uncommon to install them in the dike's berm. In theory pressure relief wells are positioned behind the dike at equal distance from the toe. In practice a contractor company sometimes has to deviate from this plan due to in situ anomalies, however that is outside the scope of this study. Therefore, this study tries to find the optimal relief well setup for the considered case study, taking soil heterogeneity into mind. A line of relief wells is assumed with longitudinal placement varying between 10-50m along the x-direction depicted in Figure 7.1. The line of wells is then also tested for various z-directions as it is not uncommon to construct a pressure relief well in the dike's berm. Figure 7.1 gives an impression of the area of interest. Exact dimensions will be given in Section 7.4.

7.2. Method for determining optimal well configuration

In Section 7.1 it was discussed that the ideal relief well placement strategy is a trade-off between lowering the aquifers hydraulic head and cost. Like in Chapter 6 two cases will be considered. The first case study considers a trajectory that consists of a stretch of 100 m in front of Wijk bij Duurstede and the second trajectory is a fictitious section in which the cross section of the first trajectory is extrapolated over a length of 2 km. First, an optimal relief well placement strategy will be defined for the 100 m trajectory as there won't be much deviation in subsoil conditions for this trajectory length. Subsequently, the result of this analysis will be used to

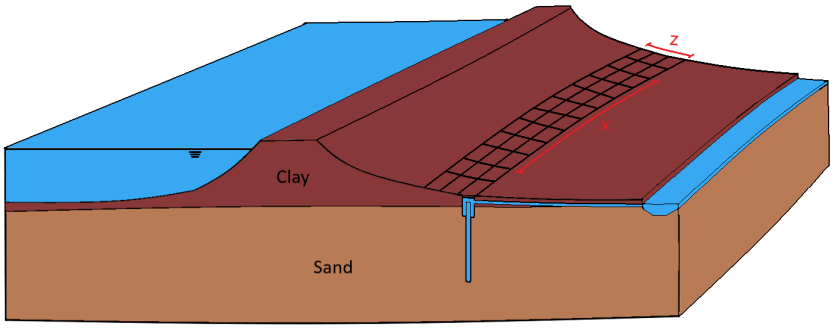

Figure 7.1: Pressure relief well placement (not to scale).

define an optimal relief well placement strategy for the 2 km section. To that end a script will be written that incorporates the soil's heterogeneity. This section provides a simplified example in which the basic principle behind this type of analysis is explained.

As was discussed in the Section 7.1 the ideal pressure relief well placement strategy is first determined for trajectory one and thereafter for trajectory two. This Section will elaborate on the applied theory for the 2000 m trajectory, as the method applied for trajectory one is relatively straightforward once one understands applied strategy for the 2000 m section. Also, implementation of the results in D-Stability will not be discussed here as again this is relatively straightforward.

For this analysis we assume that a stability analysis like the one in Section 5.4 has been performed in advance. Such an analysis shows the area below the dike prone to uplift. This 2D area overlays an area in the aquifer of similar dimensions. This area will be analysed for different set-ups of pressure relief well systems. Most of the time, the area were highest uplift pressures occur is the area in between wells. Figure 7.2 gives a realisation for a measured hydraulic head in the top layer of the aquifer. The black line indicates the hydraulic head if no relief wells would be present, the dashed line gives a realisation of the hydraulic head at the well and the blue line is a realisation of the hydraulic head measured in between wells. This Figure serves purely for illustrative purposes.

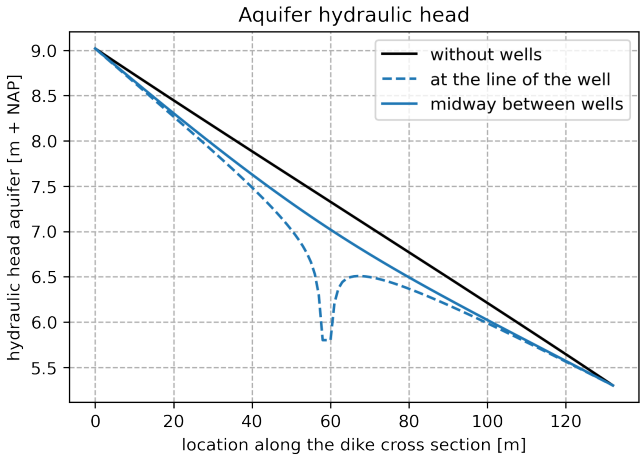

Figure 7.2: Example aquifer head with relief wells.

In this thesis the most unfavorable uplift conditions occurring in a random field will be used to assess a dikes structural integrity. As was shown in Figure 7.2 the most unfavorable conditions occur midway between wells. The results obtained to plot Figure 7.2 refer to one line of cells. The model is discretized so that 1 cell equals 1 m^3 of soil. For piping this approach seems reasonable, however for slope instability this approach

seems rather conservative as uplift pressures along one line of cells will not result in slope instability. A more thoughtful approach would be one in which uplift pressures are averaged over a certain length. Zwanenburg et al. (2013) state that a typical length along which slope stability occurs equals 50 m, this will be adopted in this thesis. This approach might seem a bit strange as one of the main goals in this thesis is to investigate the effect of heterogeneous soil conditions. However it should be realised that even with averaging uplift conditions, still the most unfavorable uplift conditions occurring in the field are taken, which is a direct product from the soil's heterogeneous character. To conclude, the most stringent uplift conditions occurring in the field, averaged over a length of 50 m, will be selected and used for slope instability analysis. This method will be elaborated further in the next paragraph along with a simplified example.

Example

Let's assume an oversimplified fictitious dike section of length 500 m. The aquifer has a width of 133 m and can be modelled with constant head boundaries representing the river's hydraulic head on one side and the hinterland phreatic level on the other side. The aquifer is modelled with the same random field generator that was used in Chapter 6 and explained in Section 6.3, only now the correlation length for soil is set to 30 m for illustrative purposes. A realisation of the hydraulic head in the aquifer is given in Figure 7.3a. The left side represents the imposed head boundary at river side, with a head of 9.02 m, and the right side represents the imposed hinterland head boundary, with a head of 5.30 m. The x-axis represents the width of the dike and the y-axis the length. Three relief wells are implemented, the locations are highlighted with red dots. Results clearly show that at the location of the relief wells the head stays constant at the imposed boundary of 5.8 m. Figure 7.3a also shows that the head in between the wells does not stay constant. Also, the hydraulic head clearly varies in between each of the subsequent wells as it is subject to the soil's heterogeneous character. This becomes more evident for shorter correlation lengths as used in this example.

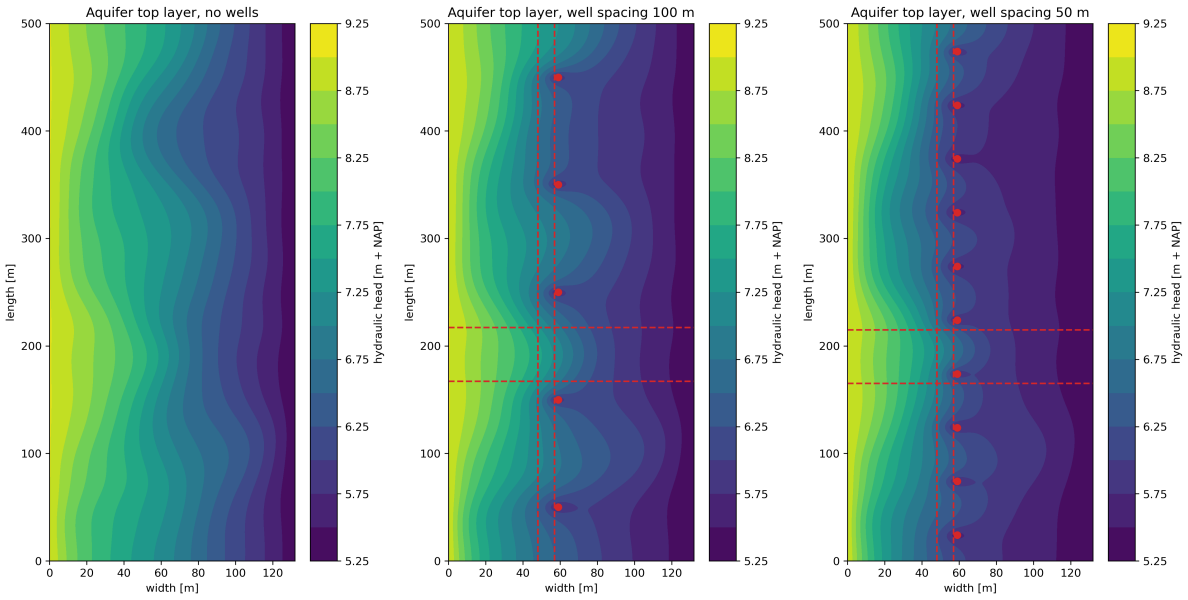

(a) Example 1 (b) Example 2 (c) Example 3

Figure 7.3: Example runs, soil correlation length and well spacing is adjusted for illustrative purposes. Both runs are executed with the same "random" soil composition. Figure 7.3a shows aquifer top layer for set-up without relief wells. Figure 7.3b shows aquifer top layer for set-up with relief wells. Red dots show well locations, vertical red lines indicate critical uplift area beneath the dike, horizontal red lines show the most critical stretch for this dike. Figure 7.3c shows how closer well spacing influences aquifer pore pressure.

The red line in Figure 7.4 shows the shear surface between the dike body and aquifer. Uplift conditions negatively impact the dike's stability in this area. The area beneath the dike that is prone to uplift is highlighted by the two vertical red lines in Figure 7.3b. The script that is written for this analysis now calculates the sum of uplift pressures for each stretch of 50m. With a total dike length of 500 m and a relevant area length of 50 m this gives a total of 450 areas, and therefore 450 uplift pressures. The script now identifies the highest uplift pressure and links it to the area it belongs to. For the current example this area is highlighted by the two

horizontal red lines. For this area the average hydraulic head is now determined for the whole cross section and ready to be used for slope stability analysis.

For the current example only one run is executed for a longitudinal well distance of 200 m. For the actual case study a section of 2 km will be investigated in which multiple longitudinal well placement strategies with y values varying between 55, 50, 45, 40, 35, 30, 25, and 20 m are investigated. Subsequently, the selected scenario will also be investigated for various placement scenarios in which the location of the wells vary over the z direction as indicated in Figure 7.1.

7.3. Specifications of the groundwater model

This section elaborates on the model that is used for evaluating the aquifer's hydraulic head with pressure relief wells. The random fields that are used for this model are again generated using GSTools. The same setup as described in Section 6.3 is used with a correlation length of 300 m. For the flow model again FloPy is used to script the MODFLOW model development, as described in Section 6.3. The implementation of pressure relief wells is discussed below.

Implementation of pressure relief wells

Pressure relief wells are implemented in MODFLOW through the boundary package. The assigned head does not equal hinterland phreatic level, as relief wells are subject to head loss. This was shown in Section 4.2. In this thesis a head loss of 0.5 m is assigned to each relief well. The hinterland phreatic level equals 5.3 m + NAP. The assigned head boundary therefore equals 5.8 m + NAP. For each well the head boundary is assigned to one cell, representing 1 m^3 of soil. For each well, adjacent cells have been given high permeability.

Stability assessment

Stability assessments are performed through D-GEO Suite Stability (van der Meij, 2019), a tool used to analyze slope instability in 2D geometry. A model representing the case study's cross section was provided by Sweco. Hydraulic head lines were pre-calculated using standard design formulas. Stability assessment is performed in a semi-probabilistic way. The aim is to show whether relief wells can be an effective way for increasing a dike's stability. To that end semi-probabilistic stability assessment calculations are assumed to be an adequate measure. Results either clearly indicate the effectiveness of the reinforcement measure or show that is a close call. In case of the latter full probabilistic calculations can be executed to provide more clarity.

Model validation

Constant head boundaries were defined in such a way that the pre-determined hydraulic gradient equals the average gradient occurring in the field. A run for a 100 m section, and therefore nearly homogeneous soil conditions, yields a factor of safety equal to 1.032. The model provided by Sweco yields a factor of safety equal to 1.031. Figure 7.4 shows the model as provided by Sweco, the hydraulic head was derived in (Sweco and Arcadis, 2019). Figure 7.5 shows the hydraulic head as was calculated with MODFLOW for a 100 m dike section with no relief wells. The red line indicates the shear surface between the dike body and aquifer. Uplift conditions negatively impact the dike's stability in this area.

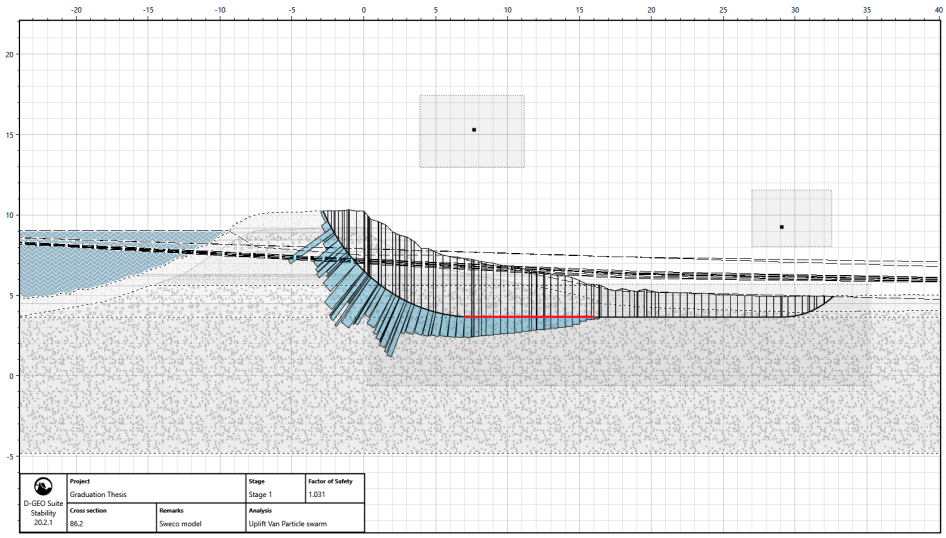

Figure 7.4: Stability model with hydraulic headline provided by Sweco.

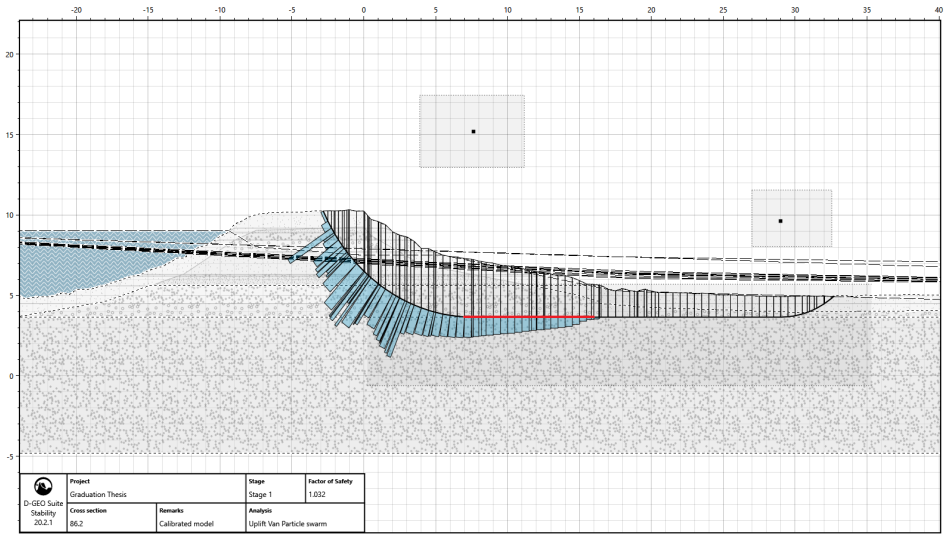

Figure 7.5: Calibrated stability model with hydraulic headline calculated with MODFLOW.

7.4. Stability analysis for varying well spacing

It was shown in Figures 7.3b and 7.3b that well spacing influences aquifer pore pressure. The closer the well spacing, the lower aquifer pore pressure will be. This Sections serves to show how failure probability changes for varying well spacing. The stability checks were executed in accordance with the method explained in Section 7.2. The stability runs are presented in Appendix G. Appendix H shows the head lines that were implemented in D-GEO Suite Stability. The confidence interval indicates head lines for various soil conditions. The results from the stability runs are shown in Table 7.1. The FoS is shown for each well spacing and for each dike trajectory. The results for the 2000 m trajectory give a lower FoS than the results for the 100 m trajectory, this can be attributed to the fact that the chance for weak spots increases with length.

Well spacing [m]	20	25	30	35	40	45	50	55	∞
Dike trajectory 100 m	1.276	1.261	1.249	1.226	1.218	1.209	1.184	1.163	1.032
Dike trajectory 2000 m	1.264	1.248	1.228	1.208	1.190	1.163	1.153	1.140	1.013

Table 7.1: Factor of Safety for well spacing derived through D-GEO Suite Stability.

The results that are derived through the method explained before are depicted in Figure 7.6. The x-axis shows the well spacing in increasing order and the y-axis shows the reliability index. The blue line refers to the 100 m trajectory and the green line to the 2000 m trajectory. The dashed red line indicates the cross-sectional target reliability index for slope instability. Results indicate that for the 100 m trajectory a wider well spacing suffices, as opposed to the 2000 m trajectory. This makes sense as the chance for possible weak spots increases with length. Figure 7.6 clearly shows that for the 100 m trajectory a well spacing of 50 m suffices and for the 2000 m trajectory a well spacing of 40 m. Section 7.5 will explore the possibility of placing wells on the inner slope as a way to meet the target reliability with wider well spacing.

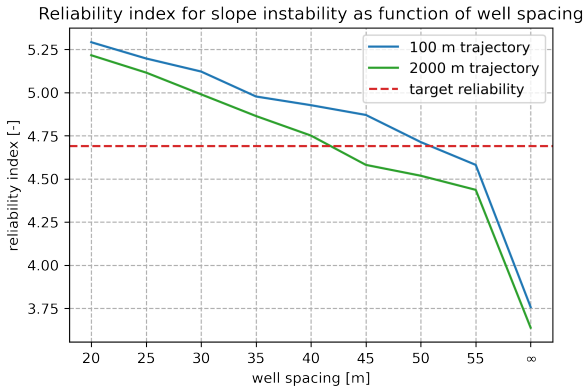

Figure 7.6: Reliability index for varying well spacing.

7.5. Placing wells on the inner slope

sec:resultswellspace It was mentioned in Section 7.1 that it was an aim to find out whether placing wells in the dike's berm can positively influence the reliability estimate for slope instability. Figure 7.7 gives a schematic overview of the considered locations for relief wells on the inner slope.

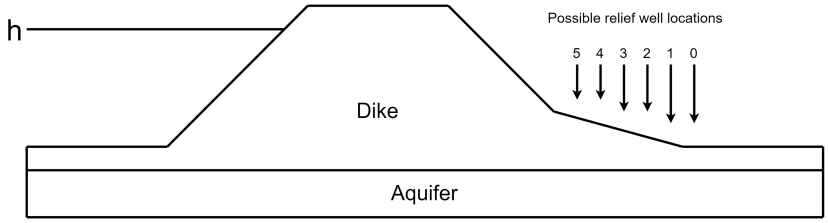

Figure 7.7: Possible relief well locations on the inner slope.

In Section 7.4 it was shown that for the 100 m trajectory a well spacing of 50 m resulted in adequate reliability and for the 2000 m trajectory a well spacing of 40 m was required. It is desired to construct relief wells as deep as possible in the aquifer layer as this positively induces artesian flow. Therefore, constructing wells near the inner toe of the dike is considered economically more attractive as the aquitard layer is thinner there compared to the dike's berm. Nevertheless constructing wells on the dike's berm can become more attractive if the reliability estimate for slope instability is guaranteed with wider well spacing. As was briefly mentioned before the 100 m trajectory required a well spacing of 50 m and the 2000 m trajectory requires a well spacing of 40 m. Therefore for the 100 m trajectory research will be performed to find out whether placing wells at a spacing of 55 m on the inner berm can guarantee the same reliability. For the 2000 m trajectory a similar approach is used, only now with wells with a spacing of 45 m. It is assumed that the maximum depth to penetrate the clay layer equals 3 m. This results in wells to be placed on the berm at a maximum distance of 5 m from the inner toe. Table 7.2 shows the FoS that was derived for placing wells on the inner berm.

Distance from the inner toe [m]	0	1	2	3	4	5
Dike trajectory 100 m, 55 m spacing	1.163	1.166	1.171	1.172	1.177	1.180
Dike trajectory 2000 m, 45 m spacing	1.163	1.169	1.173	1.178	1.182	1.186

Table 7.2: Factor of Safety for different locations in the berm derived through D-GEO Suite Stability.

It is shown that decreasing well spacing has little influence on FoS. However the reliability index is sensitive to small changes in FoS and can be used to show increase in reliability. The results depicted in Table 7.2 are used to derive the reliability estimate. Figure 7.8 displays the results. The x-axis refers to the distance of the well from the inner toe of the dike in increasing order. The y-axis shows the reliability estimate. The dashed red line shows the target reliability. Results clearly indicate that placing wells on the inner slope positively influences the reliability estimate for slope instability. It was found that for the 100 m trajectory a well spacing of 55 m could not increase the reliability estimate to an adequate level. For the 2000 m trajectory it was found that a well spacing of 45 m could assure an adequate reliability estimate when placed in the dike's berm at a distance of four metres from the inner toe.

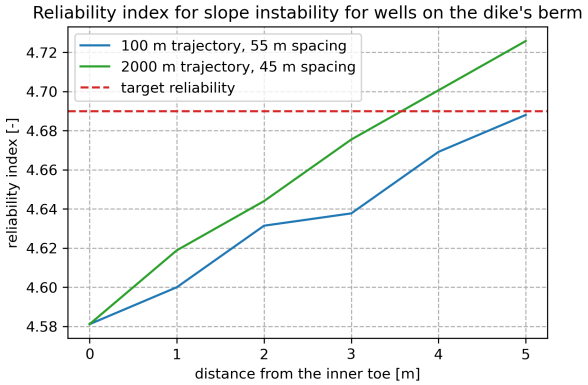

Figure 7.8: Reliability index for different well locations on the inner slope.

7.6. Reliability after reinforcement for slope instability

Calculating reliability for slope instability after reinforcement is rather straightforward. The well spacing is determined based on the assigned target reliability. As was mentioned in Section 7.5 the required well spacing for the 100 m trajectory equals 50 m and for the 2000 m trajectory 45 m. The FoS corresponding to the 100 m trajectory equals 1.184 and the FoS corresponding to the 2000 m trajectory equals 1.182. The derived failure probabilities are given in Table 7.3. Results show that the updated failure probability satisfies the target reliability.

	Old [year^{-1}]	New [year^{-1}]	Target [year^{-1}]
Dike trajectory 100 m	8.81E-5	1.22E-6	1.33E-6
Dike trajectory 2000 m	8.81E-5	1.30E-6	1.33E-6

Table 7.3: Probability of failure after reinforcement for slope instability.

7.7. Reliability after reinforcement for piping

Reliability reduction for piping is executed the same way as was done in Section 6.7. Results that are derived for the 100 m trajectory are depicted in Figure 7.10a, Figure 7.10b shows the results that were derived for the 2000 m trajectory. The implemented relief wells are situated at ground level which is at 5.3 m + NAP. It was derived in Section 4.2 that a head loss of 0.5 m would be assumed. Therefore the relief wells will only function for groundwater pressures exceeding 5.8 m + NAP at the location of the well. The required river head h_r is now calculated the same way as was done in for example Section 6.7. Figure 7.9 gives a graphical representation of h_r.

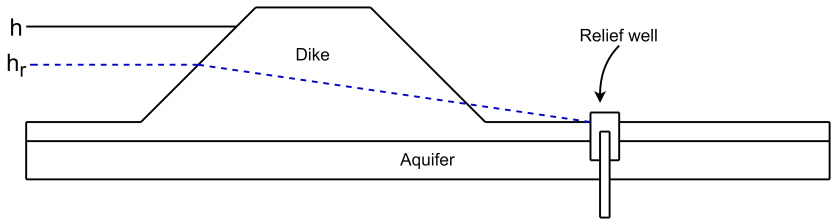

Figure 7.9: Cross section dike with minimum required river head h_r required for the wells to function.

The required hydraulic head differs slightly for the two dike trajectories as for the 2000 m trajectory relief wells are situated on the inner slope, hence the seepage length is shorter. Results are depicted in Table 7.4.

	Seepage length [m]	Required head at the well [m + NAP]	Required head difference [m]	Required river head [m + NAP]
Dike trajectory 100 m	59	5.8	1.65	7.45
Dike trajectory 2000 m	55	5.8	1.54	7.34

Table 7.4: Required river head for relief wells to function.

As was shown in Table 7.4 minimum river head is required for the relief wells to work. Hence only for river heads exceeding those minimum levels new values for λ can be acquired. The approach seems justified as failure occurs for high river water levels. The new relation between river head and hydraulic potential behind the dike is shown in Figure 7.10. Figure 7.10a shows the relation for the 100 m trajectory and Figure 7.10b for the 2000 m trajectory. Values for λ are derived the same way as was done in Section 6.6. Figures 6.10a and 6.10b therefore show the same relation only before implementation of pressure relief wells. Results are shown in Table 7.5.

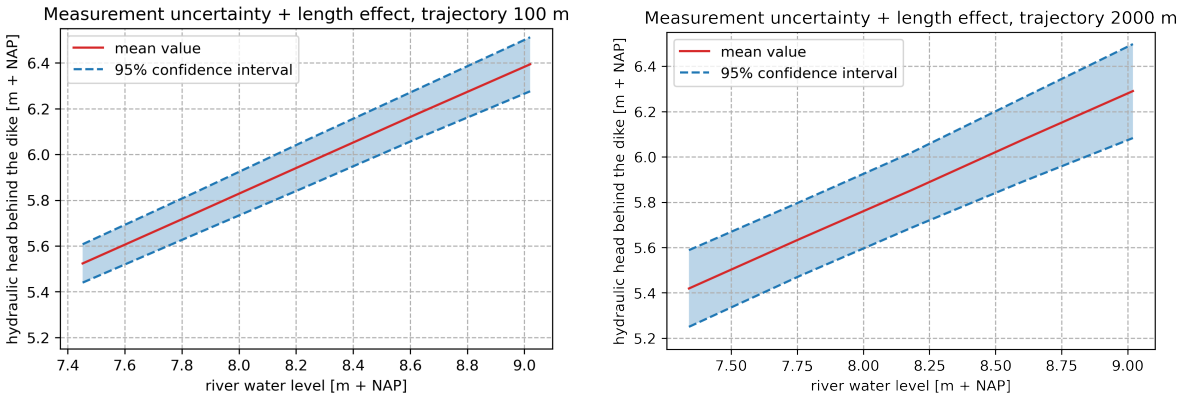

(a) Uncertainty after relief well implementation, 100 m trajectory.

(b) Uncertainty after relief well implementation, 2000 m trajectory.

Figure 7.10: Linear extrapolation aquifer head, after relief well implementation.

The limit state equations as given by Equations 6.15, 6.16 and 6.17 are used for recalculating reliability. The same procedure as in Section 6.7 is applied. The fragility curves derived through FORM are depicted in Figures 7.11a and 7.11b. The blue lines indicate the result after the first reliability update, the orange lines show

	μ	σ
Dike trajectory 100 m	0.296	0.0155
Dike trajectory 2000 m	0.266	0.0279

Table 7.5: Value for λ after relief well implementation.

the probability of failure after reinforcement. It has to be mentioned that the probability of failure determined after reinforcement is fitted to high river water levels in which relief wells function. This leads to overestimation of the failure probability at low river water levels. Nevertheless failure occurs for high river water levels and the method therefore seems justified.

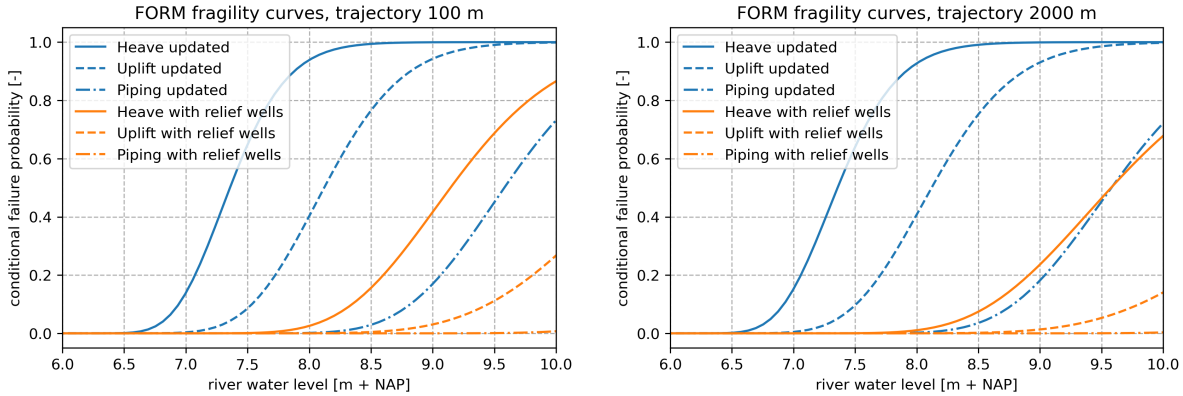

(a) Dike trajectory 100 m, after relief well implementation.

(b) Dike trajectory 2000 m, after relief well implementation.

Figure 7.11: FORM fragility curves after relief well implementation. The continuous lines indicate heave, dashed lines indicate uplift and the dashed line with dots indicates piping.

The updated probability of failure for backward internal erosion is depicted in Table 7.6.

	Uplift	Heave	Piping	Combined
Dike trajectory 100 m	3.14E-5	8.83E-4	2.03E-7	2.03E-7
Dike trajectory 2000 m	1.41E-5	4.22E-4	1.02E-7	1.02E-7

Table 7.6: Failure probability for piping with relief wells derived through FORM.

Table 7.7 shows the result for the increase in reliability for backward internal erosion. The updated failure probability now meets the target failure probability for both trajectories.

	Old [year^{-1}]	Update [year^{-1}]	With relief well [year^{-1}]	Target [year^{-1}]
Dike trajectory 100 m	5.21E-3	1.62E-4	2.03E-7	8.00E-6
Dike trajectory 2000 m	5.21E-3	1.89E-4	1.02E-7	8.00E-6

Table 7.7: Increased failure probability for piping derived through FORM.

Figure 7.12 shows the effect of the reliability increase for λ based on the expected values for hydraulic head monitoring in combination with relief wells. The blue plots show the result of the reliability update as was determined in Section 6.7. The orange plots show the pre-posterior belief of λ after relief well implementation. For both updates the dashed line represents the 2000 m trajectory and the continuous line the 100 m trajectory. The results show that for relief well implementation the PDF of the 2000 m trajectory is located further to the left than the one for the 100 m trajectory. This might seem strange as the 100 m trajectory has a higher density in piezometers. However this result can be explained by the fact that the density of relief wells is higher on the 2000 m trajectory, hence the occurring hydraulic head in between the wells is smaller.

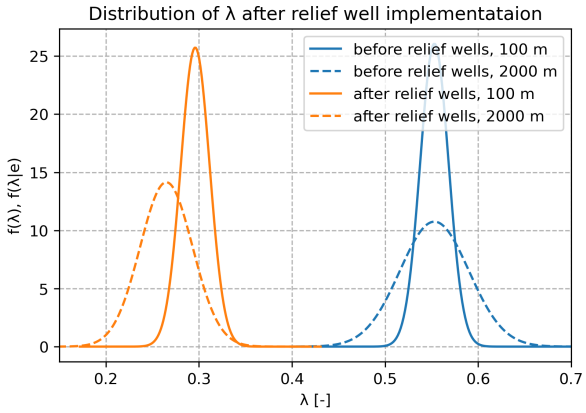

Figure 7.12: PDF for distribution of λ. Blue plots show distribution after reliability update. Orange plots show distribution after relief well implementation. Continuous lines are for 100 m trajectory and dashed line for 2000 m trajectory.

7.8. Concluding remarks

This Chapter provides answers to subquestions three and four. It was shown how an optimal configuration for pressure relief wells was derived using a combination of a finite difference model that was used to compute groundwater flow through random fields and stability software. The system was designed to mitigate risk for slope instability. It was subsequently also shown how this system in combination with pore pressure sensors can be used to increase reliability against piping. For the considered case study a combination of pore pressure monitoring and pressure relief well implementation has proven to be an adequate measure for meeting target reliability for both failure modes. For the considered case study optimal relief well spacing was found at 50 m for the 100 m trajectory and 45 m for the 2000 m trajectory. For the 2000 m trajectory it was found that placing wells on the berm had positive impact on relief well spacing. The relief well set-up was designed according to target failure probability for slope instability. Subsequently the new set-up was used in combination with pore pressure sensors to update failure probability for piping. It was shown that relief wells can be used to increase reliability up to target failure probability for slope instability and piping. Chapter 8 will now compare the combination of pore pressure monitoring and relief well implementation with more traditional reinforcement measures such as berms and sheet pile walls.

8

Comparing various design options

This Chapter evaluates whether pore pressure monitoring in combination with pressure relief wells is a cost-effective design option. Section 8.1 discusses the framework for which it is evaluated. A successful monitoring campaign depends on whether useful measurements were taken. Section 8.2 discusses possible outcomes of a monitoring campaign. General theory behind cost of a strategy is elaborated in Section 8.3. Section 8.4 then discusses some assumptions and simplifications that were made to obtain results that are also presented here. Finally Section 8.5 concludes this Chapter.

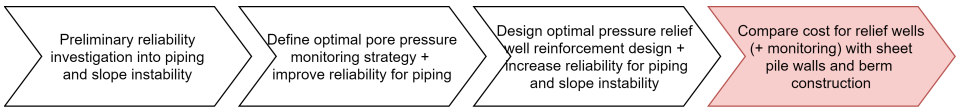

8.1. Decision framework

As has been mentioned before the aim of this thesis is to investigate whether pore pressure monitoring in combination with pressure relief wells is an adequate measure in assuring a dike's reliability estimate. To that end a case study has been performed. Results of this study will provide (part of) a framework to answer the question whether the proposed method is practical. The case study was briefly elaborated on in Chapter 5. To evaluate the benefits of pore pressure monitoring Bayesian pre-posterior analysis is used. The basic idea is that the best decisions are made based on a-priori information by evaluating all possible outcomes. For more information on this type of analysis one is referred to Section 2.1 in this thesis. In Section 1.4 a decision tree was introduced to visualise and structure analysis in this thesis. Figure 8.1 depicts the same decision tree as it provides a concise overview to structure pre-posterior decision analysis.

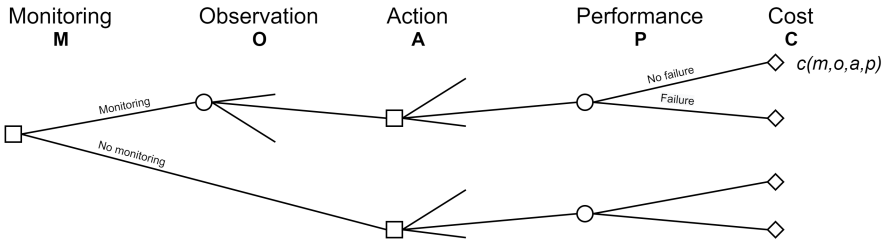

Figure 8.1: Decision tree for sequential decision on monitoring and reinforcement used in the case study. Squares indicate choice nodes and circles indicate chance nodes.

The decision tree as depicted in Figure 8.1 shows a sequence of decision nodes and outcome nodes. The squares are decision nodes, which represent possible choices for a decision maker. A decision maker for example opts to perform monitoring or not. The circles represent chance nodes and are outcomes of choices made by the decision maker. Chance nodes depend on the decision taken and prior information of the state of the system. In the evaluation of the choices on pore pressure monitoring and reinforcement measures it is

desired to evaluate the optimal strategy based on the prior belief of the system.

The first decision in the decision tree is the option to invest in pore pressure monitoring in order to reduce uncertainty with respect to hydraulic potential at the hinterland toe of the dike. The measured potential depends on outside water levels. Therefore general separation can be made between a situation in which an observation is made or not. This depends on whether river water level exceeds a certain threshold required to obtain useful measurements. In order to apply Bayesian updating, linear extrapolation between river water level and hinterland potential is applied. Background theory on this is extensively covered in Sections 3.2 and 6.7. It was discussed in Section 6.7 that at least three realisations of threshold exceedance are required. For this case study the threshold was determined at 5.30 m + NAP. Section 8.2 will elaborate further on possible outcomes of a monitoring campaign and how it is incorporated in the decision process.

The second decision in the decision tree considers possible reinforcement measures as was elaborated in Chapter 7. In this thesis the possibility of implementing a pressure relief well system is compared with more traditional reinforcement measures including berm construction and sheet pile wall installation. The case study considers a dike in a densely populated area, hence berm construction will induce relocation of houses near the inner slope which is an important cost driver. Section 8.3 elaborates further on how total cost for each reinforcement measure is determined.

8.2. Possible outcomes of the monitoring campaign

It was briefly mentioned before that a general separation is made between two scenarios, one in which useful observations are made and one in which not. In order to apply Bayesian updating as suggested in this thesis at least three useful observations are required. Useful observations are defined as observations at a river water level h higher than a predefined threshold river water level h_t. This threshold water level induces artesian groundwater conditions which are required for Bayesian updating. The probability of obtaining one valuable measurement is now computed according to:

$$P = 1 - F\big(h > h_t\big)^t \tag{8.1}$$

In which $F\big(h > h_t\big)$ equals the cumulative probability per year that $h > h_t$and t is the duration of the monitoring campaign. The duration for the monitoring campaign t was extensively discussed in Section 1.1 and equals five years for this example. It was determined in Section 6.7 that artesian groundwater conditions arise for river water level $h_t > 5.30$ m + NAP. The number of required observations equals three. Observations cannot be equal, it is assumed that they need to differ at least 10 cm. A Gumbel distribution has been fitted to river water level data from 5.3 to 6.6 m. The data was acquired through Hydra-Ring. The fit is depicted in Appendix E in Figure E.2. The Gumbel distribution has a mean value μ of 3.79 m and a standard deviation σ of 1.80 m. It is assumed that three useful observations need to differ at least 10 cm. Also, for $h_t > 5.30$ m + NAP groundwater conditions change from phreatic to artesian. It is assumed that for $h_t = 5.40$ m + NAP groundwater conditions are fully artesian. Therefore at least three water levels are required for $h_t \geq 5.40$ m + NAP with at least 10 cm in between each measurement. This means that useful measurements will be obtained for $h_t \geq 5.60$ m + NAP. Table 8.1 now depicts this water level including cumulative probability. Equation 8.1 was used to derive probability belonging to this measurement, P now equals 0.839. The probability that the monitoring campaign yields useful outcome therefore equals 0.839.

River water level [m + NAP]	Cumulative probability [year^{-1}]	P [-]
5.6	0.694	0.839

Table 8.1: River water levels with cumulative probability.

8.3. The cost of a strategy

The cost of the optimal strategy is based on the lowest cost for a branch in the decision tree as depicted in Figure 8.1. van der Krogt et al. (2020) provide a way to evaluate the cost of the optimal strategy. A similar approach will be used here. The cost of a branch in the decision tree is calculated by the sum of every individual step including the cost for expected damage given the performance: $c(m,o,a,p)$. The cost of the optimal strategy is now calculated by the sum of costs for each decision node in the branch representing the optimal strategy:

$$c(m,a) = I_m \cdot c_m + \int_{f_X(x)} c_r(a,x) + c_f(a,x)dx \tag{8.2}$$

In which I_m is an indicator variable indicating whether monitoring was executed, c_m is the cost component for a monitoring campaign, c_r is the cost component for reinforcement and c_f the cost component for failure. The cost components of reinforcement c_r and failure c_f both depend on action a and realization x.

Reinforcement measures considered in this thesis include berms, diaphragm walls and relief wells. Costs for the first two measures are relatively high, however hardly any maintenance is required after installation. Initial costs for relief wells are relatively low compared to berms or diaphragm walls, however regular maintenance is required over the lifetime of the wells. Therefore in order to compare those reinforcement measures a life cycle costing (LCC) approach is used. This approach considers all costs that will be incurred during the lifetime of the reinforcement. Maintenance costs are assumed to be constant in time. Therefore for maintenance costs c_m an infinite time horizon is considered. Using LCC the present value for a dike reinforcement with an infinite time horizon can now be determined according to:

$$LCC = c_r + \frac{c_{m,f}}{r} \tag{8.3}$$

In which c_r is initial investment for reinforcement, $c_{m,f}$ is the constant future value of maintenance cost and r the discount rate. For the present value of failure cost the same approach is used. The annual failure probability is assumed to stay constant in time. The present value for failure costs $c_f(a,x)$, for convenience here denoted as LCR, is now given by:

$$LCR = \frac{P(F|a,x) \cdot D}{r} \tag{8.4}$$

In which $P(F|a,x)$ represents the chance of failure given action a and realization x, D represents the expected damage in case of a flood and r is the discount rate. The total cost (TC) is now simply given by the summation of LCC and LCR:

$$TC = LCC + LCR \tag{8.5}$$

Decision analysis in this thesis uses the Value of Information (VoI) principle to quantify the expected increase in utility due to additional information. The principle was first explored by Raiffa and Schlaifer (1961). The lower branch in the decision tree depicted in Figure 8.1 is regarded the base-case scenario without monitoring. The cost of the base-case scenario is defined as c_0. The VoI of a strategy with monitoring is now determined according to:

$$VoI = c_0(a) - c(m,a) \tag{8.6}$$

Table 8.2 shows the parameters that were used for cost analysis. Values for r, D and c_m were used before in van der Krogt et al. (2020) and seem reasonable. Values for c_b, c_s and c_r were acquired through Movares (2021) in which a similar like comparison was made between relief wells and more traditional reinforcement techniques. The cost for removing a house was used before in Klerk et al. (2019a) and is adopted in this thesis. Values for relief well maintenance are difficult to define as the technique is relatively new and few reference projects are available. Based on USACE (1992) values for c_{rm} were estimated.

Parameter	Unit	Description	Value
r	[-]	annual discount rate	0.035
D	[million €]	damage in case of flooding	5000
c_m	[million €]	cost per km for 5 years of pore pressure monitoring	0.1
c_b	[million €]	cost per km for constructing a berm monitoring	3
c_s	[million €]	cost per km for installing a sheet pile wall	7
c_r	[million €]	cost for installing one relief well	0.1
c_{rm}	[thousand €]	cost per year per relief well for maintenance	1
c_h	[million €]	cost for removing one house	0.5

Table 8.2: Parameters used for cost analysis.

8.4. Results

The parameters as used for deriving total cost per strategy are shown in Table 8.2. The chance for obtaining useful results through monitoring were derived in Section 8.2 and equal 0.839. Figure 8.2 shows the obtained results. Some assumptions and simplifications that were made are discussed.

Risk

The cost for risk was calculated according to Equation 8.4. For relief well implementation (+ maintenance) risk was derived based on probabilities of failure as derived in Sections 7.6 and 7.7. It is assumed that for other failure modes target failure probability is met. For reinforcement methods berm and sheet pile wall it is also assumed that reinforcement was applied up until target reliability level.

Construction and maintenance

The cost for construction and maintenance were determined according to Equation 8.3 and are based on values presented in Table 8.2. It is assumed that berm construction and sheet pile wall installation increase reliability up until target reliability level for cost as given in Table 8.2. Construction cost for relief well implementation plus monitoring are based on the number of relief wells for the 2000 m trajectory. The number of relief wells is derived from results on well spacing that was determined in Sections 7.4 and 7.5. For relief well implementation without monitoring it was found that well spacing decreased from a spacing of 45 m to a spacing of 40 m. Maintenance cost are obtained from HDSR (2017) and were determined for the number of relief wells on a trajectory. It is assumed that maintenance for berms and sheet pile walls is nil and is therefore not taken into account for this analysis.

Relocating houses

For berm construction additional space behind the dike is required. It is assumed that an average of 10 houses per kilometer are located at the hinterland toe of the dike. It has to be mentioned that only cost for relocation are included. Societal impact of relocating houses is not expressed in cost and therefore not taken into account.

Monitoring

Cost for pore pressure monitoring are included for design option relief well plus monitoring. The value as presented in Table 8.2 is incorporated.

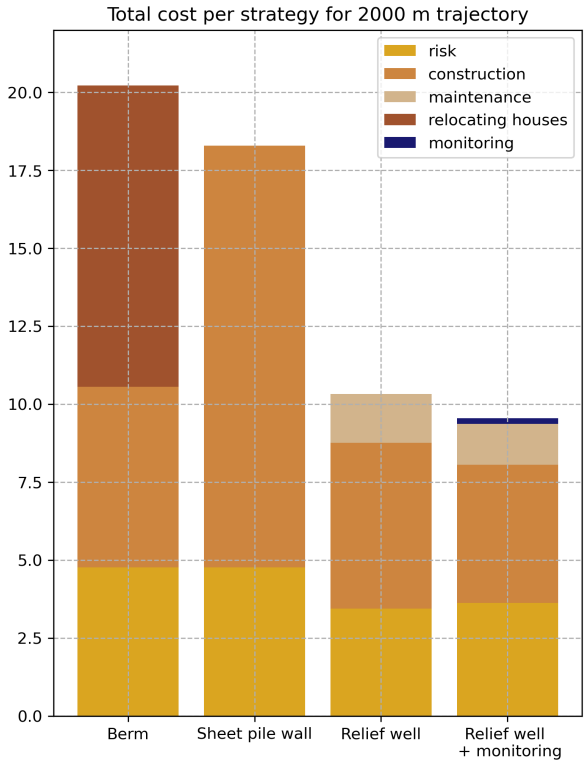

Figure 8.2: Net present value of total cost per strategy for the case study, colours indicate the contribution of various components to total cost of a strategy.

Results show that construction cost for sheet pile walls exceeds construction cost for the other design options. Nevertheless berm construction is the most expensive design option as relocation of houses forms an important cost driver. Relief wells form most cost-effective design option. The LCC approach is applied and it is shown that maintenance cost for relief wells remain manageable. For the considered dike trajectory it is concluded that net present value is most attractive for pressure relief wells. Relocation cost for houses and maintenance cost for relief wells are very case specific. In order to provide insight into the preferred option for other values of house removal cost or relief well maintenance cost Figure 8.3 provides more insight.

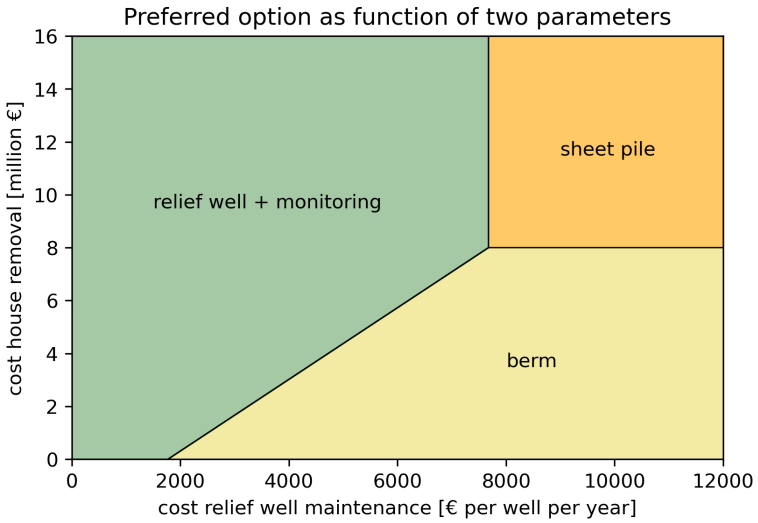

Figure 8.3: Preferred design option as function of cost for house removal and cost for relief well maintenance.

Value of information

The VoI is determined according to Equation 8.6 and is simply stated the total cost for a situation without monitoring minus a situation with monitoring. In this thesis monitoring was only applied in the situation for relief well implementation, hence VoI is only determined for relief wells versus monitoring and relief wells. Table 8.3 shows the results. It is shown that for the considered case study total cost have decreased from 10.3 million € to 9.5 million €, hence the VoI equals 0.8 million €.

Strategy	Total cost [million €]
Without monitoring	10.3
With monitoring	9.5
Value of information	0.8

Table 8.3: Value of information obtained through pore pressure monitoring for relief well implementation.

8.5. Concluding remarks

This Chapter provides an answer to subquestion five. For the considered case-study pressure relief wells provide a good design alternative for reinforcement. It was shown that compared to more traditional reinforcement measures such as berms and sheet pile walls, pressure relief wells provide a more economically attractive design alternative. It has to be mentioned that for berm construction total cost are relatively high as relocation of houses forms an important cost-driver. If relocation of houses would be ignored total cost would approach that of relief well implementation. It was shown that for this case-study pore pressure monitoring yields a positive VoI of 0.8 million €.

9

Conclusion and recommendations

The objective of this thesis was to investigate benefits of pore pressure monitoring and pressure relief wells in spatially variable soils. Section 9.1 gives answers to the research questions. Section 9.2 presents some discussion and recommendations for future research.

9.1. Answers to the research questions

The main research question that was posed at the beginning of this thesis was:

How can the effect of pore pressure monitoring and pressure relief wells on dike reliability and resulting reinforcement be assessed in spatially variable soils?

This thesis has shown how spatial variability in soil can be incorporated in reliability analysis. Spacial variability in soil was modelled using random fields that represent soil heterogeneity. Pore pressure was calculated by means of a finite difference model that was used to calculate groundwater flow through random fields. Results were subsequently used to perform 2D analyses for the relevant failure modes. Backward internal erosion was assessed through probabilistic analyses using limit state equations. For piping the revised Sellmeijer formula was used. Slope instability was assessed using stability software. Limit equilibrium model Uplift-Van was used for semi-probabilistic stability checks. The research was split into parts and five sub-questions were created to help answer the main question. The sub-questions and their corresponding answer are listed as follows.

1. How can spatially variable soils be incorporated in optimizing a pore pressure monitoring strategy?

This thesis focused on defining an optimal pore pressure monitoring strategy for describing pore pressure at the hinterland toe of the dike. The goal was to find optimal longitudinal spacing for sensors taking soil heterogeneity into mind. Pore pressure was determined by modelling groundwater flow through random fields. Measurement errors were included in pore pressure measurements. The aim was to measure as much variation in pore pressure with the least amount of sensors. It was found that for the 100 m trajectory four piezometers measure 85.4 % of the variation in pore pressure and for the 2000 m trajectory six piezometers measure 88.6 % of the variation in pore pressure. The increase in measured variation significantly drops when more peizometers are added and it was therefore concluded that this was the optimal set-up.

2. What is the effect of including pore pressure monitoring on piping reliability estimate for the considered case study?

The pore pressure monitoring set-up was implemented and used for improving piping reliability estimate. It was found that for both trajectories the reliability estimate increased significantly. For the 100 m trajectory the reliability estimate improved from 5.21E-3 per year to 1.62E-4 per year. For the 2000 m trajectory the reliability estimate improved from 5.21E-3 per year to 1.89E-4 per year. For both trajectories target reliability was not reached. However it can be concluded that the pore pressure monitoring approach did significantly improve piping reliability estimate.

3. How can spatially variable soils be accounted for in determining the configuration of pressure relief wells?

An optimal configuration for pressure relief wells in spatially variable soils was derived. Again aquifer pore pressure was calculated by modelling groundwater flow through random fields. Pore pressure was averaged over 50 m and most unfavourable conditions were used for stability analysis. For the considered case-study a straight dike trajectory was assumed, relief wells were therefore equally spaced and positioned on one line. The configuration was designed based on target reliability for slope instability. For the 100 m trajectory it was found that a spacing of 50 m along the hinterland toe of the dike increased reliability for slope instability up until target reliability level. Placing wells on the inner slope of the dike did increase reliability, however spacing between the wells could not be reduced. For the 2000 m trajectory it was found that a spacing of 40 m increased reliability for slope instability up until target reliability level. Locating relief wells on the inner slope did increase reliability to such an extent that well spacing could be increased to 45 m.

4. What is the effect of including relief wells on the reliability against piping and slope instability for the considered case study?

The relief well set-up was designed based on target reliability for slope instability. It was shown that for the considered case study it was possible to increase reliability with pressure relief wells. For the 100 m trajectory reliability for slope instability increased from 8.81E-5 per year to 1.22E-6 per year. For the 2000 m trajectory reliability increased from 8.81E-5 per year to 1.30E-6 per year. Target reliability for slope instability was equal to 1.33E-6 per year. Pore pressure monitoring was used to increase piping failure probability. For the 100 m trajectory it was found that probability of failure increased from 1.62E-4 per year to 2.03E-7 per year. For the 200 m trajectory probability of failure increased from 1.89E-4 per year to 1.02E-7 per year. With a target reliability equal to 8.00E-6 per year both trajectories satisfied stability requirements.

5. To what extent can pore pressure monitoring and/or pressure relief wells contribute to more cost effective dike reinforcement designs?

For the considered case study it was concluded that implementation of pressure relief wells can be economically attractive compared to sheet pile walls and berms. Initial cost for sheet pile walls are high and in urban areas relocation of houses forms an important cost driver in the case of stability/piping berms. It was found that a combination of pore pressure monitoring and pressure relief wells yielded a positive value of information of 0.8 million € compared to a situation in which a pressure relief well system would be designed without prior knowledge acquired through pore pressure monitoring.

9.2. Recommendations for future research

In this thesis finite modelling software MODFLOW was used in combination with a random field generator GSTools, the length-effect was therefore incorporated through random fields. A correlation length for soil of 300 m has been used throughout this thesis. This approach has shown that more optimized designs can be realized when the lengt-effect effect is incorporated through random field modelling instead of through a length-effect factor. It is recommended to conduct more analyses with other values for correlation lengths to check whether the outcome changes significantly. Also, the effect of anomalies have not been included in this analysis and should be investigated as it can significantly influence the outcome.

In this thesis it was assumed that flow through a relief well could be disposed on surface water in the hinterland. However many waterboards in the Netherlands are reticent when it comes to disposing water in the hinterland. A practicality assessment should therefore be carried out to check whether it is feasible. In Section 4.2 realistic values were derived for flow through a relief well that can be used for such an assessment. If not possible, it should be investigated whether it is feasible to pump water back over the dike during high water conditions.

Pore pressure monitoring was used to update piping failure probability. If pore pressure sensors are installed in a row perpendicular to the direction of the dike it is also possible to improve reliability against slope instability with pore pressure monitoring. It is recommended to conduct more research on this as in some cases required well spacing might increase making the proposed design alternative more cost-effective. Slope instability was assessed with semi-probabilistic analysis. It should be investigated whether probabilistic analysis

can generate new insights and possible result in a more economic relief well design.

Information on pressure relief wells is scarce in the Netherlands. As such some (conservative) assumptions were made in this thesis. It should be investigated to what extent clogging affects flow through a relief well over lifetime. It is also desired to have a more in-depth analysis on required maintenance in order to have a better grip on costs over the lifetime of a relief well. In that way a more accurate estimate can be made and used as blueprint for other reinforcement projects.

The research conducted in this thesis was based on a case study. As such permeability and hydraulic head boundary conditions that were pre-determined were implemented in the groundwater model. It is recommended for future research to evaluate results for varying permeability values and varying boundary conditions.

Bibliography

J.P. Aguilar-López and T.A. Bogaard. Dike Monitoring Methods. Technical report, DOMINO, 2014a.

J.P. Aguilar-López and T.A. Bogaard. Expertise Interviews on Dike Monitoring. Technical report, DOMINO, 2014b.

J. Allgeier, A. González-Nicolás, D. Erdal, W. Nowak, and O.A. Cirpka. A Stochastic Framework to Optimize Monitoring Strategies for Delineating Groundwater Divides. *Frontiers in Earth Science*, 8, 11 2020. ISSN 2296-6463. doi: 10.3389/feart.2020.554845. URL `https://www.frontiersin.org/articles/10.3389/feart.2020.554845/full`.

S. Bakkenist, O. van Dam, A. van der Nat, F. Thijs, and W. de Vries. *Directorate-General for Public Works and Water Management*. Stowa, Amersfoort, 2012. ISBN 978.90.5773.542.4. URL `www.stowa.nl`.

S.W. Bakkenist and W.S. Zomer. *Inspectie van waterkeringen, een overzicht van meettechnieken*. STOWA, Amersfoort, 2010. ISBN 978.90.5773.486.1.

M. Bakker, V. Post, C. D. Langevin, J. D. Hughes, J. T. White, J. J. Starn, and M. N. Fienen. Scripting MODFLOW Model Development Using Python and FloPy. *Groundwater*, 54(5):733–739, 9 2016. ISSN 17456584. doi: 10.1111/gwat.12413.

M. Baudin, A. Dutfoy, B. Iooss, and A. Popelin. OpenTURNS: An industrial software for uncertainty quantification in simulation. 2015.

P.T. Bennett and R.A. Barron. Design Data for Partially Penetrating Relief Wells. Technical report, 1957.

P. Bernardini and H. Knoeff. HWBP Handreiking verkenning versie 2. Technical report, HWBP, 9 2017.

S. Bersan and A.R. Koelewijn. Temperature monitoring in piping-prone hydraulic structures. In *Engineering Geology for Society and Territory - Volume 2: Landslide Processes*, pages 1409–1413. Springer International Publishing, 1 2015. ISBN 9783319090573. doi: 10.1007/978-3-319-09057-3{_}249.

S. Bersan, A.R. Koelewijn, and P. Simonini. Application of distributed temperature sensors in piping-prone dikes. In *Proceedings of the Ninth International Symposium on Field Measurements in Geomechanics, 9-11 September 2015, Sydney, Australia*, page 829, Perth, 2015. Australian Centre for Geomechanics. ISBN 9780992481025.

M. Bishop, J.B. Dunbar, and L.P. Peyman-Dove. Integration of remote sensing (LIDAR, electromagnetic conductivity) and geologic data toward the condition assessment of levee systems. In *Remote Sensing for Environmental Monitoring, GIS Applications, and Geology II*, volume 4886, page 400. SPIE, 3 2003. doi: 10.1117/12.462112.

W.G. Bligh. Dams, barrages and weirs on porous foundations. *Engineering News*, 1910.

A. Casas, D. Riaño, J. Greenberg, and S. Ustin. Assessing levee stability with geometric parameters derived from airborne LiDAR. *Remote Sensing of Environment*, 117:281–288, 2 2012. doi: 10.1016/j.rse.2011.10.003.

Y. Choung. Mapping risk of levee overtopping using LiDAR data: A case study in Nakdong River Basins, South Korea. *KSCE Journal of Civil Engineering*, 19(2):385–391, 2015. doi: 10.1007/s12205-015-0452-7.

D. Closson, N.A. Karaki, H. Hansen, D. Derauw, C. Barbier, and A. Ozer. Space-borne radar interferometric mapping of precursory deformations of a dyke collapse, Dead Sea area, Jordan. *International Journal of Remote Sensing*, 24(4):843–849, 2 2003. doi: 10.1080/01431160210147388.

CRED. Natural disasters 2018. Technical report, CRED, 2019.

S.L. Cundill, M. Van Der Meijde, and H.R.G.K. Hack. Investigation of remote sensing for potential use in dike inspection. *IEEE Journal of Selected Topics in Applied Earth Observations and Remote Sensing*, 7(2):733–746, 2 2014. doi: 10.1109/JSTARS.2013.2293617.

T. Dahlin, P. Sjödahl, and S. Johansson. Embankment Dam Seepage Evaluation from Resistivity Monitoring Data. In *Near Surface 2008 - 14th EAGE European Meeting of Environmental and Engineering Geophysics*. European Association of Geoscientists & Engineers, 2008. ISBN 978-90-73781-56-6. doi: 10.3997/2214-4609.20146268. URL https://www.earthdoc.org/content/papers/10.3997/2214-4609.20146268.

G. de Vries, A.R. Koelewijn, and V. Hopman. IJkdijk Full Scale Underseepage Erosion (Piping) Test: Evaluation ofInnovative Sensor Technology. HENRY, 2010. doi: 20.500.11970.

Deltares. Parameterlijst Complete WTI parameterlijst Aquo, 2016.

Deltares. *Gebruikershandleiding Riskeer*. Deltares, Delft, 19.1.1 edition, 4 2019.

M.H. Faber. Lecture Notes Risk and Safety in Civil Engineering. Technical report, 2007. URL http://www.ibk.ethz.ch/fa/education/ws_safety/.

J. C. Fisher and B. V. Twinning. Multilevel Groundwater Monitoring of Hydraulic Head and Temperature in the Eastern Snake River Plain Aquifer. Technical report, U.S. Geological Survey, Reston, Virginia, 2011.

D.M. Frangopol and M. Soliman. Life-cycle of structural systems: recent achievements and future directions. *Structure and Infrastructure Engineering*, 12(1):1–20, 1 2016. ISSN 17448980. doi: 10.1080/15732479.2014.999794.

R.B. Haarbrink and A.M. Shutko. Sensor Wavelength Specs Use Passive Microwave Scanner. Firenze, Italy, 2008. IEEE. doi: 10.1109/MICRAD.2008.4579460.

R.F. Hanssen and F.J. Van Leijen. Monitoring water defense structures using radar interferometry. In *2008 IEEE Radar Conference, RADAR 2008*, 2008. ISBN 9781424415397. doi: 10.1109/RADAR.2008.4720874.

A.W. Harbaugh. MODFLOW-2005, The U.S. Geological Survey Modular Ground-Water Model-the Ground-Water Flow Process. Technical report, 2005. URL http://water.usgs.gov/software/ground_water.html/.

HDSR. Drainagesysteem in de verkenning. Technical report, 1 2017. URL www.witteveenbos.com.

F. Heße, V. Prykhodko, S. Schlüter, and S. Attinger. Generating random fields with a truncated power-law variogram: Acomparison of several numerical methods. *Environmental Modelling and Software*, 55:32–48, 5 2014. ISSN 13648152. doi: 10.1016/j.envsoft.2014.01.013.

W.L. Hsu and K.T. Chang. Cross-estimation of soil moisture using thermal infrared images with different resolutions. *Sensors and Materials*, 31(1):387–398, 2019. ISSN 09144935. doi: 10.18494/SAM.2019.2090.

M.J. Hvorslev. Time lag and soil permeability in ground-water observations. Technical report, Waterways Experiment station, US Army Corps of Engineers, Vicksburg, 1951.

S.J. Ikard, J. Rittgers, A. Revil, and M.A. Mooney. Geophysical investigation of seepage beneath an earthen dam. *Groundwater*, 53(2):238–250, 3 2015. doi: 10.1111/gwat.12185.

J. Johnstone. *An Account of the Most Approved Mode of Draining Land, According to the System Practised by Mr. Joseph Elkington*. 1797.

C. Jones, G. Bawden, S. Deverel, J. Dudas, and S. Hensley. Characterizing land surface change and levee stability in the Sacramento-San Joaquin Delta using UAVSAR radar imagery. In *International Geoscience and Remote Sensing Symposium (IGARSS)*, pages 1638–1641, 2011. ISBN 9781457710056. doi: 10.1109/IGARSS.2011.6049546.

C.E. Jones, G. Bawden, S. Deverel, J. Dudas, S. Hensley, and S-H. Yun. Study of movement and seepage along levees using DINSAR and the airborne UAVSAR instrument. In *SAR Image Analysis, Modeling, and Techniques XII*, volume 8536, page 85360E. SPIE, 11 2012. ISBN 9780819492760. doi: 10.1117/12.976885.

R.B. Jongejan and B. Maaskant. Quantifying flood risks in the Netherlands. *Risk Analysis*, 35(2):252–264, 2 2015. ISSN 15396924. doi: 10.1111/risa.12285.

S.N. Jonkman, R.D.J.M. Steenbergen, O. Morales-Nápoles, A.C.W.M. Vrouwenvelder, and J.K. Vrijling. Probabilistic Design: Risk and Reliability Analysis in Civil Engineering Lecture notes CIE4130. Technical report, Delft University of Technology, 2015.

S.N. Jonkman, R.E. Jorissen, T. Schweckendiek, and J.P. Van Den Bos. Flood defences Lecture notes CIE5314 3rd edition 2018. Technical report, 2018a.

S.N. Jonkman, H.G. Voortman, W.J. Klerk, and S. van Vuren. Developments in the management of flood defences and hydraulic infrastructure in the Netherlands. *Structure and Infrastructure Engineering*, 14(7): 895–910, 7 2018b. doi: 10.1080/15732479.2018.1441317.

W. Kanning. *The weakest link : spatial variability in the piping failure mechanism of dikes*. [s.n.], 2012. ISBN 9789461860880.

W. Kanning, A. Teixeira, M. van der Krogt, and K. Rippi. Derivation of the semi-probabilistic safety assessment rule for inner slope stability. Technical report, Deltares, Delft, 2017.

J.M. Kind. Economically efficient flood protection standards for the Netherlands. *Journal of Flood Risk Management*, 7(2):103–117, 2014. doi: 10.1111/jfr3.12026.

W.J. Klerk, F. den Heijer, and T. Schweckendiek. Value of information in life cycle management of flood defences. In *Safety and Reliability of Complex Engineered Systems - Proceedings of the 25th European Safety and Reliability Conference, ESREL 2015*, pages 931–938. CRC Press/Balkema, 2015. ISBN 9781138028791. doi: 10.1201/b19094-125.

W.J. Klerk, W. Kanning, N.J. van Veen, and M. Kok. Influence of Monitoring on Investment Planning of Flood Defence Systems. In *Proceedings of the 7th International Symposium on Geotechnical Safety and Risk (ISGSR 2019)*, pages 792–797, Singapore, 2019a. Research Publishing Services. ISBN 978-981-11-2725-0. doi: 10.3850/978-981-11-2725-0-IS4-10-cd. URL `http://rpsonline.com.sg/proceedings/9789811127250/html/IS4-10.xml`.

W.J. Klerk, T. Schweckendiek, F. Den Heijer, and M. Kok. Value of information of structural health monitoring in asset management of flood defences. *Infrastructures*, 4(3), 8 2019b. doi: 10.3390/infrastructures4030056.

W.J. Klerk, W. Kanning, M. Kok, and R. Wolfert. Optimal planning of flood defence system reinforcements using a greedy search algorithm. *Reliability Engineering & System Safety*, 207, 3 2021. ISSN 09518320. doi: 10.1016/j.ress.2020.107344.

J.M. Ko and Y.Q. Ni. Technology developments in structural health monitoring of large-scale bridges. *Engineering Structures*, 27(12 SPEC. ISS.):1715–1725, 2005. ISSN 01410296. doi: 10.1016/j.engstruct.2005.02.021.

A.R. Koelewijn and M.T. van der Meer. Handreiking Life Cycle Monitoring-Groene Versie Geotechnische monitoring van dijken. Technical report, 2019.

K. Kosugi. Lognormal distribution model for unsaturated soil hydraulic properties. *Water Resources Research*, 32(9):2697–2703, 9 1996. ISSN 00431397. doi: 10.1029/96WR01776.

L.L. Kupper. Probability, Statistics, and Decision for Civil Engineers. *Technometrics*, 13(1), 2 1971. ISSN 0040-1706. doi: 10.1080/00401706.1971.10488770.

R. Lancellotta. *Geotechnical Engineering, Second Edition*. 2 edition, 2008.

E.W. Lane. Security from Under-Seepage-Masonary Dams on Earth Foundations. *American Society of Civil Engineers*, 100(1919):1235–1272, 1935.

O. Langhorst and B. Bouwens. De Waterontspanner. *Civiele Techniek*, 1-2, 2015.

C.P. Lin and S.H. Tang. Development and Calibration of a TDR Extensometer for Geotechnical Monitoring. Technical Report 5, 2005. URL `www.astm.org`.

Z. Lu and G.V. Wilson. Acoustic Measurements of Soil Pipeflow and Internal Erosion. *Soil Science Society of America Journal*, 76(3):853–866, 5 2012. doi: 10.2136/sssaj2011.0308.

C.I. Mansur, G. Postol, and R.J. Salley. Performance of Relief Well Systems Along Mississippi River Levees. *Journal of Geotechnical and Geoenvironmental Engineering*, 126(8):727–738, 2000.

N.B. Melnikova, V.V. Krzhizhanovskaya, and P.M.A. Sloot. Modeling earthen dikes using real-time sensor data. *Journal of Hydrology*, 496:154–165, 2013. doi: 10.1016/j.jhydrol.2013.05.031.

P. Mériaux and P. Royet. *Surveillance, maintenance and diagnosis of flood protection dikes A practical handbook for owners and operators*. Quae, 2007. ISBN 2.7592.0037.5.

M. Mesquita, S.O. Moraes, and J.E. Corrente. More adequate probability distributions to represent the saturated soil hydraulic conductivity. *Scientia Agricola*, 59(4), 12 2002. ISSN 0103-9016. doi: 10.1590/S0103-90162002000400025.

C.A. Miranda Eguez. Probabilistic Design of Relief Wells as Piping Mitigation Measure. Technical report, Delft University of Technology, 2014. URL `http://repository.tudelft.nl/`.

O. Monserrat, M. Crosetto, and G. Luzi. A review of ground-based SAR interferometry for deformation measurement. *ISPRS Journal of Photogrammetry and Remote Sensing*, 93:40–48, 2014. doi: 10.1016/j.isprsjprs.2014.04.001.

Movares. https://waterontspanner.nl/, 1 2021.

M. Muskat. *The Flow of Homogeneous Fluids Through Porous Media*, volume 46. McGraw-Hill, New York, 2 edition, 1937.

J.W. Nieuwenhuis, M. van der Meer, S. Bakkenist, Y. Pluijmers, R. Clemens, and W. Zomer. LiveDijk XL Noorderzijlvest State of the Art 2015. Technical report, 2016.

N. Nöther, A. Wosniok, K. Krebber, and E. Thiele. A distributed fiber optic sensor system for dike monitoring using Brillouin optical frequency domain analysis. In *Smart Sensor Phenomena, Technology, Networks, and Systems 2008*, volume 6933, page 69330T. SPIE, 3 2008. ISBN 9780819471192. doi: 10.1117/12.775133.

I.E. Özer, S.J.H. Rikkert, F.J. van Leijen, S.N. Jonkman, and R.F. Hanssen. Sub-seasonal Levee Deformation Observed Using Satellite Radar Interferometry to Enhance Flood Protection. *Scientific Reports*, 9(1), 12 2019. doi: 10.1038/s41598-019-39474-x.

M.L. Parekh, W. Kanning, C. Bocovich, M.A. Mooney, and A.R. Koelewijn. Backward erosion monitored by spatial-temporal pore pressure changes during field experiments. *Journal of Geotechnical and Geoenvironmental Engineering*, 142(10), 10 2016. doi: 10.1061/(ASCE)GT.1943-5606.0001528.

T. Planès, M.A. Mooney, J.B.R. Rittgers, M.L. Parekh, M. Behm, and R. Snieder. Time-lapse monitoring of internal erosion in earthen dams and levees using ambient seismic noise. *Geotechnique*, 66(4):301–312, 4 2016. doi: 10.1680/jgeot.14.P.268.

V.E.A. Post and J.R. von Asmuth. Revue : Mesure du niveau piézométrique-nouvelles technologies, pièges classiques. *Hydrogeology Journal*, 21(4):737–750, 6 2013. ISSN 14312174. doi: 10.1007/s10040-013-0969-0.

H. Raiffa and R. Schlaifer. *Applied Statistical Decision Theory*. Cambridge University Press., Cambridge, 1961.

Rijkswaterstaat. Flood prone areas in the Netherlands, 2010. URL `http://www.pbl.nl`.

Rijkswaterstaat. Regeling veiligheid primaire waterkeringen 2017. Technical report, Ministerie van Infrastructuur en Milieu, 2017. URL `http://www.helpdeskwater.nl/onderwerpen/waterveiligheid/pri`.

Rijkswaterstaat. Schematiseringshandleiding piping. 11 2019. URL `www.helpdeskwater.nl`.

J. Rings, A. Scheuermann, K. Preko, and C. Hauck. Soil water content monitoring on a dike model using electrical resistivity tomography. Technical report, 2008.

S. Rödelsperger and A. Meta. MetaSensing's FastGBSAR: ground based radar for deformation monitoring. In *SAR Image Analysis, Modeling, and Techniques XIV*, volume 9243, page 924318. SPIE, 10 2014. ISBN 9781628413069. doi: 10.1117/12.2067243.

L. Schenato, L. Palmieri, M. Camporese, S. Bersan, S. Cola, A. Pasuto, A. Galtarossa, P. Salandin, and P. Simonini. Distributed optical fibre sensing for early detection of shallow landslides triggering. *Scientific Reports*, 7(1), 12 2017. doi: 10.1038/s41598-017-12610-1.

L. Schueler and S. Mueller. GeoStat-Framework/GSTools: Volatile Violet v1.2.1, 2020.

T. Schweckendiek. Reassessing Reliability Based on Survived Loads. Technical report, Delft University of Technology, Delft, 2010.

T. Schweckendiek. *On Reducing Piping Uncertainties*. PhD thesis, 2014.

T. Schweckendiek and A.C.W.M. Vrouwenvelder. Reliability updating and decision analysis for head monitoring of levees. *Georisk*, 7(2):110–121, 6 2013. ISSN 17499518. doi: 10.1080/17499518.2013.791034.

J.B. Sellmeijer. *On the Mechanism of Piping Under Impervious Structures*. PhD thesis, Delft University of Technology, 1988.

J.B. Sellmeijer. Numerical computation of seepage erosion below dams (piping). (GeoDelft), 2006.

S.N.P. Sharma. Partially Penetrating Multiple-Well System in a Confined Aquifer with Application to Relief Well Design. *Journal of Hydrology*, 23:1–37, 1974.

D. Straub. Reliability updating with equality information. *Probabilistic Engineering Mechanics*, 26(2):254–258, 4 2011. ISSN 02668920. doi: 10.1016/j.probengmech.2010.08.003.

Sweco and Arcadis. Beoordeling Piping en heave, dijkversterking Wijk bij Duurstede - Amerongen. Technical report, 2019.

R. 't Hart, H. De Bruijn, and G. de Vries. Fenomenologische beschrijving Faalmechanismen WTI. Technical report, Deltares, Delft, 2016.

TAW. Technisch rapport waterspanningen bij dijken. Technical report, 2004.

A. Teixeira, K. Wojciechowska, and W. ter Horst. Derivation of the semi-probabilistic safety assessment for piping WTI 2017: Cluster C, piping failure mechanism. Technical report, Deltares, Delft, 2016.

C. Terzaghi. Wellpoint Method for Handling Excavation of Foundation Pit at New Sewage Pumping Station. *J. of the Boston Soc. of Civil Eng.*, XIV(7):63–71, 1927.

K. Terzaghi and R.B. Peck. *Soil Mechanics in Engineering Practice.* John Wiley & Sons, 2nd edition, 1967. ISBN 9780471852735.

S. Thöns. Monitoring based condition assessment of offshore wind turbine support structures. Technical report, 2011.

M.E. Tipping and C.M. Bishop. Probabilistic Principal Component Analysis. *Journal of the Royal Statistical Society: Series B (Statistical Methodology)*, 61(3), 8 1999. ISSN 1369-7412. doi: 10.1111/1467-9868.00196.

USACE. Miss. River Levees Underseep. Studies - BlackBayou Levee. Vicksburg, 1939.

USACE. Design, construction, and maintenance of relief wells. Technical report, USACE, Washington, 1992.

V.M. van Beek. *Backward Erosion Piping Initiation and Progression.* 2015. ISBN 978-94-6259-940-6.

G. van der Kamp and C.K. Keller. Casing Leakage in Monitoring Wells: Detection, Confirmation, and Prevention. *Groundwater Monitoring & Remediation*, 13(4), 11 1993. ISSN 10693629. doi: 10.1111/j.1745-6592.1993.tb00457.x.

M.G. van der Krogt, W.J. Klerk, W. Kanning, T. Schweckendiek, and M. Kok. Value of information of combinations of proof loading and pore pressure monitoring for flood defences. *Structure and Infrastructure Engineering*, 12 2020. ISSN 1573-2479. doi: 10.1080/15732479.2020.1857794.

R. van der Meij. *D-Stability User Manual.* Delft, 2019.

van Essen. Product Manual TD-Diver™ & Baro-Diver®-DI8xx Series. Technical report, 2016. URL `www.eijkelkamp.com`.

H.A.J.M. van Gelder. *Statistical Methods for the Risk-Based Design of Civil Structures.* 2000. ISBN 9090134522.

G.A.M. van Meurs, J. Niemeijer, J.J. van Meerten, O.S. Langhorst, and H.D.C. Meuwese. POV Drainagetechnieken. 5 2018.

L. van Vliet, A.R. Koelewijn, and M. van der Vat. MonitoringStowa. 2011.

R. Vergouwe. The National Flood Risk Analysis for the Netherlands. Technical report, Rijkswaterstaat, 2014.

J. Weijers, G.T. Elbersen, A.R. Koelewijn, and N. Pals. *Macrostabiliteit IJkdijk: Sensor-en meettechnologie.* Rijkswaterstaat, 2009. ISBN 978.90.5773.432.8.

M. Wewer. *Development of an optimal sensing strategy for dike monitoring of backward erosion piping with fibre optic cable based sensors.* PhD thesis, Technische Universitat Dresded, Dresden, 2 2019.

C.M. White. The equilibrium of grains on the bed of a stream. Technical report, Imperial College of Science and Technology, London, 1940.

C. Zwanenburg, A. van Duinen, and A. Rozing. Technisch Rapport Macrostabiliteit. Technical report, Deltares, Delft, 2013.

A

Target probability of failure

The formulas to derive a target probability of failure are given by:

$$\beta_{r,j} = -\phi^{-1}(P_f) \tag{A.1}$$

$$P_f = \frac{P_{r,j} \cdot w_j}{N_j} \tag{A.2}$$

$$N_j = 1 + \frac{a_j * L}{b_j} \tag{A.3}$$

In which a_j and b_j are failure mechanism specific parameters, L the length of the trajectory, N_j resembles the length effect factor, $P_{r,j}$ the required probability of failure obtained from Riskeer, w_j a parameter that defines the maximum contribution of a failure mechanism to the system failure probability, P_f the target probability of failure and $\beta_{r,j}$ the target reliability index. Values for a_j and b_j are given in (Jonkman et al., 2015) and equal:

Failure mode	Location	a_j	b_j
Piping	Upper Rhine	0.9	300
	Other parts	0.4	300
Stability	All	0.033	50

Table A.1: Default parameters length effect

The default settings for the maximum contribution of a failure mechanism to the system failure probability w_j for dikes are given in (Jonkman et al., 2015) and are depicted below:

Failure type	Overflow	Piping	Stability	Revetments	Structure	Other
w_j	0.24	0.24	0.04	0.10	0.08	0.30

Table A.2: Default parameters for failure mechanism contribution w_j

For parameters that are best described by a lognormal distribution the location ζ and scale λ parameters are determined according to:

$$\zeta = \sqrt{\ln(1 + V^2)} \tag{A.4}$$

$$\lambda = \ln(\mu) - 0.5\zeta^2 \tag{A.5}$$

Calibration formulas for uplift, heave and piping are given by respectively (Rijkswaterstaat, 2019):

$$P_{f,u} = \phi\left[- \frac{ln\left(\frac{F_u}{0.48}\right) + 0.27\beta_r}{0.46} \right] \tag{A.6}$$

$$P_{f,h} = \phi\left[-\frac{ln\left(\frac{F_h}{0.37}\right) + 0.3\beta_r}{0.48} \right] \tag{A.7}$$

$$P_{f,p} = \phi\left[-\frac{ln\left(\frac{F_p}{1.04}\right) + 0.43\beta_r}{0.37} \right] \tag{A.8}$$

B

USACE design method

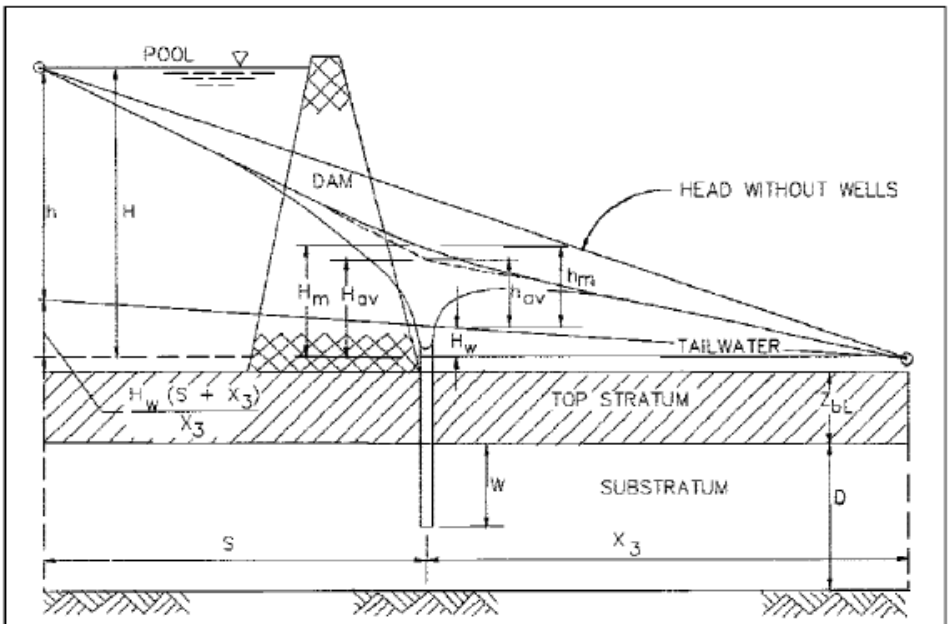

$$h = H - H_w \left(\frac{S + X_3}{X_3} \right) \quad (7\text{-}1)$$

$$h_{av} = \frac{h\theta_a}{\frac{S}{a} + \left(\frac{s + X_3}{X_3} \right)^{\theta_a}} \quad (7\text{-}2)$$

$$H_{av} = H_w + h_{av} \quad (7\text{-}3)$$

$$h_m = h_{av} \frac{\theta_m}{\theta_a} = \frac{h\theta_m}{\frac{S}{a} + \left(\frac{s + X_3}{X_3} \right)^{\theta_a}} \quad (7\text{-}4)$$

$$H_m = H_w + h_m \quad (7\text{-}5)$$

$$\Delta M = \frac{H - H_{av}}{S} - \frac{H_{av}}{X_3} \quad (7\text{-}6)$$

$$Q_w = a \Delta M \, k_f \, D \quad (7\text{-}7)$$

$$\text{or } Q = \frac{h k_f D}{\frac{S}{a} + \left(\frac{s + X_3}{X_3} \right)^{\theta_a}} \quad (7\text{-}8)$$

$$h_m = a \Delta M \theta_m \quad (7\text{-}9)$$

$$h_{av} = a \Delta M \theta_a \quad (7\text{-}10)$$

Figure B.1: Formulas for design of relief wells at toe of dam (USACE, 1992)

Flow through the well is calculated with the iterative method given by USACE (1992):

$$h = H - H_w\left(\frac{S + X_3}{X_3}\right) \tag{B.1}$$

$$h_{av} = \frac{h\theta_a}{\frac{S}{a} + \left(\frac{S+X_3}{X_3}\right)^{\theta_a}} \tag{B.2}$$

$$H_a v = H_w + h_a v \tag{B.3}$$

$$h_m = h_{av}\frac{\theta_m}{\theta_a} = \frac{h\theta_m}{\frac{S}{a} + \left(\frac{S+X_3}{X_3}\right)^{\theta_a}} \tag{B.4}$$

$$H_m = H_w + h_m \tag{B.5}$$

$$\Delta M = \frac{H - H_{av}}{S} - \frac{H_{av}}{x_3} \tag{B.6}$$

$$Q_w = a\Delta M k_f D G_p \tag{B.7}$$

$$h_m = a\Delta M\theta_m \tag{B.8}$$

$$h_a v = a\Delta M\theta_a \tag{B.9}$$

For partially penetrated wells the discharge is reduced by a factor G_p:

$$G_p = \frac{W}{D}\left(1 + 7\left(\sqrt{\frac{r_w}{2W}}\cos\left(\frac{\pi W}{2D}\right)\right)\right) \tag{B.10}$$

C

Well losses USACE

The following Figures provide empirical relations for determining filter head loss and entrance head loss as provided by USACE (1992). Figure C.1 shows a relation to determine filter head loss for a clean filter. Figure C.2 shows some relations to estimate filter head loss over time.

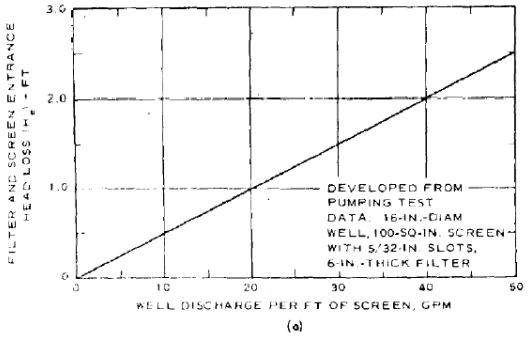

Figure C.1: Filter head loss (USACE, 1992)

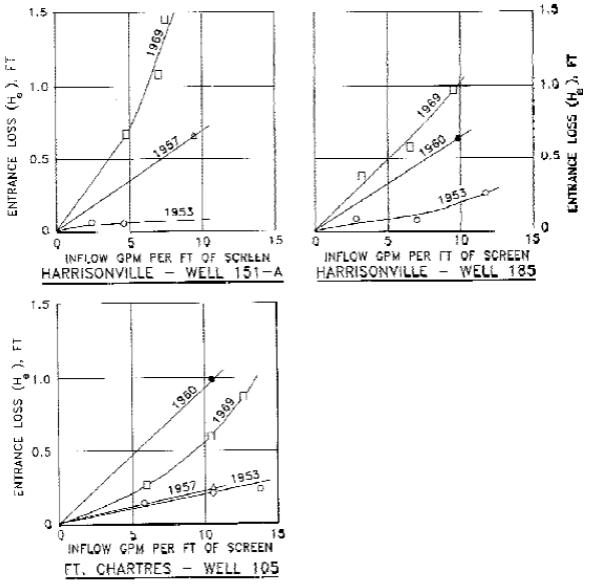

Figure C.2: Filter head loss over time (USACE, 1992)

D

Flow in a relief well

The considered relief wells are artesian wells. Flow through the well is modelled as laminar flow through a pipe. Flow through the filter can be modelled as fluid flowing through a packed bed of solids.

Entrance head loss in screen and filter

Flow through the filter is calculated with Kozeny-Carman equation, here expressed as pressure drop Δp::

$$\Delta p = 180 \cdot \frac{\mu}{g} \frac{(1-p)^2}{p^3} \frac{v}{d_h^2} L \cdot \rho g \tag{D.1}$$

In which μ is the fluids kinematic viscosity, g gravitational constant, p the filters porosity, v superficial flow velocity, d_h filter material diameter, ρ density of water, L the length of the filter.

Friction head loss

Darcy-Weisbach equation is an empirical equation that relates head loss to friction. In a cylindrical pipe, pressure is characterized as follows:

$$\Delta p = f_D \cdot \rho \cdot \frac{L}{D} \cdot \frac{< v >^2}{2} \tag{D.2}$$

In which f_D is the Darcy friction factor calculated with Colebrook-White:

$$\frac{1}{\sqrt{f}} = -2\log\left(\frac{\epsilon}{3.7 D_h} + \frac{2.51}{Re\sqrt{f}}\right) \tag{D.3}$$

In which Reynolds number is defined through:

$$Re = \frac{VD}{v} \tag{D.4}$$

Where V is the mean velocity of the fluid flow, D pipe diameter and v kinematic viscosity. Another empirical relationship that relates flow of water in a pipe to pressure drop due to friction is the Hazen-Williams equation. The advantage of the Hazen-Williams equation is that its roughness coefficient C is not a function of the Reynolds number, making it computationally much more easy to use. Rewriting the Hazen-Williams equation to pressure drop yields:

$$\Delta p = \frac{10.67 \cdot Q^{1.852}}{C^{1.852} \cdot d^{4.8704}} \cdot \rho \cdot g \tag{D.5}$$

In which Q is the flow through the pipe, C the roughness coefficient and d the pipe's diameter.

Velocity head loss

Velocity head loss H_v is calculated according to:

$$\Delta p = \frac{v^2}{2g} \cdot \rho \cdot g \tag{D.6}$$

In which v resembles the velocity, g gravitational constant and ρ water density.

Well flow

Hagen-Poiseuille equation is used to describe the flow through the well as a function of pressure:

$$Q = \frac{\Delta p \pi r^4}{8 \mu L} \tag{D.7}$$

In which Δp resembles pressure difference, r the well's radius, L the pipe's length and μ the dynamic viscosity related to the kinematic viscosity:

$$v = \frac{\mu}{\rho} \tag{D.8}$$

The equation is invalid for low viscosity or wide/short pipes. If the pipe is too short, the relation can result in unrealistically high flow volumes. The flow is bounded by Bernoulli's principle under less restrictive conditions:

$$Q_{max} = \pi r^2 \sqrt{\frac{2\Delta p}{\rho}} \tag{D.9}$$

E

Function fit water level

Figures E.1 and E.2 show function fits to water level data acquired through Hydra-Ring. Figure E.1 shows a fit for high water levels derived through an interpolation fit. Figure E.2 shows a Gumbel fit for water level between 5.3 and 6.6 m + NAP.

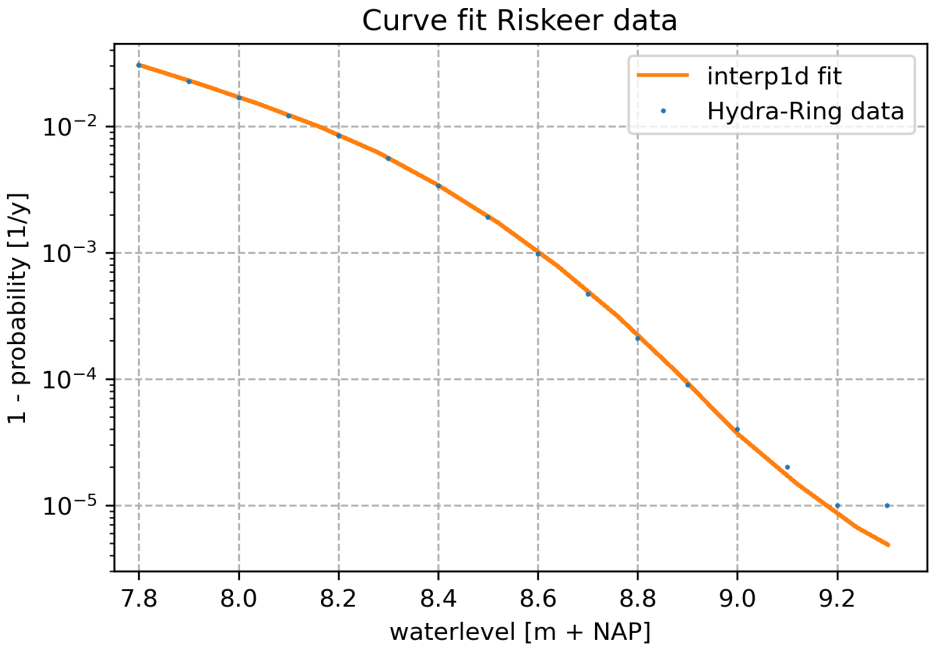

Figure E.1: CDF fit for extreme water levels obtained through Hydra-Ring, constructed with interpolation

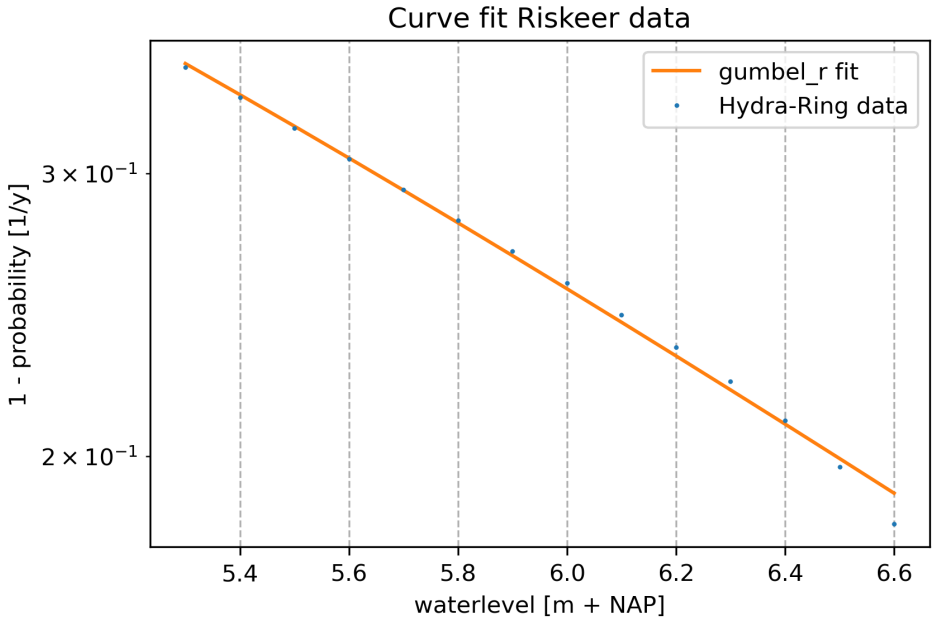

Figure E.2: CDF gumbel_r fit for river water levels varying between 5.3-6.6 m obtained through Hydra-Ring, $\mu = 3.79$ and $\sigma = 1.80$.

F

FORM vs MC

The following fragility curves have been created in order to show that the results derived from FORM analysis don't deviate much from the results derived through MC analysis. Because MC analyses demand much more computational time, most of the calculations will therefore be performed with FORM. Figures F.1, F.2 and F.3 depict the FORM and MC fragility curves derived for respectively uplift, heave and piping.

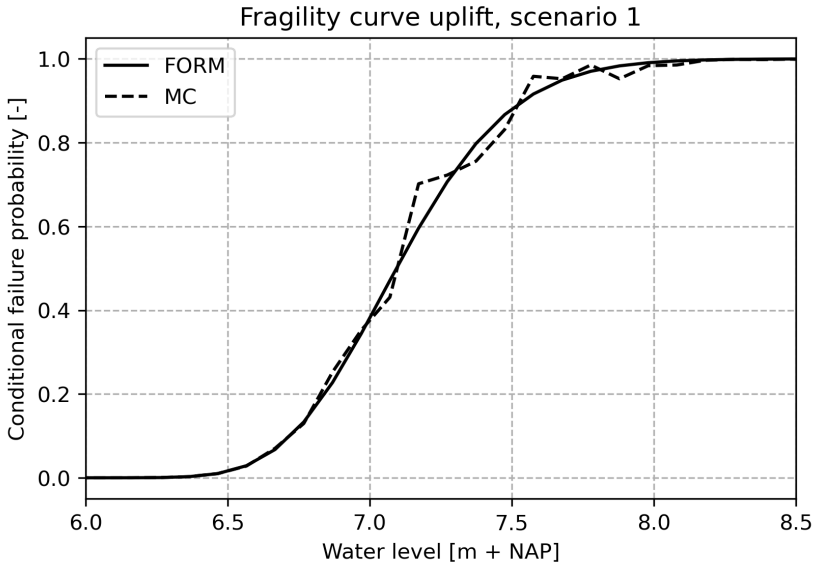

Figure F.1: Fragility curves uplift, FORM & MC

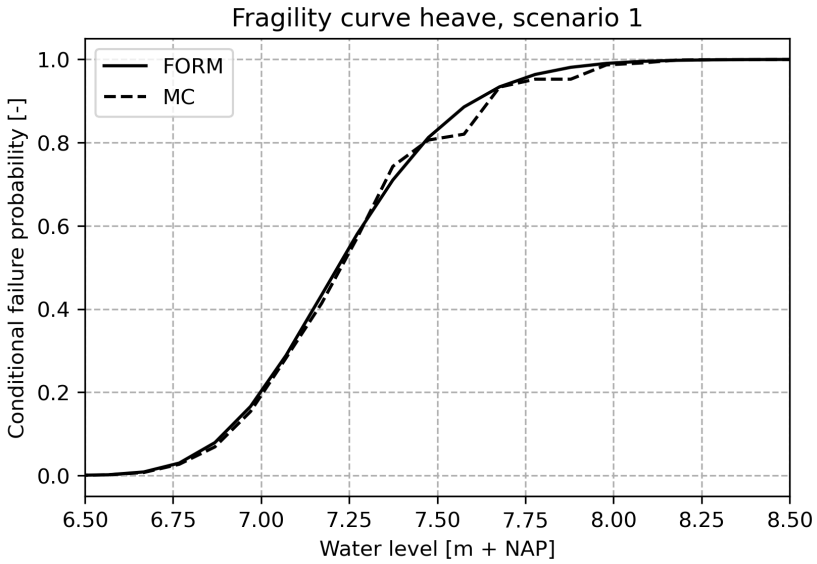

Figure F.2: Fragility curves heave, FORM & MC

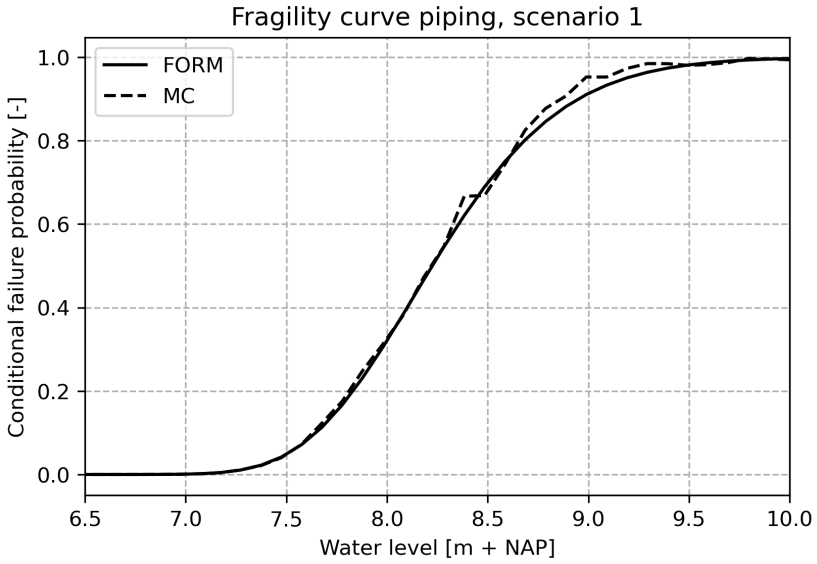

Figure F.3: Fragility curves piping, FORM & MC

G

Slope stability analysis

Preliminary stability checks

Figures G.1, G.2 and G.3 provide stability calculations derived through D-GEO Suite Stability for preliminary analysis. Figure G.1 provides a Bishop calculation, Figure G.2 an Uplift-Van calculation and Figure G.3 a Spencer calculation. All analyses are performed with the hydraulic head line as determined by Sweco.

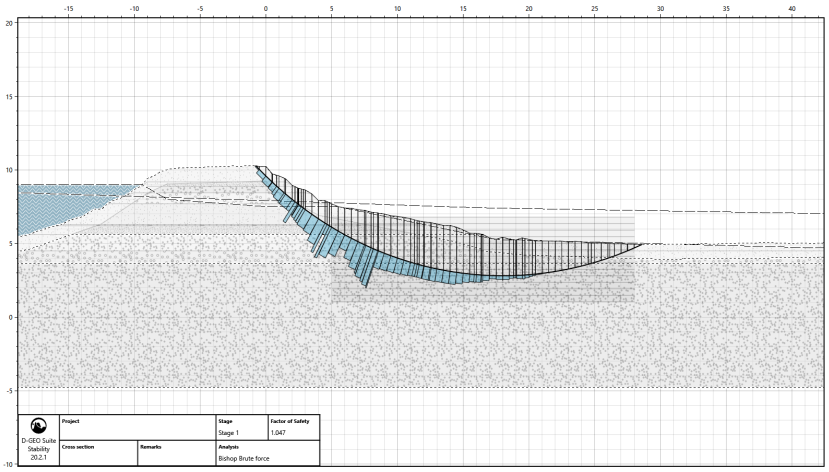

Figure G.1: Result Bishop calculation, shear stress

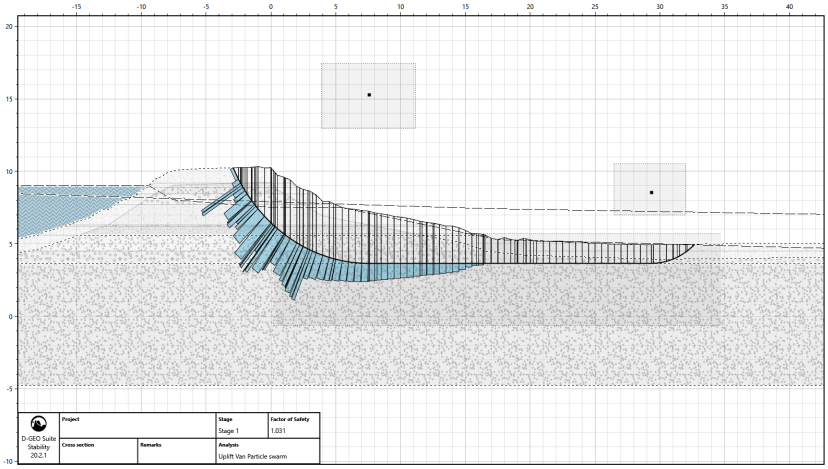

Figure G.2: Result Uplift-Van calculation, shear stress

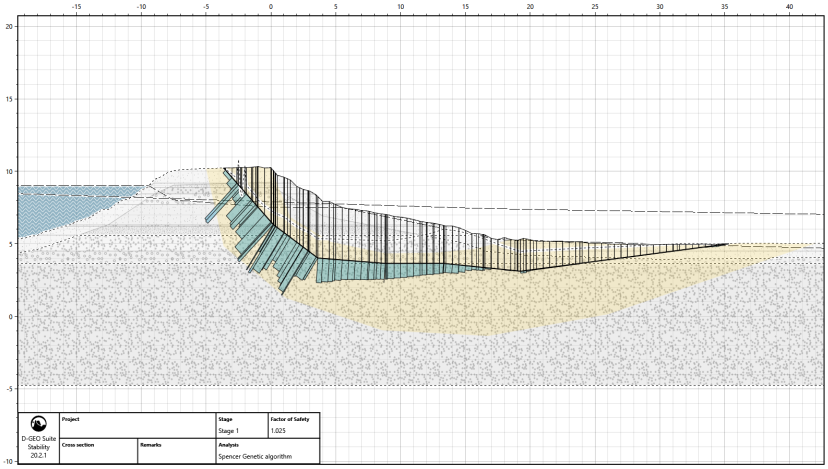

Figure G.3: Result Spencer calculation, shear stress

Pressure relief well analysis, 100 m trajectory

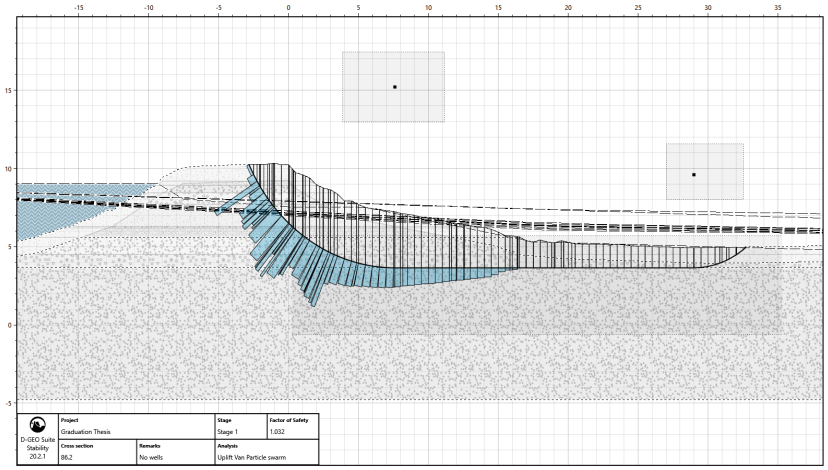

Figure G.4: No wells, FoS = 1.032

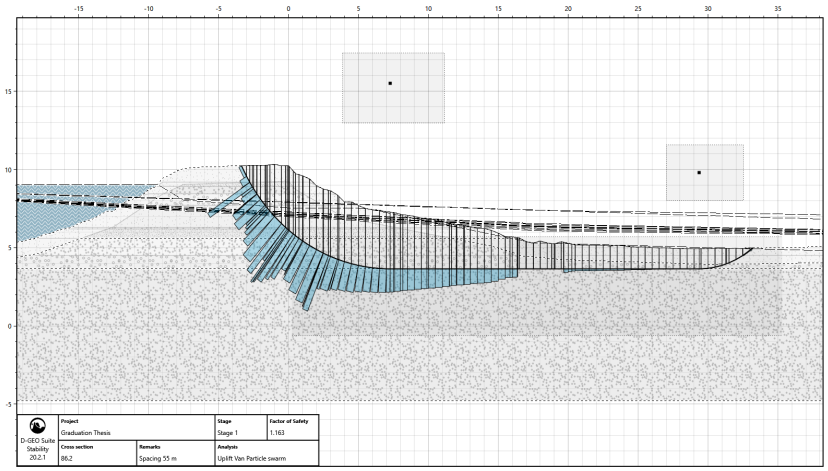

Figure G.5: Spacing 55 m, FoS = 1.163

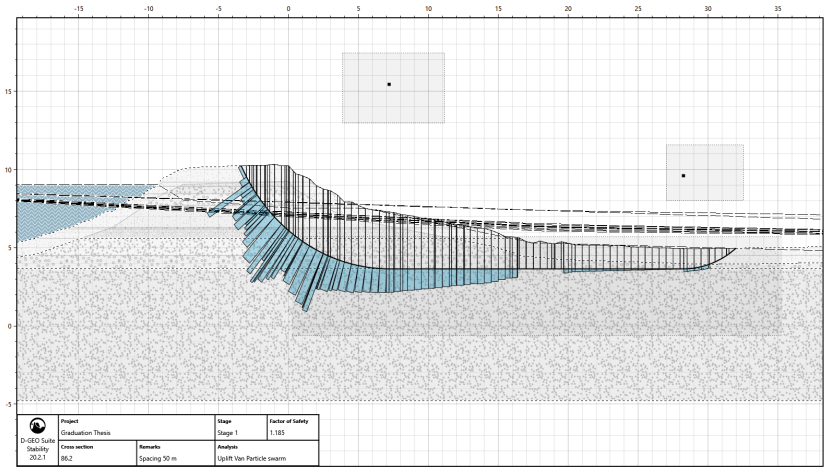

Figure G.6: Spacing 50 m, FoS = 1.185

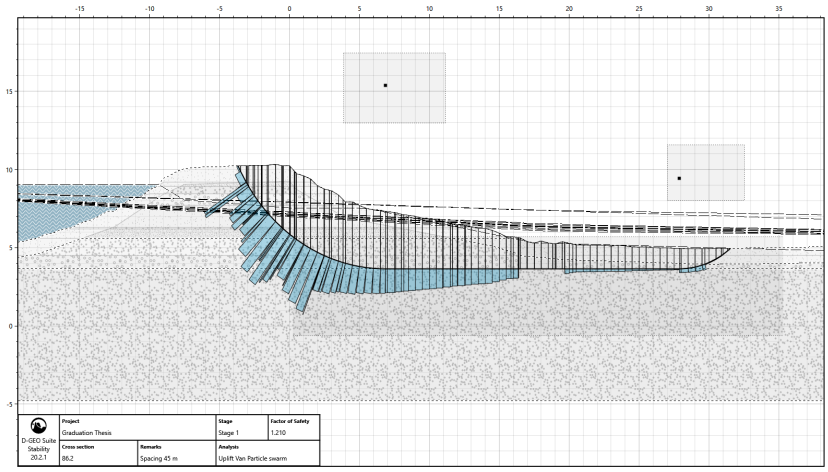

Figure G.7: Spacing 45 m, FoS = 1.210

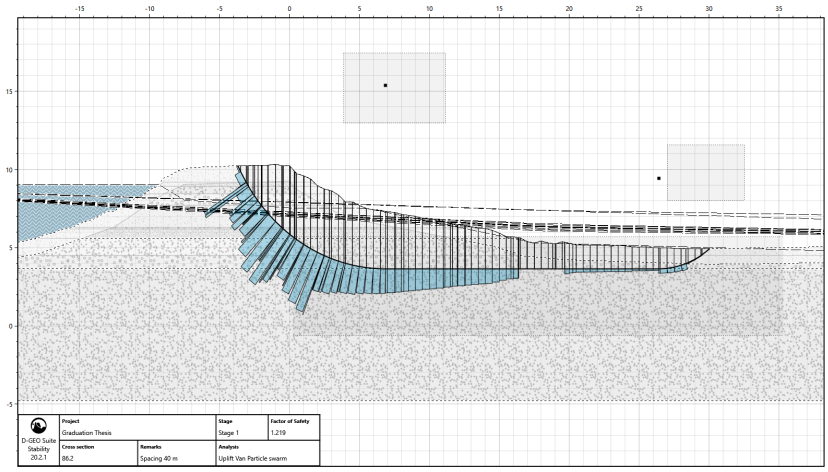

Figure G.8: Spacing 40 m, FoS = 1.219

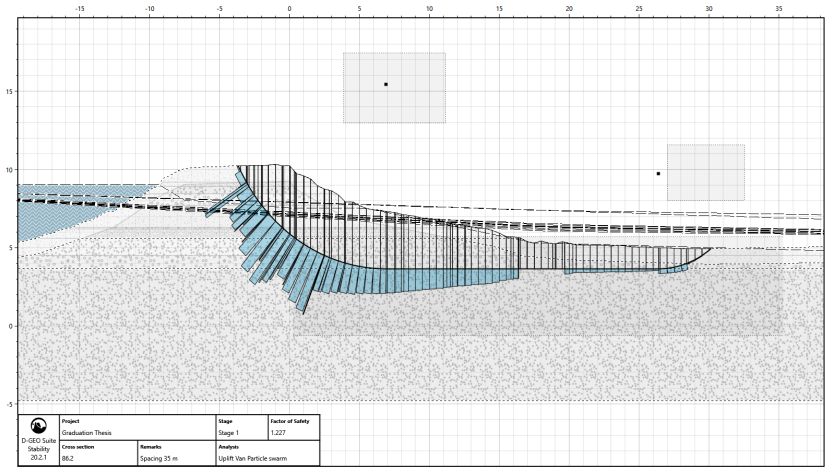

Figure G.9: Spacing 35 m, FoS = 1.227

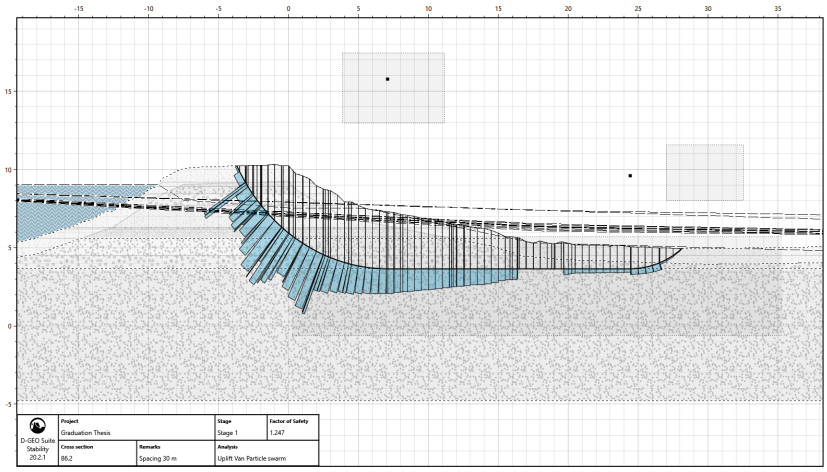

Figure G.10: Spacing 30 m, FoS = 1.247

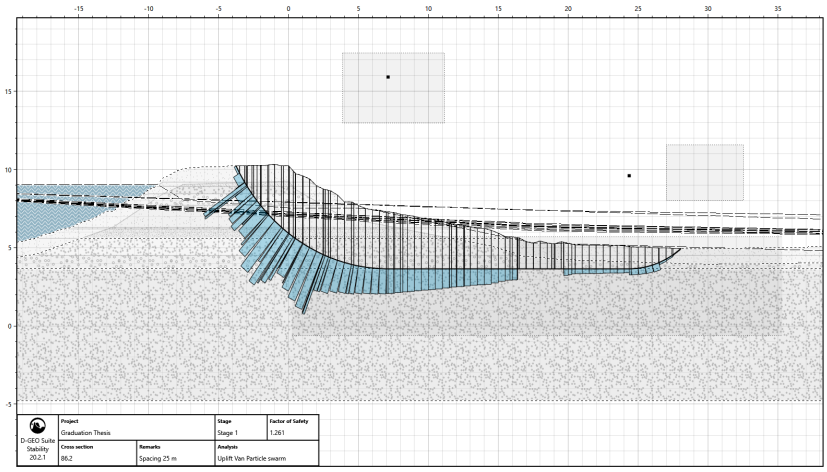

Figure G.11: Spacing 25 m, FoS = 1.261

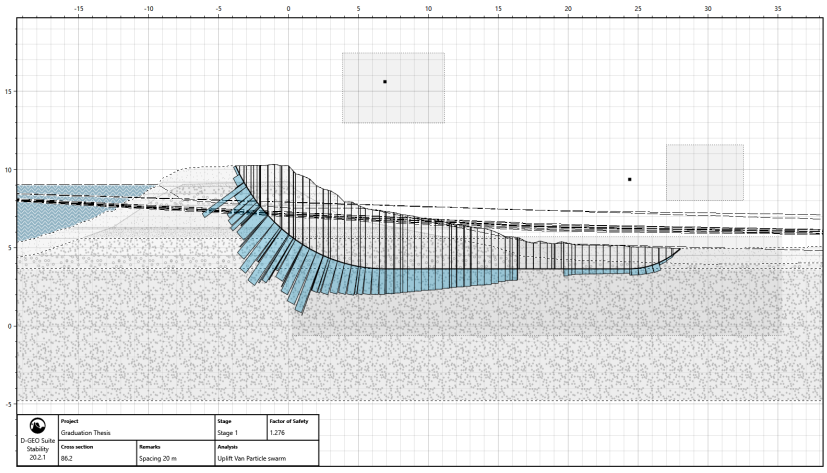

Figure G.12: Spacing 20 m, FoS = 1.276

Pressure relief well analysis, 2000 m trajectory

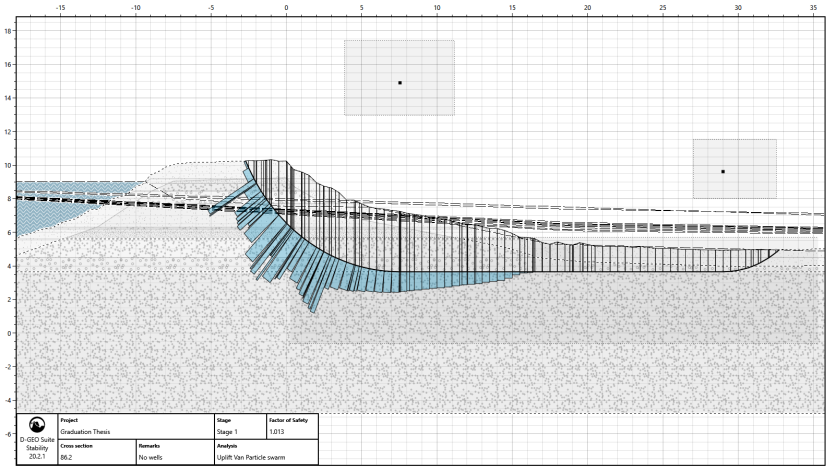

Figure G.13: No wells, FoS = 1.013

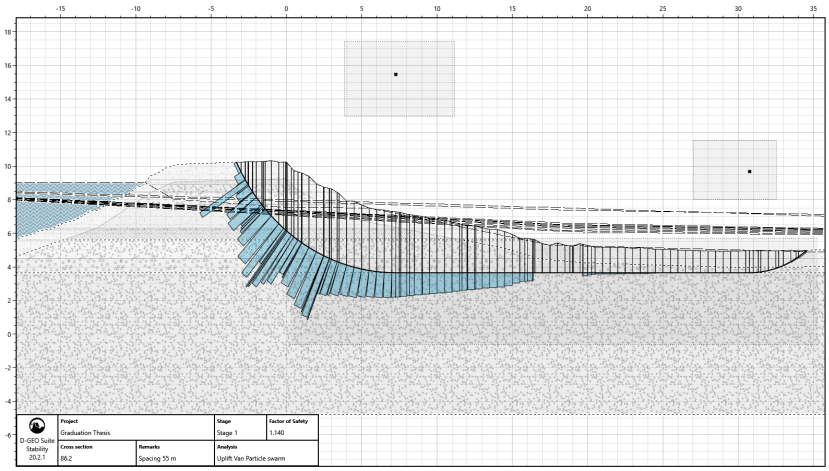

Figure G.14: Spacing 55 m, FoS = 1.140

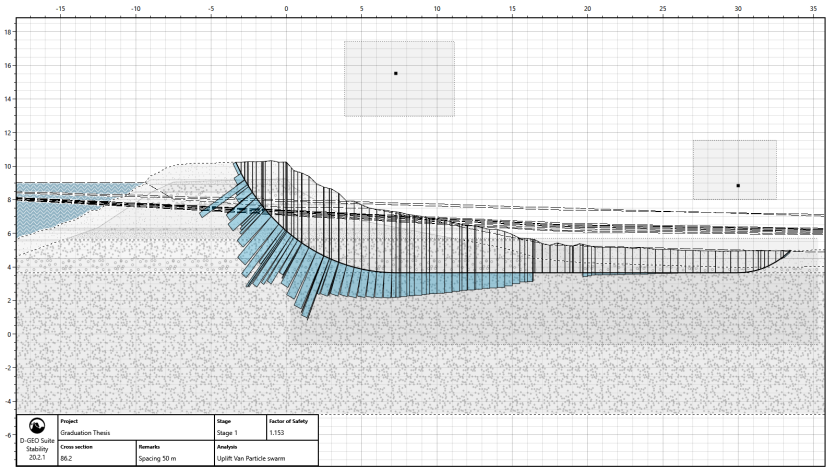

Figure G.15: Spacing 50 m, FoS = 1.153

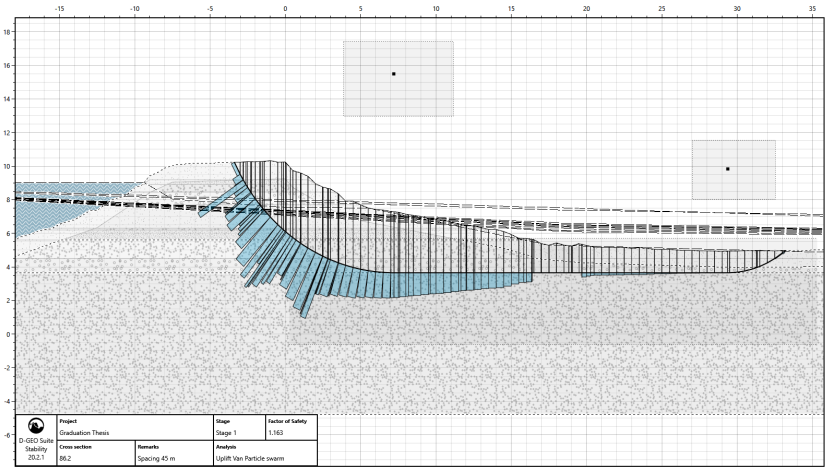

Figure G.16: Spacing 45 m, FoS = 1.163

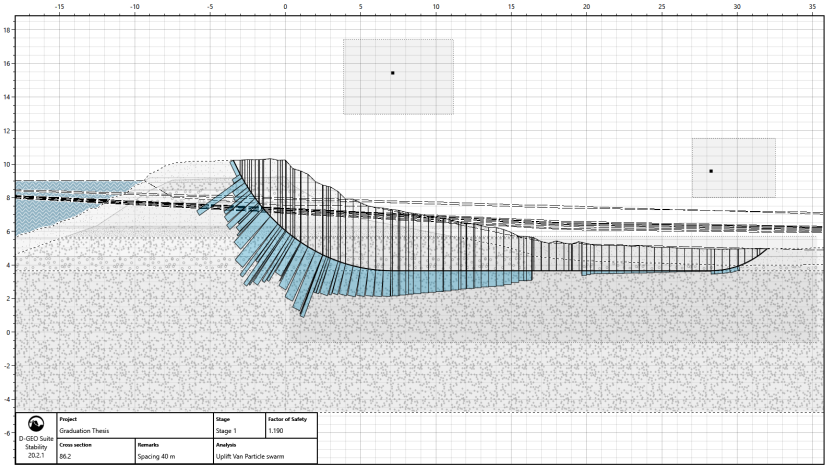

Figure G.17: Spacing 40 m, FoS = 1.190

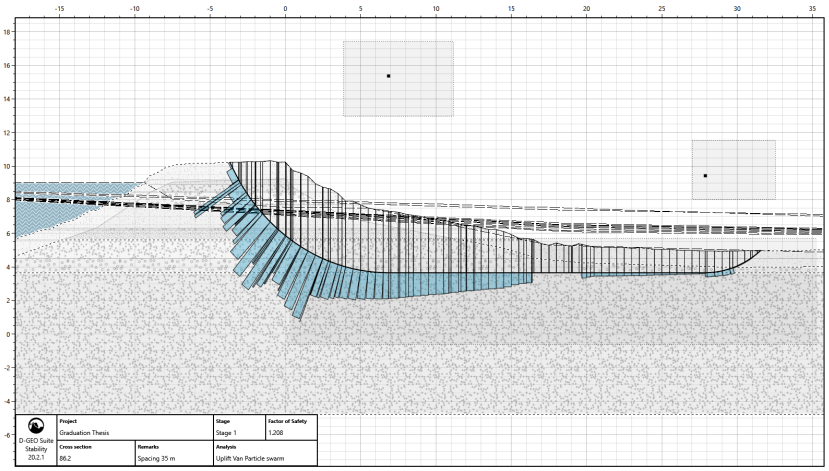

Figure G.18: Spacing 35 m, FoS = 1.208

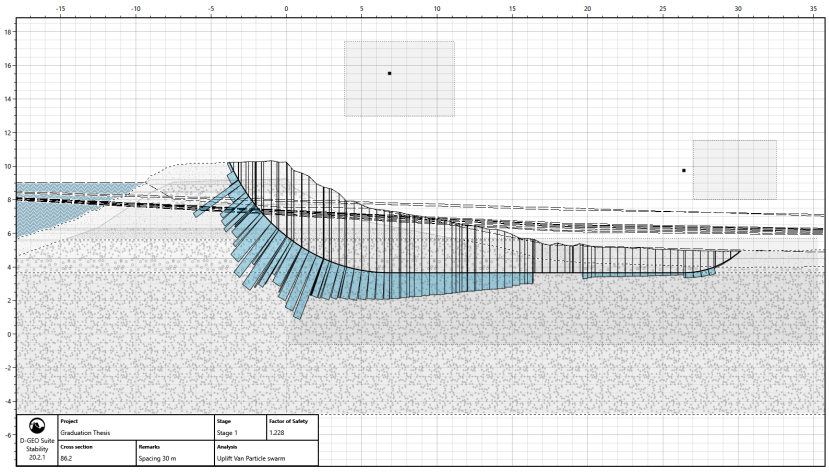

Figure G.19: Spacing 30 m, FoS = 1.228

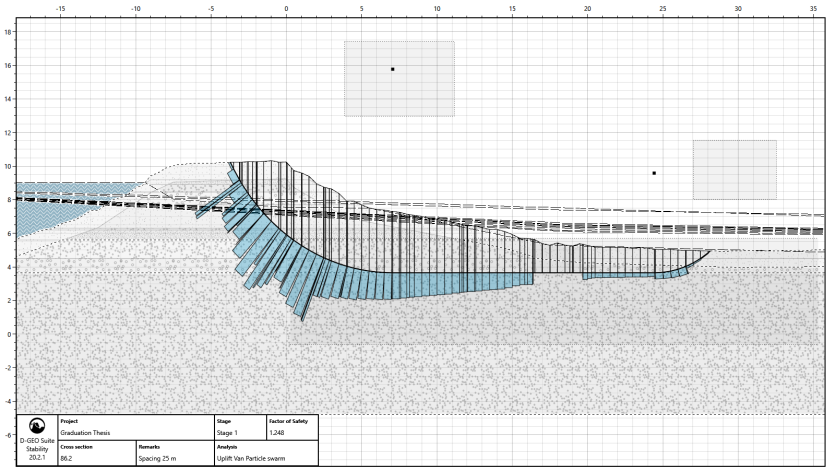

Figure G.20: Spacing 25 m, FoS = 1.248

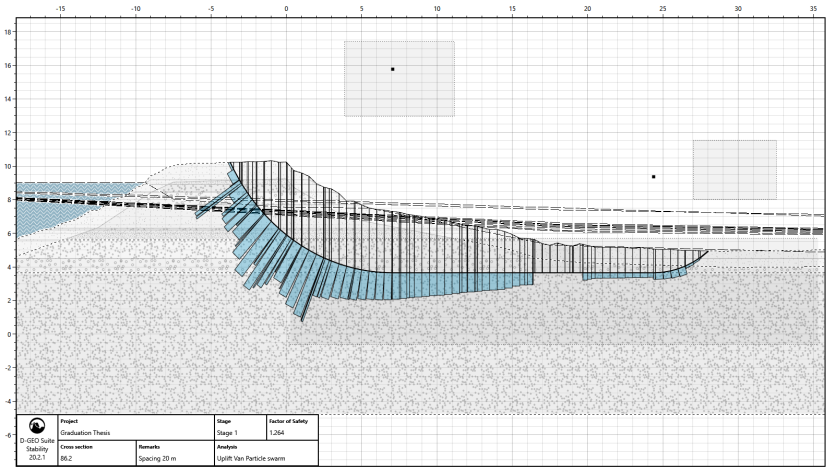

Figure G.21: Spacing 20 m, FoS = 1.264

Pressure relief well analysis, 100 m trajectory

The following checks are executed to assess the effect of placing the well in the berm at different locations.

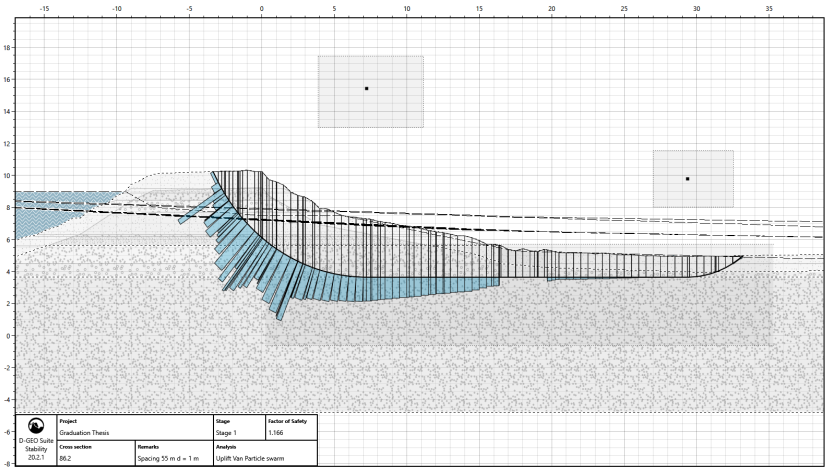

Figure G.22: Spacing 55 m, FoS = 1.166, d = 1 m

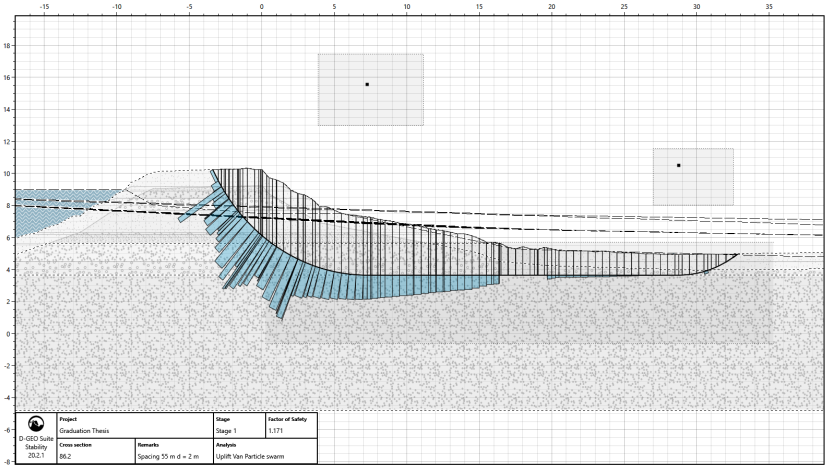

Figure G.23: Spacing 55 m, FoS = 1.171, d = 2 m

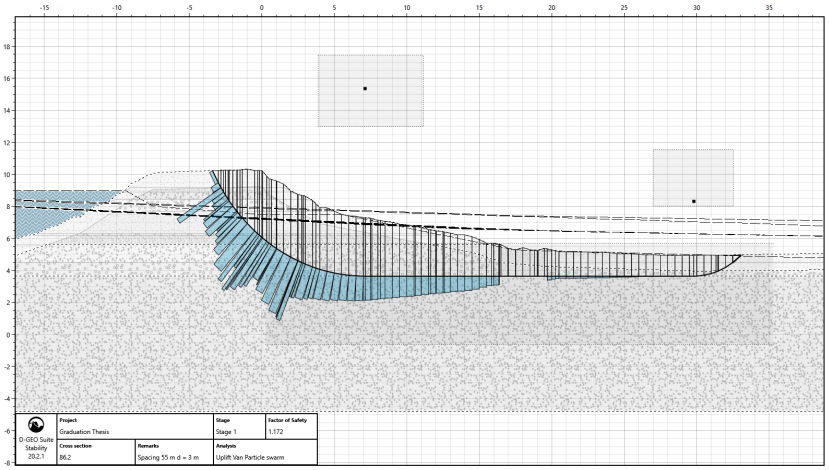

Figure G.24: Spacing 55 m, FoS = 1.172, d = 3 m

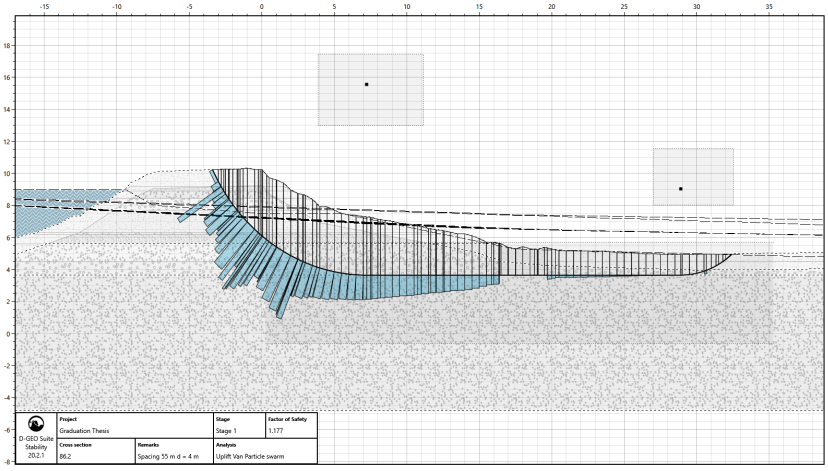

Figure G.25: Spacing 55 m, FoS = 1.177, loc = 4 m

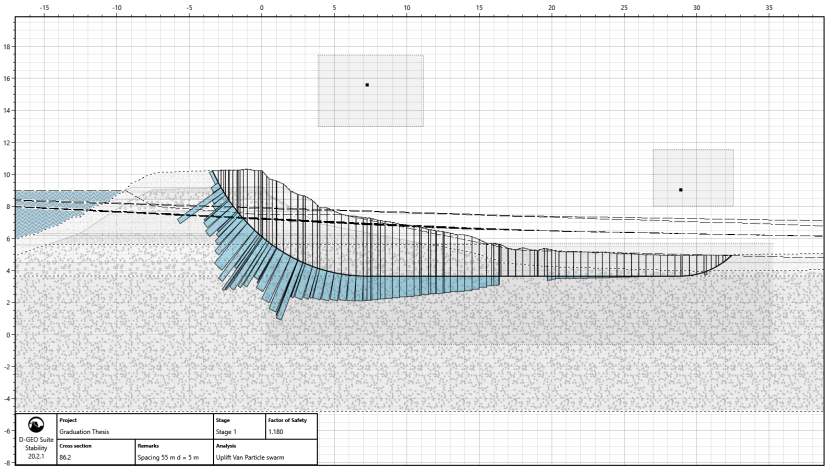

Figure G.26: Spacing 55 m, FoS = 1.180, d = 5 m

Pressure relief well analysis, 2000 m trajectory

The following checks are executed to assess the effect of placing the well in the berm at different locations.

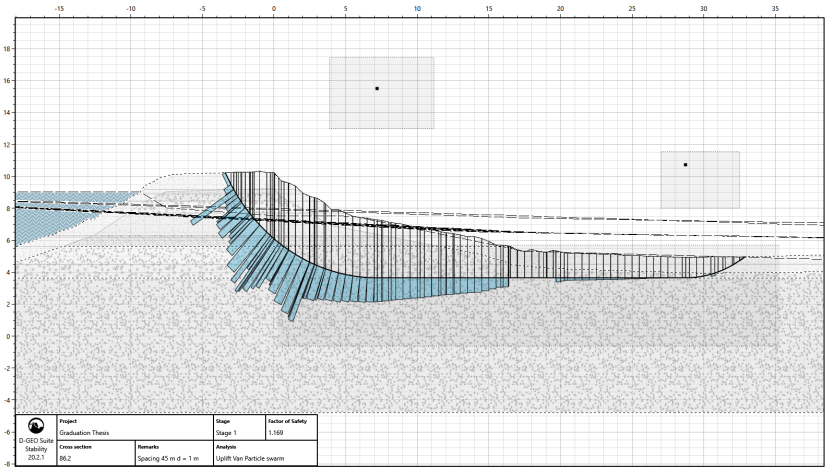

Figure G.27: Spacing 45 m, FoS = 1.169, d = 1 m

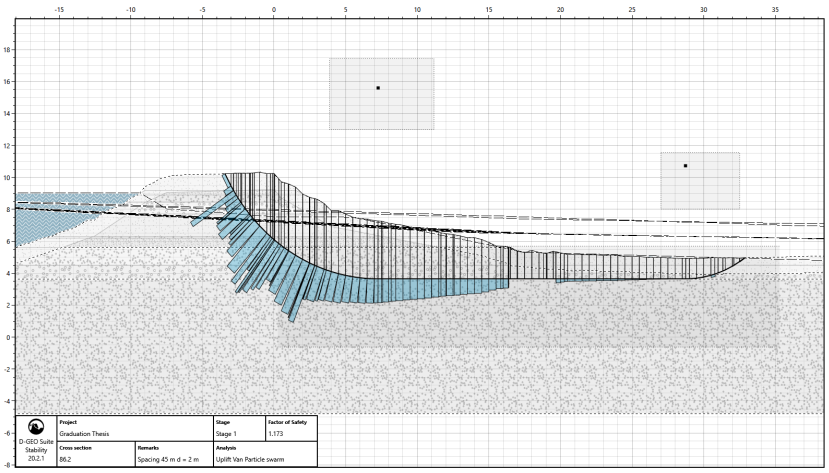

Figure G.28: Spacing 45 m, FoS = 1.173, d = 2 m

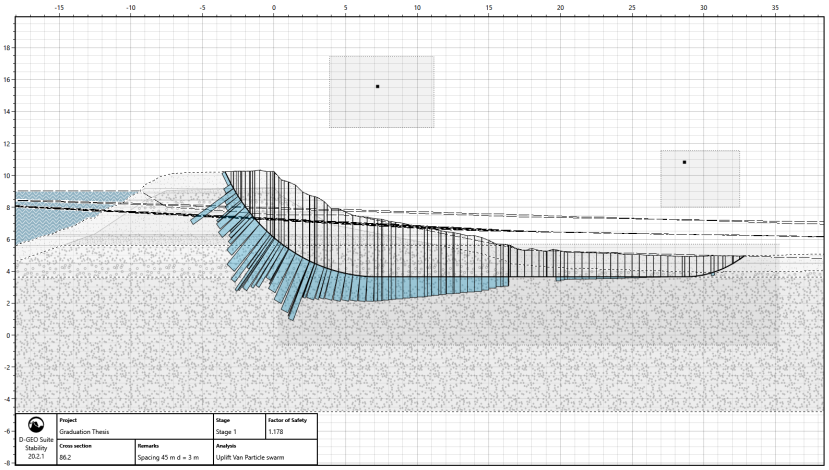

Figure G.29: Spacing 45 m, FoS = 1.178, d = 3 m

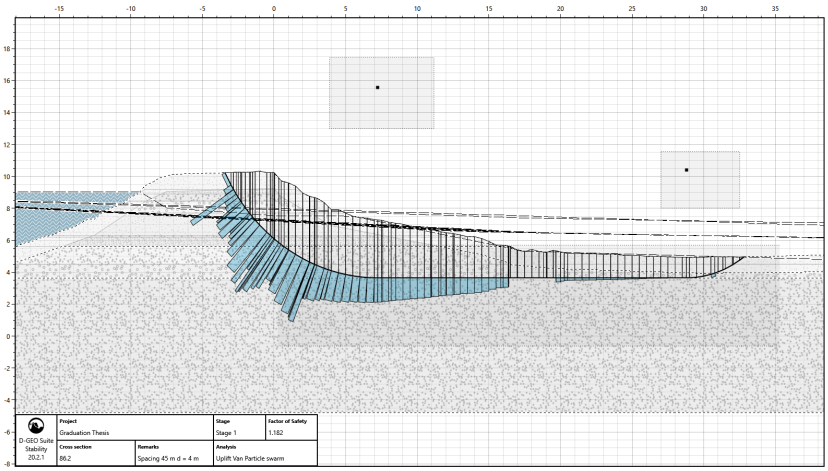

Figure G.30: Spacing 45 m, FoS = 1.182, d = 4 m

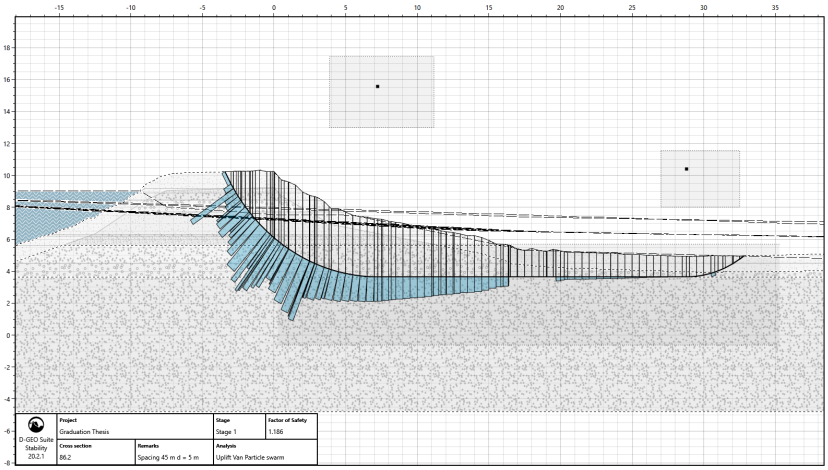

Figure G.31: Spacing 45 m, FoS = 1.186, d = 5 m

H

Hydraulic head lines

Dike trajectory 100 m

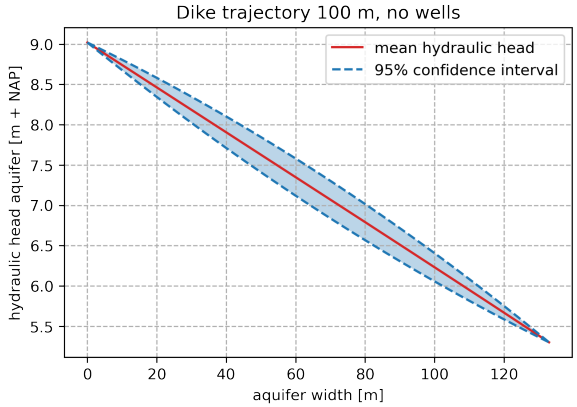

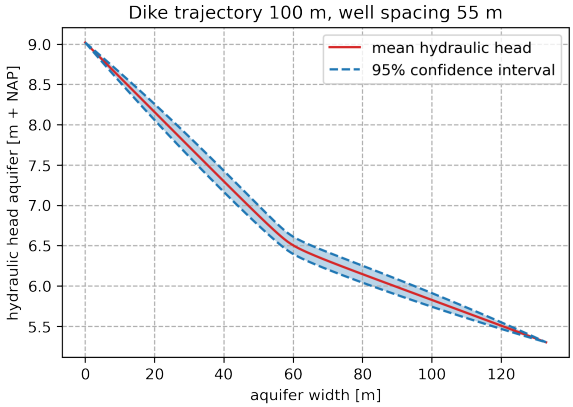

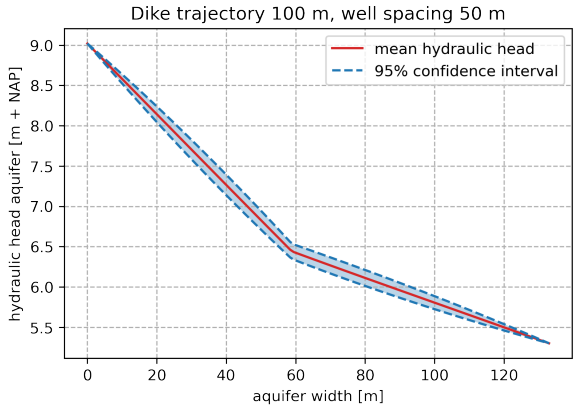

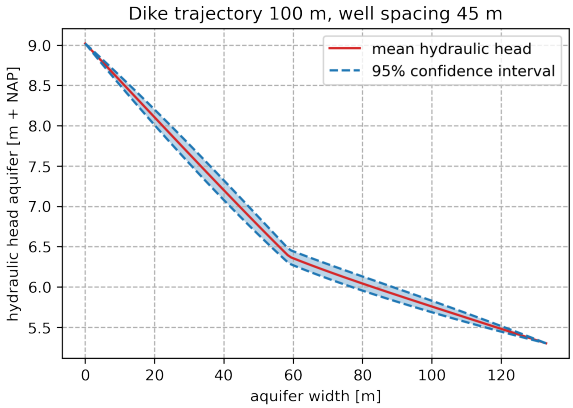

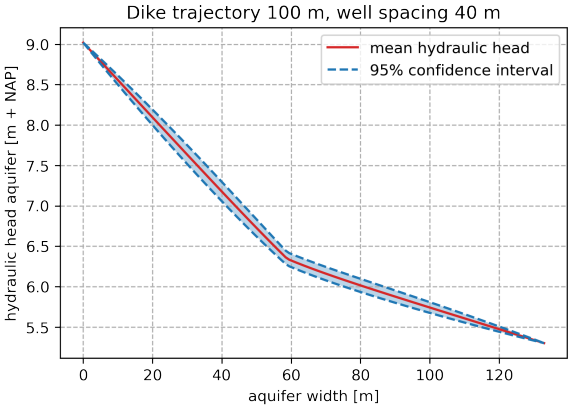
Dike trajectory 100 m, well spacing 40 m
mean hydraulic head
95% confidence interval
hydraulic head aquifer [m + NAP]
aquifer width [m]

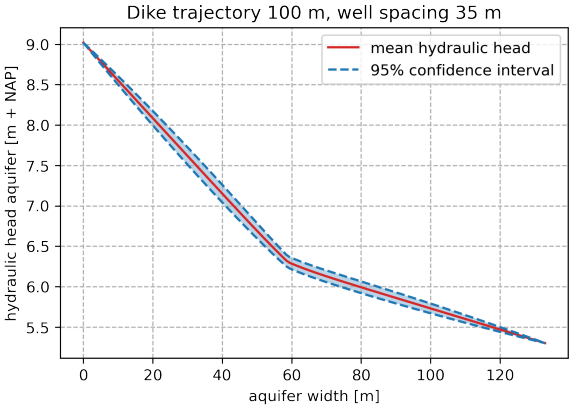
Dike trajectory 100 m, well spacing 35 m
mean hydraulic head
95% confidence interval
hydraulic head aquifer [m + NAP]
aquifer width [m]

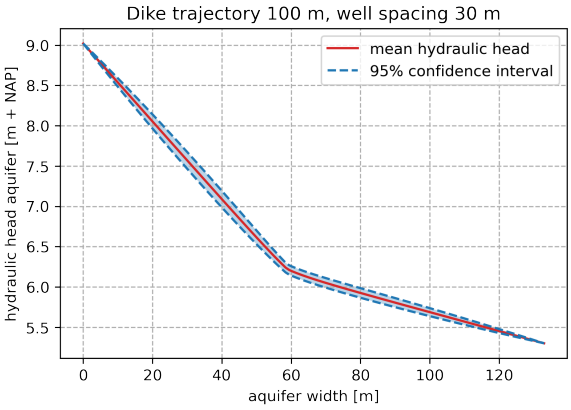
Dike trajectory 100 m, well spacing 30 m
mean hydraulic head
95% confidence interval
hydraulic head aquifer [m + NAP]
aquifer width [m]

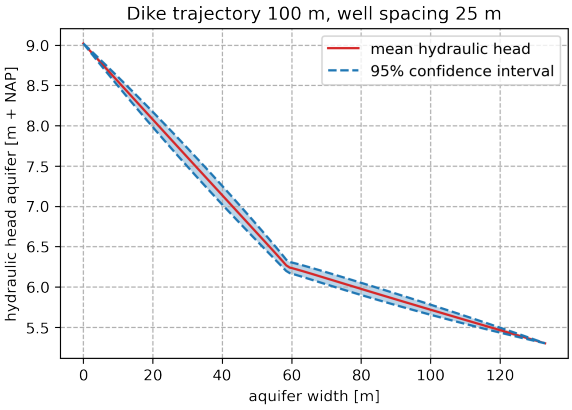
Dike trajectory 100 m, well spacing 25 m
mean hydraulic head
95% confidence interval
hydraulic head aquifer [m + NAP]
aquifer width [m]

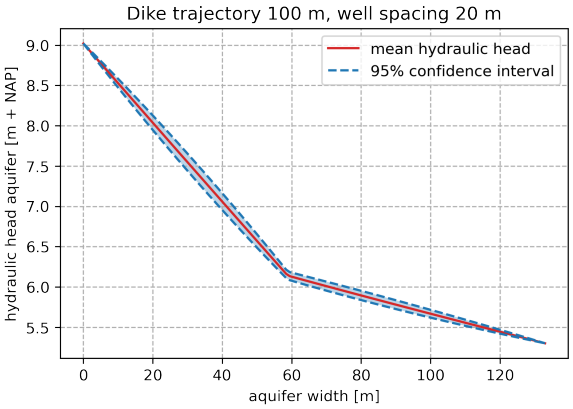
Dike trajectory 100 m, well spacing 20 m
mean hydraulic head
95% confidence interval
hydraulic head aquifer [m + NAP]
aquifer width [m]

Dike trajectory 2000 m

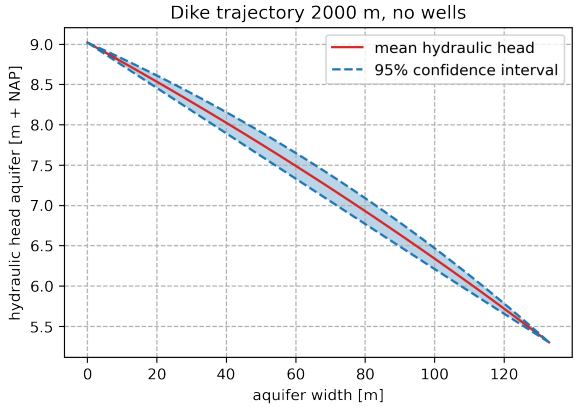

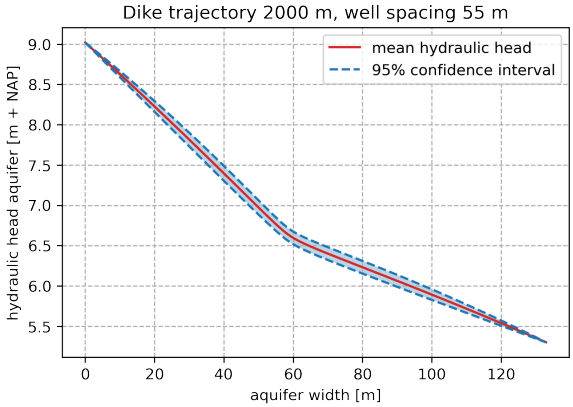

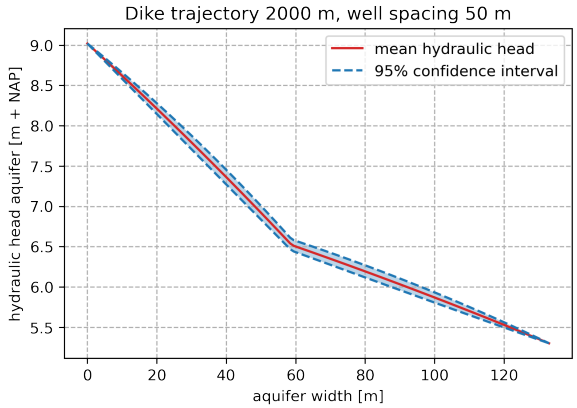

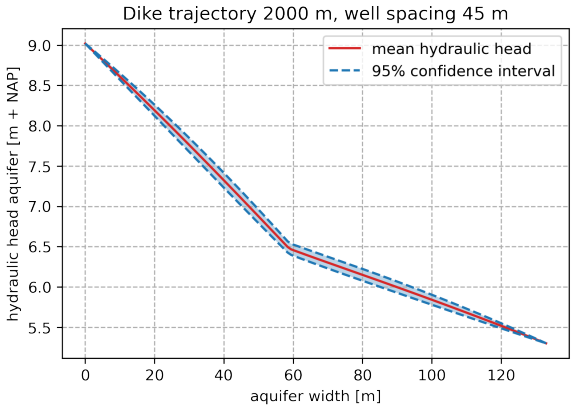

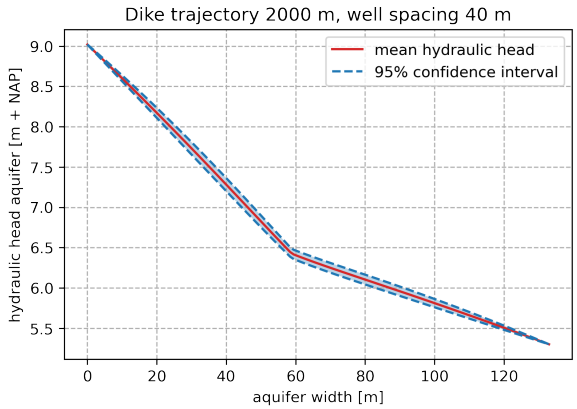

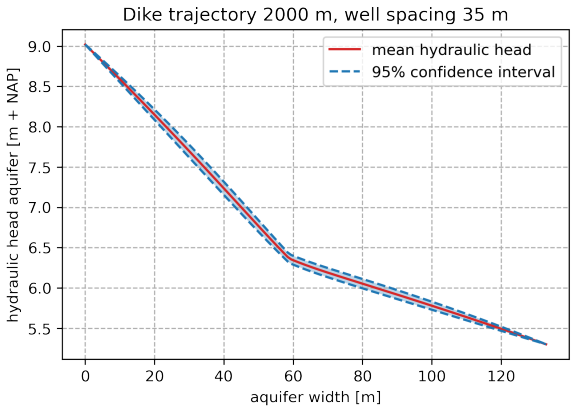

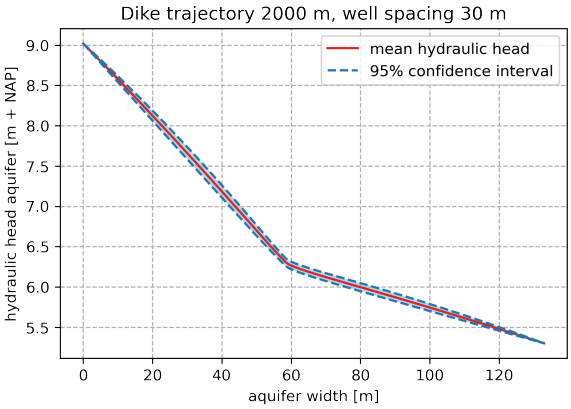
Dike trajectory 2000 m, well spacing 30 m
mean hydraulic head
95% confidence interval
hydraulic head aquifer [m + NAP]
aquifer width [m]

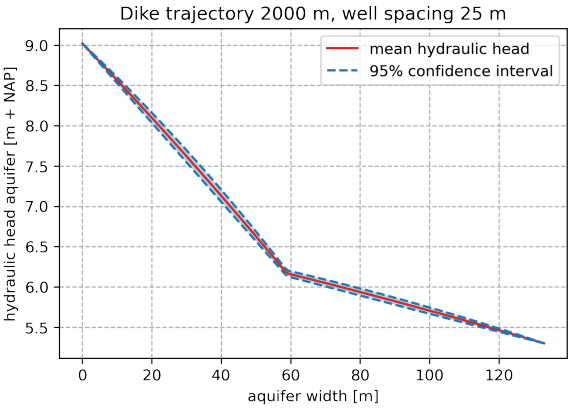
Dike trajectory 2000 m, well spacing 25 m
mean hydraulic head
95% confidence interval
hydraulic head aquifer [m + NAP]
aquifer width [m]

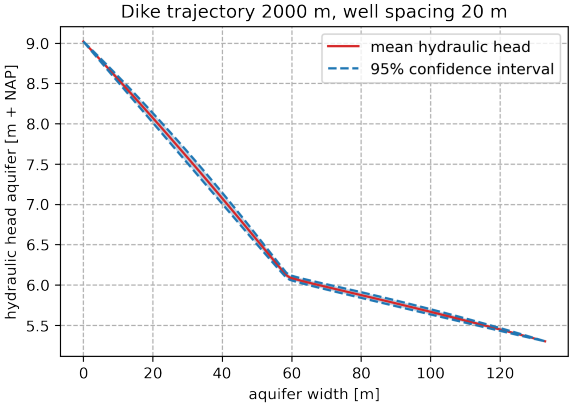
Dike trajectory 2000 m, well spacing 20 m
mean hydraulic head
95% confidence interval
hydraulic head aquifer [m + NAP]
aquifer width [m]

Dike trajectory 100 m

The following head lines are used to assess the effect of placing the well in the berm at different locations.

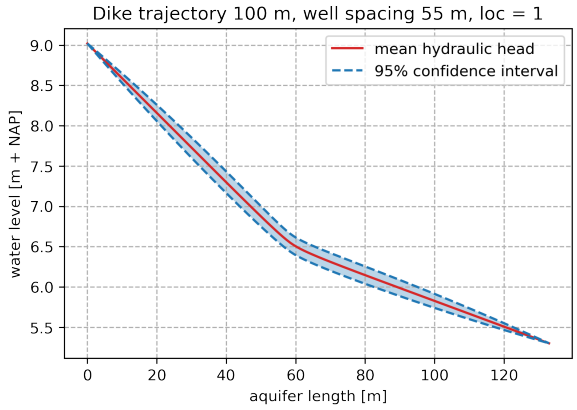

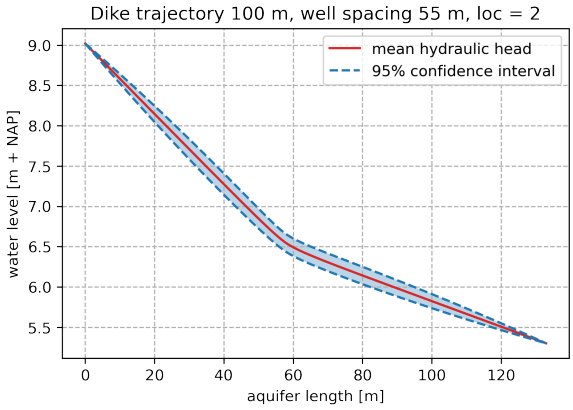

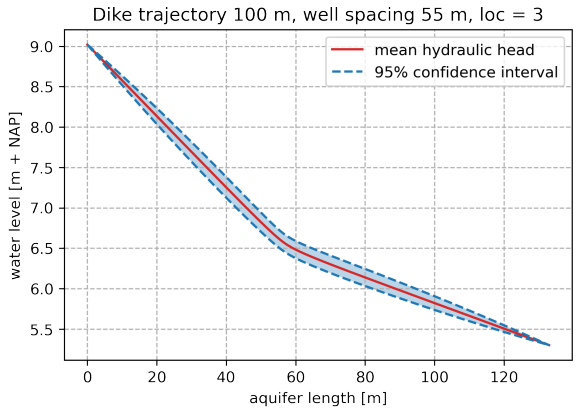

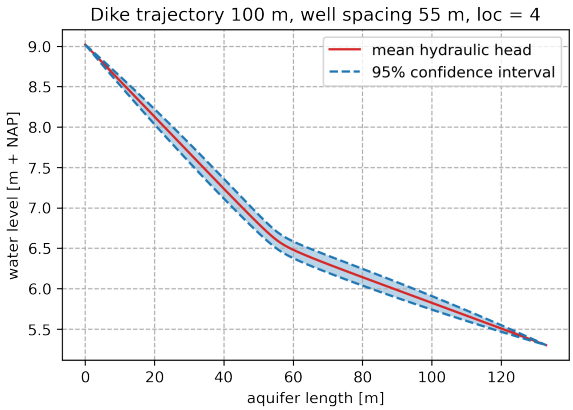

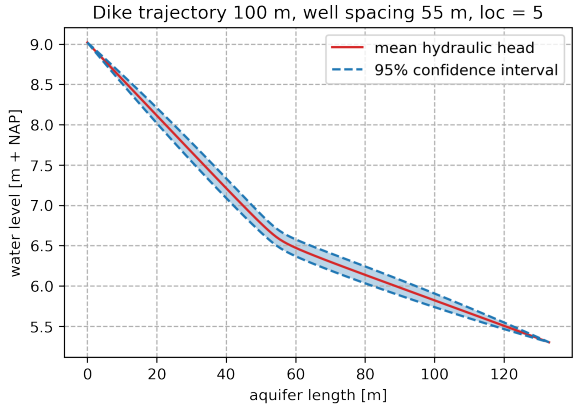

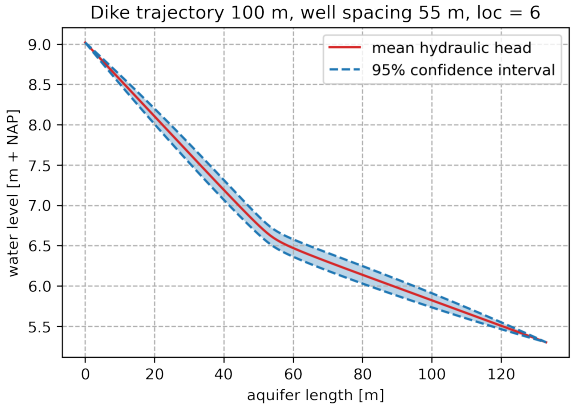

Dike trajectory 2000 m

The following head lines are used to assess the effect of placing the well in the berm at different locations.